

HOST-ROCK CONTAMINATION AND SULFIDE  
IMMISCIBILITY IN THE FRANKLIN LARGE IGNEOUS  
PROVINCE, VICTORIA ISLAND, CANADA

Matthew J. Hryciuk

April 2013

Department of Earth and Planetary Sciences

McGill University

Montréal, Québec

A thesis submitted to the Faculty of Graduate Studies and Research in partial  
fulfillment of the requirements of the degree of Master of Science

© M.J Hryciuk, 2013

## ABSTRACT

Contamination in the intrusive plumbing system of large igneous provinces (LIPs) by country rocks can lead to sulfide immiscibility, which is a vital step in the formation of nickel-copper-platinum group element (PGE) ore deposits. On Victoria Island, arctic Canada, exceptional preservation enables the relationships between sills and dikes of the Neoproterozoic Franklin LIP and their host sedimentary rocks to be studied in detail. We use sulfur isotope values and major and trace elements concentrations of intrusions and host rocks and Fe-Ti oxide oxybarometry of intrusions to evaluate contamination in the Franklin LIP and the effect of contamination on sulfur solubility.

There is minimal evidence of host rock contamination in carbonate- and shale-hosted sills. These sills tend to have homogeneous  $\delta^{34}\text{S}$  values between +3 and +4‰ (V-CDT, Vienna Canyon Diablo Troilite). We document how sulfur contamination in a prominent dike led to  $\delta^{34}\text{S}$  values as low as -4‰. Major and trace element profiles document a net depletion of sulfur and trace metals in host carbonates proximal to the dike. We propose that sulfur advected into the dike carried by contact metamorphic fluids generated by carbonate devolatilization reactions.

We present field evidence linking host-rock contamination to oxygen fugacity ( $f\text{O}_2$ ) and sulfide immiscibility. Sills hosted by carbonates and shales have oxygen fugacity conditions in the range where sulfides are stable below  $\Delta\text{FMQ}+1$  (log units relative to the fayalite-magnetite-quartz buffer). In these sills, oxygen fugacity ( $f\text{O}_2$ ) is not correlated to sulfur isotope values. Evaporite-hosted sills record much wider ranges of sulfur isotope values and oxygen fugacities.

Evaporite-hosted sill samples with  $\delta^{34}\text{S}$  values less than +5‰ recorded uniformly reducing  $f\text{O}_2$  conditions below  $\Delta\text{FMQ}-1$ . The sill with the most positive  $\delta^{34}\text{S}$  in its interior (up to +13‰) recorded the most homogeneously oxidizing  $f\text{O}_2$  conditions ( $\Delta\text{FMQ}+1$  to  $\Delta\text{FMQ}+2$ ) in the transitional range between sulfide and sulfate melt speciation. Mixing calculations indicate that up to 0.7wt% anhydrite needed to be assimilated to explain the S-isotopic signatures. However, half the added sulfur predicted by the mixing calculations is missing, and it is inferred that this may be due to immiscible sulfide segregation upstream of the sill emplacement site.

Although sulfide immiscibility in a mafic melt, such as that accompanying host-rock contamination, is a necessary prerequisite to the formation of an economic magmatic sulfide deposit, it does not guarantee that further ore-forming processes, such as metal tenor upgrading, will occur. With this caution in mind, the data presented in this thesis suggest that evaporite assimilation in dikes is the best way to generate the immiscible sulfides needed to initiate an ore-forming sequence in a large igneous province plumbing system.

## RÉSUMÉ

La contamination par des roches encaissantes ayant lieu dans les conduits qui alimentent les effusions basaltiques de grande envergure (LIP = large igneous province) pourrait déclencher l'immiscibilité entre les liquides sulfureux et silicatés, et représente une étape vitale dans la formation de gîtes de nickel-cuivre-ÉGP (éléments du groupe du platine) magmatiques. Sur l'île de Victoria (Canada arctique), la préservation exceptionnelle permet l'étude en détail des relations entre les roches sédimentaires encaissantes et les filons couches et dykes basaltiques du LIP Franklin d'âge Néoprotérozoïque. Nous utilisons les éléments majeurs et traces, ainsi que les isotopes de soufre des intrusions et encaissants, ainsi que l'oxy-barométrie sur les oxydes de Fe-Ti provenant des intrusions, afin d'évaluer l'importance de la contamination dans le LIP Franklin et son effet sur la solubilité du soufre.

Il y a peu d'évidences de contamination par les roches encaissantes dans les filons couches encaissés par les carbonates et shales. Ces filons ont des valeurs assez homogènes du  $\delta^{34}\text{S}$ , entre +3 et +4‰ par rapport à la troilite de Vienna Canyon Diablo (V-CDT). Nous documentons comment la contamination dans un dyke a généré des valeurs de  $\delta^{34}\text{S}$  aussi basses que -4‰. Des profils géochimiques dans les roches sédimentaires adjacentes au dyke impliquent un appauvrissement en S et autres métaux traces. Nous proposons que le soufre a été incorporé dans le dyke par advection, transporté par des fluides métamorphiques générés par des réactions de dévolatilisation.

Nous présentons des evidences de terrain reliant la contamination par les encaissants à des variations dans la fugacité de l'oxygène ( $f\text{O}_2$ ) et l'immiscibilité



des sulfures. Les filons encaissés par les shales et carbonates ont des conditions de  $fO_2$  sous  $\Delta FMQ+1$  (unités logarithmiques relatif au tampon fayalite-magnétite-quartz), et il n'y a aucune corrélation entre le  $fO_2$  et la composition isotopique du S; alors que les filons couches encaissés par les évaporites enregistrent un spectre de  $\delta^{34}$  et  $fO_2$  beaucoup plus large. Les échantillons provenant des filons encaissés par ces évaporites ayant des valeurs de  $\delta^{34}S$  inférieures à +5‰ enregistrent des conditions réductrices du  $fO_2$  sous  $\Delta FMQ-1$ . Le filon ayant les valeurs de  $\delta^{34}S$  les plus positives dans son intérieur (maximum de +13‰) correspond à des conditions plus oxydantes du  $fO_2$  ( $\Delta FMQ+1$  à  $\Delta FMQ+2$ ), dans la zone transitionnelle entre une spéciation sous forme de sulfures et sulfates du S dans le magma. Des calculs indiquent que jusqu'à 0.7wt% d'anhydrite doit être assimilé pour expliquer les signatures isotopiques du S dans cette intrusion. Cependant, la moitié du S prédit par les calculs en est absent, et nous soupçonnons que ce filon a perdu des sulfures par immiscibilité avant d'avoir été mis en place.

Quoique l'immiscibilité d'un liquide sulfureux à partir de magmas mafiques, comme celle qui accompagnerait la contamination par une roche encaissante comme les évaporites, représente un pré-requis pour la formation d'un gîte économique de sulfures magmatiques; cela ne garanti pas que les autres processus nécessaires à la formation d'un gîte (e.g. l'enrichissement des grades) auront nécessairement lieu. Avec cet avertissement, les données présentées dans cette Thèse suggèrent que l'assimilation des évaporites par des basaltes dans des dykes est la meilleure façon de générer des sulfures immiscibles qui constituent le point de base pour le création d'un gîte de sulfures magmatiques dans les conduits alimentant un LIP.

## CONTRIBUTION OF AUTHORS

This thesis includes two manuscripts intended for scientific publication. Chapter 2, *Dynamic dikes and sterile sills: contamination in the Neoproterozoic Franklin large igneous province, Victoria Island, Canada* documents a mechanism by which contamination occurred in a flowing magma conduit. This manuscript is co-authored by Matthew Hryciuk (MH), Jean Bedard (JB), Peter Nabelek (PN) and Boswell Wing (BW). Chapter 4, *Evaporite assimilation and immiscible sulfides in a mafic magma conduit system: insights from the Franklin LIP, Victoria Island, Canada* presents new field evidence for how mafic magmas can reach sulfur saturation. This manuscript is co-authored by Matthew Hryciuk, Jean Bedard, William Minarik (WM), and Boswell Wing. All co-authors contributed to the intellectual ideas and edited their respective manuscripts.

MH was responsible for most of the sample collection, sample preparation, scientific analysis, data processing, interpretation and writing. JB coordinated field logistics and the overall approach to sampling, and assisted with the collection of major and trace element and platinum-group element (PGE) concentrations and acted as a co-supervisor. BW coordinated the sulfur isotope laboratory logistics and was the principal in-house supervisor. WM directly assisted with the collection of electron microprobe data and associated methodologies and was also part of the thesis advisory committee. PN assisted with sample collection and was the resident expert on metamorphic petrology in the field, which is a crucial aspect of the contamination mechanism proposed in Chapter 2.

## **ACKNOWLEDGEMENTS**

This thesis is part of the Geological Survey of Canada's Geomapping for Energy and Minerals (GEM) megaproject, and was a collaborative effort involving many people, so please accept my apologies if I do not mention you specifically. See the Bedard et al. (2012) acknowledgements for a more comprehensive list of organizations involved. First of all, I would like to thank Jean Bedard for his work pulling the strings in assembling and managing the Silly Crew, as well as your continual effort to get the most out of me and the rest of the field crew for the duration of the project. I would like to thank the other 2 parts of the 3-headed monster, Rob Rainbird and Keith Dewing, for making the Victoria Island GEM project a reality. Camp life was an unforgettable experience thanks to the contributions of Greg, Darcy, Gary and the rest of the helicopter pilots, mechanics and fixed wing crews; Isaac and the rest of the camp managers; Derek, Noah (C'est Bon!, CS) and the rest of the wildlife and environmental managers; Peter and the rest of the visiting scientists; Sharon, Rosanda and Susie for providing fresh baking daily; Etienne and the rest of the IT crew; the high school mapping crew; and the one-year students Adam, Gilly, Kat, Jeff, Charlie, Fannie, Dylan, and Ziggy. Thank you to the people of Ulukhaktok for letting us work in your spectacular landscape and for your tremendous hospitality. Special thanks to Nicole Williamson, Danielle Thomson, Ben Hayes, Trent Dell'Oro, John Prince and last but not least Durbatron for making life on an arctic field mapping crew an unforgettable once-in-a-lifetime experience, twice.

Thank you a million times over to Boz Wing, who managed my efforts at McGill on a day-to-day basis. You were probably thinking that you didn't get the

student advertised when a 22 year old scatterbrained Albertan showed up on your doorstep seemingly more interested in enjoying life away from parents for the first time in Montreal than scientific research. You gave me a chance to work through my mistakes, discover ideas on my own, and helped keep me on course over the 2 years of my Master's thesis, and for that I am eternally thankful.

I would like to thank everybody I have encountered in the McGill Department of Earth and Planetary Sciences, the best department in the world; it is thanks to you people that I got the most out of Montreal academically and socially. First of all, I would like to thank Bill Minarik for assisting me with my microprobe analyses and interpretations, despite my seemingly short-term memory on how to run the darn thing, and to Lang Shi for helping train me. Anne, Kristy, Angela, and Brigitte helped make life run easily on a day-to-day basis. Thank you to everyone in my lab group PROPS (particularly Kristyn, Andre, Hao, Grant, Marcus, Lucie, Emma and Libby) for your patience in teaching me lab procedures, providing a stimulating working environment, and general companionship. If I hadn't gone to McGill I might never have experienced a Wine and Cheese, a Pub Golf and "The List" (thanks Sam Scher), Carnival, Hype Week and Jeux des Geos, epic jam sessions (Ryan Libbey says repent), a thrilling round of beer baseball, or the magnificent Stoners hockey team. Departmental trips took me to as varied locations as Tanzania (Willy Trip 2011), Newfoundland (Grad Trip 2011), an island sauna near Sudbury, a sugar shack an orchard and a mountain, and an unusual dance floor outside a cabin in the Gatineau hills.

Last but certainly not least I would like to thank my parents for encouraging me to pursue my passions and for your unwavering support.

## TABLE OF CONTENTS

Abstract .....	i
Résumé.....	iii
Contribution of authors .....	v
Acknowledgements.....	vi
Table of contents.....	viii
List of figures and tables.....	xii

<b>Chapter 1: Introduction .....</b>	<b>1</b>
--------------------------------------	----------

<b>Chapter 2: Dynamic dikes and sterile sills: contamination in the Neoproterozoic Franlin large igneous province, Victoria Island, Canada .....</b>	<b>4</b>
2.1 Abstract .....	4
2.2 Introduction .....	5
2.3 Background geology.....	7
2.4 Sampling.....	8
2.5 Methods .....	9
2.6 Elemental profiles.....	10
2.7 Sulfur isotope profiles .....	11
2.8 Discussion .....	12
2.8.1 Preservation of original geochemical distributions within sill profiles.	13
2.8.2 Ni, Cu and S depletion halos around dikes.....	14

2.8.3 Sulfur isotope constraints on mass transfer into dikes .....	15
2.9 Conclusions .....	19
2.10 Acknowledgments .....	19
2.11 References .....	20
Figure Captions .....	25
Figures .....	27
Tables .....	33
 <b>Chapter 3: Connections between manuscripts.....</b>	 <b>34</b>
 <b>Chapter 4: Evaporite assimilation and immiscible sulfides in a mafic magma conduit system: insights from the Franklin LIP, Victoria Island, Canada ...</b>	 <b>36</b>
4.1 Abstract .....	36
4.2 Introduction .....	37
4.3 Background geology.....	39
4.4 Sampling.....	40
4.5 Methods .....	41
4.6 Results .....	43
4.6.1 Carbonate-hosted and shale-hosted sills.....	43
4.6.2 Evaporite-hosted sills .....	43
4.7 Fe-Ti oxide temperature and oxygen fugacity constraints .....	44

4.8 Discussion .....	46
4.8.1 S-isotopic evolution in the Franklin magmatic plumbing system .....	46
4.8.1.1 Source of sulfur isotope values and sulfur concentrations in sills C1 and S1 .....	46
4.8.1.2 Sulfur isotope shifts in sill chilled margins .....	47
4.8.1.3 Contamination in the evaporite-hosted sills .....	48
4.8.2 Location and mechanisms of S incorporation .....	49
4.8.3 Evaporite assimilation, oxygen fugacity and sulfide immiscibility .....	51
4.8.4 Implications for Ni-Cu mineralization and LIPs .....	53
4.9 Conclusions .....	54
4.10 Acknowledgements .....	55
4.11 References .....	56
Figure captions .....	62
Figures .....	65
Tables .....	72
<b>Chapter 5: Conclusions and applications .....</b>	<b>76</b>
5.1 Scientific contributions.....	76
5.2 From ore-forming processes to exploration models.....	78
5.3 Application: carbonate contamination.....	79
5.3.1 Sampling.....	79

5.3.2 S-isotope results.....	79
5.3.3 Element abundances .....	80
5.3.4 Discussion.....	81
5.4 Application: evaporite contamination .....	83
5.5 Concluding statements and future research directions .....	85
<b>References .....</b>	<b>86</b>
<b>Appendices .....</b>	<b>89</b>
Appendix A: Sample descriptions .....	90
Appendix B: Supplemental S-isotope values .....	97
Appendix C: S, Ni, Cu and MgO contents .....	100
Appendix D: PGE contents .....	101
Appendix E: Magnetite-Ilmenite pair $fO_2$ and T constraints .....	102
Appendix F: Relationship between Fe-Ti oxide morphology and calculated T and $fO_2$ .....	Supp Files



## **LIST OF FIGURES AND TABLES**

### **Figures**

**Figure 2.1-** Victoria Island Geology Map

**Figure 2.2a-** West NFD S-isotopes

**Figure 2.2b-** East NFD S-isotopes

**Figure 2.2c-** NFD S concentrations

**Figure 2.3a-** West NFD isocons

**Figure 2.3b-** East NFD isocons

**Figure 4.1-** Victoria Island Geology Map

**Figure 4.2-** Evaporite-hosted sill sampling profiles

**Figure 4.3-** Sill E1 S-isotopes

**Figure 4.4-** Sill E3 S-isotopes

**Figure 4.5-** Evaporite-hosted sill S-isotopes vs.  $fO_2$

**Figure 4.6-** Evaporite-hosted sill S-contents vs.  $fO_2$

**Figure 4.7-** Sill E3 missing S model

### **Tables**

**Table 2.1-** Mass changes for NFD isocon profiles

**Table 4.1-**  $\delta^{34}S$  values of sills hosted by the Wynniatt Formation

**Table 4.2-**  $\delta^{34}S$  values and S contents of evaporite-hosted sills

**Table 4.3-** Magnetite-Ilmenite  $fO_2$  and T constraints (Ghiorso and Evans 2008) for Wynniatt-hosted and evaporite-hosted sill samples

**Table 4.4-** Sulfur isotopes and added anhydrite for evaporite-hosted sills

## **Chapter 1: Introduction**

Country rock sulfur addition to mafic magmas has often been inferred to be important in the formation of magmatic nickel-copper-platinum group element (PGE) deposits (Li et al., 2001; Ripley and Li, 2007; Keays and Lightfoot, 2010). However, studies of mafic magmas associated with these ore deposits generally lack direct field evidence of the process of host rock contamination and its subsequent effects on magmatic conditions such as oxygen fugacity and sulfur solubility.

The Franklin large igneous province (LIP), Victoria Island, arctic Canada, is an ideal location for evaluating the effects of host-rock contamination in a magmatic plumbing system. The effects of chemical weathering, structural deformation, and metamorphism are minimal, allowing the relationships between sills, feeder dikes, flood basalts and host rocks to be studied in detail. As well, the effect of lithology on host rock contamination can be evaluated because of the range of sedimentary rocks exposed from carbonates to shales to sandstones to evaporites.

We use sulfur isotopes in this thesis as a critical tracer for evaluating interactions between intrusive magmas and host rocks. Sedimentary rocks tend to have a much larger range of  $\delta^{34}\text{S}$  values than igneous rocks: sedimentary sulfides can have  $\delta^{34}\text{S}$  values far below -30‰ [referenced to the Vienna Canyon Diablo Troilite (VCDT)] whereas sedimentary sulfates can have  $\delta^{34}\text{S}$  values in excess of +30‰ (Seal, 2006). Typical igneous rocks tend to have  $\delta^{34}\text{S}$  values between -2 and +5‰ (Seal, 2006). The large isotopic differences among igneous sulfur, sedimentary sulfides, and sedimentary sulfates allow sulfur isotopes to track host

rock contamination of an igneous system, even at low levels of contamination. By coupling sulfur isotope measurements with changes in major and trace element abundances, the net fluxes of sulfur and trace metals into and out of intrusions can be evaluated.

In order to determine whether magmatic sulfur isotope shifts are caused by host rock contamination, a number of other processes need to be evaluated. These include: fractional crystallization (Janecky and Shanks, 1988); degassing (de Hoog et al., 2001; Ripley et al, 2003; Mandeville et al., 2009); diffusive exchange (Ripley and Li, 2003); and subsolidus recrystallization driven by hydrothermal fluids (Ripley, 1983). Each of the processes should affect the sulfur isotopes and abundances in a unique way. Fractional crystallization should lead to increasing sulfur abundances from a sill base to a sill top with minimal isotopic fractionation. Degassing would lead to lower sulfur abundances and positive or negative isotopic fractionations depending on the oxygen fugacity during degassing. Pure diffusive isotope exchange would affect sulfur isotope compositions but not sulfur abundances. Because of the discrete fracture-controlled nature of most hydrothermal fluid pathways, variable sulfur concentrations and isotopic changes would be characteristic of subsolidus hydrothermal recrystallization. By studying intrusions that are similar except for one key difference, such as host-rock lithology or intrusive geometry, the effects of contamination can be further constrained.

Magmatic-stage contamination by host rocks has the potential to lead to sulfide immiscibility, which is where sulfur solubility is reached and a sulfide melt phase segregates from the silicate melt. However, contamination can also

lead to changes in oxygen fugacity (Li et al., 2009b). Sulfur solubility in a mafic melt increases by a factor of ten from reduced oxygen fugacities, where sulfides are stable, to oxidized oxygen fugacities where sulfates are stable (Jugo et al., 2005). We combine Fe-Ti oxide geothermometry and oxybarometry with sulfur isotope geochemistry to evaluate how host rock contamination can lead to sulfide immiscibility in the plumbing system of the Franklin large igneous province. The potential for such immiscibility is a crucial step in the formation of a magmatic sulfide deposit.

## **Chapter 2: Dynamic dikes and sterile sills: Contamination in the Neoproterozoic Franklin large igneous province, Victoria Island, Canada**

Matthew J. Hryciuk<sup>1\*</sup>, Jean H. Bédard,<sup>2</sup> Peter I. Nabelek<sup>3</sup>, Boswell A. Wing<sup>1</sup>

<sup>1</sup>Department of Earth and Planetary Sciences, McGill University, Montreal, Québec H3A 2A7, Canada

<sup>2</sup>Geological Survey of Canada (GSC-Québec), Québec City, Québec G1K 9A9, Canada

<sup>3</sup>Department of Geological Sciences, University of Missouri, Columbia, Missouri 65211, USA

**2.1 Abstract:** Voluminous mafic intrusions have the potential to form large nickel and copper and/or PGE-bearing deposits when contaminated by silica or sulfur rich country rocks. Although the effects of contamination in magma chambers have been comprehensively studied, there has been less documentation of the mechanisms of assimilation. On Victoria Island, Canada, a well-exposed network of sills and dikes preserves a record of interaction between magma and host rocks in the feeder system for the Neoproterozoic Franklin large igneous province. Although the feeder system is sill-dominated, dikes occur in syn-magmatic fault-guided transfer zones. Diabase sills we have examined show little evidence of host rock contamination, with homogeneous sulfur isotope compositions characterized by  $\delta^{34}\text{S}$  values between +3 and +4‰ (V-CDT, Vienna Canyon Diablo Troilite). A prominent dike has sulfur isotopes ranging from typical magmatic  $\delta^{34}\text{S}$  values of +4.1‰ in the core to  $\delta^{34}\text{S}$  values as low as -4.2‰ at the margins. This implies that the dike was contaminated during transport by its wallrock carbonates, which have strong negative  $\delta^{34}\text{S}$  values as low as -27.0‰

---

\*E-mail: [matthew.hryciuk@mail.mcgill.ca](mailto:matthew.hryciuk@mail.mcgill.ca)

(V-CDT) on the west side of the dike. Major and trace element profiles suggest a net depletion of sulfur and nickel from the carbonates adjacent to the dike over a distance of 20m. We propose that up to 50% of the sulfur from these host carbonates was transported into the dike by metamorphic fluids generated during devolatilization reactions.

## 2.2 INTRODUCTION

The deposition of many magmatic sulfide deposits has been linked to the addition of crustal silica and sulfur-rich rocks into mafic magmas, which can trigger sulfide immiscibility (Mungall and Naldrett, 2008). For example, the giant Noril'sk-Talnakh Ni, Cu and platinum-group element (PGE) ore deposits were formed in a continental flood basalt feeder system. Elevated  $\delta^{34}\text{S}$  values from +8 to +12‰ in these ores have been attributed to the assimilation of sulfate evaporites (Li et al., 2009a) or  $\text{H}_2\text{S}$  gas from coals and pyritic shales (Grinenko, 1985).

However, multiple lines of evidence suggest that the Noril'sk-Talnakh ores could not have formed *in situ* from the magma at the site of emplacement in thick sills. Undepleted nickel concentrations in olivine in the silicate magmas in ore-bearing intrusions indicate that these were not the source of metals in the immiscible sulfides (Arndt et al., 2003). Mantle-like Os isotopes in sulfide ores indicate that Os in sulfide melts is not derived directly from an assimilation event, and that large volumes of uncontaminated magma would have interacted with early-formed immiscible sulfides (Arndt et al., 2003). These observations led to the interpretation that initial sulfide immiscibility was triggered in deep crustal

magma staging chambers, potentially by the assimilation of granodiorite (Lightfoot and Keays, 2005). Large deep staging chambers could also provide the immense magma volumes necessary to upgrade nickel and PGE contents in sulfides (Naldrett, 1992; Li et al., 2009b).

Contamination during magma transport in a feeder system is theoretically possible (Huppert and Sparks, 1985) and has been indirectly inferred (Mungall, 2007). However, limited direct field and geochemical evidence have prevented the quantitative evaluation of this as a viable alternative hypothesis to deep crustal contamination in a staging chamber. In the Franklin large igneous province, Victoria Island, Canada, unusually complete preservation enables the contact relationships and chemical interactions between dikes, sills, host sedimentary rocks and flood basalts to be studied in detail.

This contribution will examine the plausibility and extent of localized contamination within Franklin sills and dikes. Sulfur isotopes were chosen as a tracer to investigate intrusive-host rock interactions because the wide variety of sedimentary rocks present have a much larger range of isotopic values than mantle-derived igneous rocks. Reduced pyrites in shales and carbonates can have  $\delta^{34}\text{S}$  values [referenced to the Vienna Canyon Diablo Troilite (VCDT)] as low as -30‰ and sulfates in evaporites can have  $\delta^{34}\text{S}$  values in excess of +30‰, whereas mafic igneous rocks are typically restricted to  $\delta^{34}\text{S}$  values between 0 and +5‰ (Seal, 2006). Major and trace element geochemistry will also be utilized to evaluate relative component mobility into and out of the intrusions.

## 2.3 BACKGROUND GEOLOGY

The Neoproterozoic Franklin large igneous province, emplaced around 723 Ma (Heaman et al., 1992), extends over 2500km across northern and arctic Canada from the Mackenzie Mountains in the west to Baffin Island and western Greenland in the east (Fahrig, 1987; Shellnutt et al., 2004; Denyszyn et al., 2009; Ernst and Bleeker, 2010). The Minto Inlier on Victoria Island is proximal to the inferred magma source of the Franklin event (Fig. 2.1). Here, the Neoproterozoic Shaler Supergroup (Thorsteinsson and Tozer, 1962; Rainbird et al. 1994; Long et al., 2008) is intruded by the sill-dominated Franklin intrusives, and overlain by the consanguineous Natkusiak flood basalts (also part of the Franklin event, Dostal et al., 1986; Dupuy et al., 1995). The Shaler Supergroup is dominated by carbonates interpreted to have formed in a shallow intracontinental sea (Young, 1981) and also contains significant proportions of sandstone, shale and gypsiferous evaporites.

The Franklin sills range in thickness between a few and over 100m in thickness, with many sills being traceable for several to tens of kilometers. The Franklin intrusives consist mostly of diabase and gabbro, with picritic to olivine-bearing intrusions also occurring in the lower part of the intrusive complex, which is well-exposed north of Minto Inlet. Dikes tend to be associated with prominent NNW-trending magnetic lineaments (Kiss and Oneschuk, 2010), cataclasites, and syn-magmatic normal faults which guided magma ascent (Bédard et al., 2012). Rocks of the south-western Minto Inlier are gently folded (with dips typically less than 10°) with fold axes trending to the ENE. The stratigraphy is disrupted by a



large number of similarly aligned horst and graben structures produced by post-Devonian normal faults (Bédard et al., 2012).

## **2.4 SAMPLING**

Samples were collected in transects oriented perpendicular to intrusive margins with continuous host rock exposure. Both sides of intrusions were sampled. Transects were collected far from other intrusive bodies in order to best constrain local intrusive-host rock interactions. Detailed sampling profiles and the coupling of isotopic and chemical analyses make it possible to quantify the magnitude and direction of mobile component fluxes.

A dike and two sills were targeted for sampling in order to determine the sites and mechanisms by which contamination occurred in the Franklin plumbing system. Dike and host rock samples were collected from the Northern Feeder Dike (NFD) of Bédard et al. (2012) and Nabelek et al. (2013), which is hosted by silty limestones of the Boot Inlet Formation (Fig 2.1.). The NFD dips approximately 45° to the E and was emplaced along a syn-magmatic NNW-trending fault with east-side down throw, such that a different part of the stratigraphy is exposed on either side of the dike. The calculated dike thickness is ≈26m along the sampling transect. Because there is significant stratigraphic variation in isotopic signatures in the carbonates (Jefferson et al., 1994), sample transects were collected roughly parallel to bedding (dips approximately 5 degrees to the SE) to minimize this source of variability. Apparent distances from the dike margin were corrected to reflect true distances orthogonal to the dike.

Two sill sample profiles were collected from the Wynniatt Formation (Fig. 2.1). One of these was a partial profile of host rock and sill samples from within 5 meters of the lower contact of an approximately 20m thick intrusion, carbonate-hosted sill C1. The sedimentary rocks in this profile are dominated by dark calcareous shales with nearly pure limestone nodules. Like the host rocks present at the NFD, these are dominantly carbonates with a significant clastic component, allowing us to contrast the effects of sill vs. dike emplacement. To further investigate the effect of lithology on contamination, a complete profile was taken through a 16m thick intrusion, shale-hosted sill S1, hosted by black shales with significant sandstone horizons.

## **2.5 METHODS**

Whole-rock powders for major and trace element analyses were ground from crushed samples using an agate mill. Whole-rock powders for S-isotope analyses were ground using tungsten carbide and case-hardened steel mills. Major and some trace element concentrations were analysed by ICP-AES and the remainder of the trace elements were analysed by ICP-MS at INRS-ETE in Québec City, Québec.

We extracted sulfide sulfur from rock powders with an acidic Cr-reducing solution (Canfield et al., 1986) to produce  $H_2S$ . The  $H_2S$  was trapped as  $ZnS$  in a zinc acetate solution, and then reacted with  $AgNO_3$  to produce  $Ag_2S$ . Filtered  $Ag_2S$  was weighed into aluminum foil packets and fluorinated in Ni bombs at  $\sim 250^\circ C$  to produce  $SF_6$ . The resulting  $SF_6$  was purified cryogenically and chromatographically and its isotopic composition was measured on a

ThermoElectron MAT 253 gas-source mass spectrometer. Reproducibility for the extraction and mass spectrometry of samples was equal to or less than 0.20‰ (1 $\sigma$ ) for  $\delta^{34}\text{S}$  values. We report  $\delta^{34}\text{S}$  values on the V-CDT scale, defined by the isotopic composition of the international standard silver sulfide powder IAEA-S-1 ( $\delta^{34}\text{S}_{\text{IAEA-S-1}} \equiv -0.3\text{‰ V-CDT}$ ).

## 2.6 ELEMENTAL PROFILES

Major element abundances are similar in host rocks proximal and distal to the sill margins in both sill profiles. For example, in the shale-hosted sill S1 profile,  $\text{SiO}_2$  in the shales is restricted between 57.0 and 61.7 wt% whereas  $\text{Al}_2\text{O}_3$  ranges between 17.5 and 20.5 wt%. Nor do trace element distributions (e.g., S, Cu, and Ni) show any clear trends vs. distance from the sill margins. The two sills are broadly similar in overall composition, though there are some important differences. Sulfur concentrations, for example, are roughly twice as high in sill S1 (0.076 to 0.097 wt%) as they are in sill C1 (0.037 to 0.048 wt%).

In direct contrast to the sill profiles, the dike and host rock elemental profiles show clear enrichment and depletion trends. In the eastern section carbonates, for example, host rocks show progressive enrichment in  $\text{SiO}_2$ ,  $\text{Al}_2\text{O}_3$ ,  $\text{FeO}_{\text{total}}$ ,  $\text{TiO}_2$ ,  $\text{MgO}$ ,  $\text{Na}_2\text{O}$  and Zr as the dike margin is approached. Specifically,  $\text{SiO}_2$  increases from a minimum of 21.0 wt% to a maximum of 43.3 wt%, whereas  $\text{Al}_2\text{O}_3$  increases from a minimum of 3.6 wt% to a maximum of 6.4 wt%. The western section carbonates have similar enrichments, except in the 2 samples closest to the dike margin where there are slight elemental depletions. Sulfur,

nickel and copper abundances counter the prevailing trend, with the most distal sample from the western dike contact (0.42 wt% S, 41 ppm Ni, 24 ppm Cu) having the highest concentrations, with significant depletions being evident as the dike margins are approached (Fig. 2.2c). Despite a gradation from microdiabase at dike contacts to medium-grained diabase in the core, the dike shows no clear trends of variation of SiO<sub>2</sub>, CaO, MgO, Al<sub>2</sub>O<sub>3</sub> and FeO<sub>total</sub>. The sulfur concentrations in the dike are fairly low and homogeneous between 0.039 and 0.051wt% (Fig. 2.2c), but show important variations in S isotopic composition.

## 2.7 SULFUR ISOTOPE PROFILES

Overall, the range of  $\delta^{34}\text{S}$  values in the 2 sill interiors examined is restricted, ranging between +3.6 and +4.0‰. In sill S1, interior  $\delta^{34}\text{S}$  values range from +3.7 to +4.0‰, whereas the lower chilled margin has a slightly higher  $\delta^{34}\text{S}$  value of +5.6‰. Similarly, in sill C1, two samples of the sill interior have  $\delta^{34}\text{S}$  values of +3.6 and +3.9‰, whereas two samples of the lower chilled margin show more variable values of +1.0 and +3.3‰. Sulfur isotope values in the sedimentary rocks hosting the sills exhibit a much larger range (-10.4 to +8.9‰) than those found in the sills, and clear isotopic shifts are not seen as sill margins are approached.

In direct contrast to the sulfur isotope profiles in the sills,  $\delta^{34}\text{S}$  values from the northern feeder dike environment vary smoothly from the host sedimentary rocks into the dike interior. The western carbonate profile passes from the most  $^{34}\text{S}$ -depleted values ( $\delta^{34}\text{S} = -27.0$  to  $-20.8$ ‰) in the six outermost samples, to -

14.5‰ within less than 1.5m of the dike margin (Fig. 2.2a). The  $\delta^{34}\text{S}$  values within the dike continue this pattern, with a  $\delta^{34}\text{S}$  value of -4.2‰ in the western chilled margin, ultimately defining a sigmoidal profile that reaches a maximum  $\delta^{34}\text{S}$  value of +4.1‰ in the center of the dike that is indistinguishable from that of typical sill interior magmas.

The eastern dike profile has less overall variability, with relatively  $^{34}\text{S}$ -enriched values in the outermost carbonates ( $\delta^{34}\text{S}=+3.5\text{‰}$ ) dropping to a  $\delta^{34}\text{S}$  value of -0.2‰ within 10m of the dike margin (Fig. 2.2b). This trend reverses sharply within the dike, with the most negative  $\delta^{34}\text{S}$  values in the eastern profile (-0.7‰) found in the chilled margin, followed by a gradual climb back to  $\delta^{34}\text{S}$  values near +4‰ in the dike center. Importantly, the  $\delta^{34}\text{S}$  gradient within the dike is steeper in the western profile than in the eastern profile.

## 2.8 DISCUSSION

Three observations highlight how sills and dikes may affect magmatic contamination differently. The first is the absence of chemical and isotopic trends across sill-country rock profiles. The second is the distinct elemental enrichment and depletion halos in host rocks surrounding the dike. The third is the smoothly varying  $\delta^{34}\text{S}$  profiles extending from the local country rock into the dike. We discuss the constraints placed on the contamination process by these observations in turn.

### **2.8.1 Preservation of original geochemical distributions within sill profiles**

In the sill wallrock elemental profiles, Ni, Cu, and S abundances are uncorrelated, and show no progressive changes towards sill margins. The host shales and carbonate shales in both profiles show no evidence of a convergence towards magmatic sulfur isotope values. The most likely explanation for these elemental and isotopic patterns is primary sedimentary heterogeneity of the host carbonates and black shales.

The restricted range of  $\delta^{34}\text{S}$  values from +3.6 to +4.0‰ within the interiors of sills S1 and C1 makes it unlikely that either of these intrusions contain a significant amount of locally-derived host rock sulfur. Simple isotopic mixing models (Ripley and Li, 2003) inputting the maximum  $\delta^{34}\text{S}$  difference of 0.4 per mil in the sill C1 interior (with 450ppm sulfur) indicate that at most 15ppm sulfur was assimilated from the host carbonate shales.

The overlapping restricted range of  $\delta^{34}\text{S}$  values in both sills, despite there being two times as much sulfur in sill S1 vs. sill C1, precludes extensive sulfur removal by degassing, as degassing should lead to isotopic fractionation (de Hoog et al., 2001). As well, sill samples deviating from the homogeneous range of  $\delta^{34}\text{S}$  values from +3.6 to +4.0‰ are only present in the lower 2 meters of each sill, and in each case are shifted towards average values of the local country rocks. This suggests only limited sulfur mobility in the sill profiles, perhaps because chilled margin formation restricted interactions between sill magmas and host rocks. Near-pervasive carbonate metasomatism commonly extends several cm into chilled margins of carbonate-hosted sills, suggesting that diffusional exchange

occurred at subsolidus conditions and perturbed the chilled margin S-isotope signatures. We interpret the range of sill  $\delta^{34}\text{S}$  values from +3.6 to +4.0‰ as a primary magmatic signature for the Franklin gabbros in the Minto Inlier.

### **2.8.2 Ni, Cu and S depletion halos around dikes**

Contact metamorphism around dikes can lead to dehydration and devolatilization reactions, liberating mobile components that can be redistributed by diffusion and fluid advection (Breeding and Ague, 2002). If this leads to mass gains or losses, immobile element concentrations will increase or decrease systematically as reactions progress. These changes are the basis of the isocon method (Grant, 1986), which constrains the relative mobility of a large number of major and trace elements simultaneously. In this study,  $\text{Al}_2\text{O}_3$ , Zr, and  $\text{TiO}_2$  plot in robust linear arrays allowing isocons of no-net elemental movement to be defined for the western and eastern carbonate profiles.

The isocon method reveals significant net depletions of sulfur, iron and trace metals around the Northern Feeder Dike. Average mass losses of 30 to 60%  $\text{FeO}_{\text{total}}$ , Ni, S and Cu were calculated in the NFD western carbonate profile (Fig. 2.3a). The isocons indicate that maximum mass losses occurred between 10 and 20m from the dike. The overall mass changes are roughly correlated to loss on ignition values (Table 2.1), thought to be mainly  $\text{CO}_2$  in these carbonate-rich lithologies. Metamorphic decarbonation is therefore hypothesized to be the driving process of the mass losses. Sulfur may potentially be partitioned as an aqueous species into the continuously generated metamorphic fluid (Li et al.,

2003), whereas the correlated behavior of S with Ni, Cu, and FeO<sub>total</sub> suggests that devolatilized sulfur scavenged and transported these metals.

There are similar S, Cu, FeO<sub>total</sub> and Ni mass loss trends in the carbonate profile from east of the NFD (Fig. 2.3b). However, the most proximal sample to the eastern dike margin exhibits a minimal gain of FeO<sub>total</sub>, and less loss of Ni, Cu and S than the other sample in the profile. Interpretations of this anomalous sample are complicated by two factors. The first is the limited sampling density in the inner part of the eastern carbonate profile, which makes it difficult to know how representative this anomaly is. The second is the oxygen-isotope evidence for localized magmatic fluid flux in the host rocks of the NFD (Nabelek et al., 2013). Minor metasomatism of country rocks close to the eastern margin of the NFD may have resulted from passage of this magmatic fluid, which may have caused the anomalous mass gain in SiO<sub>2</sub> seen in the most proximal eastern carbonate sample (Table 2.1). Notwithstanding the anomalous behaviour of this sample, the dominant pattern in the wall rocks of the NFD is for broad and intense depletion of Ni, Cu, and S over many meters (Figs. 2.3a and 2.3b). Our data imply that the country rocks lost nearly their full complement of these elements over extended zones comparable to the width of the NFD itself.

### **2.8.3 Sulfur isotope constraints on mass transfer into dikes**

The magnitude of <sup>34</sup>S-depletion in the NFD up to 8‰ per mil relative to primary magmatic values of +3.6 to +4.0‰ and the presence of negative δ<sup>34</sup>S values in the carbonates far from the western margin of the NFD suggest that the sulfur and base metals lost from the host rocks may have been transferred into the



dike during intrusion. We suggest that transport in fluids derived from metamorphic devolatilization is the dominant mechanism for assimilation of Ni, Cu, and S by magmas passing through this dike. As discussed in the next paragraphs, alternative causes for the geochemical patterns in the NFD are unlikely.

Degassing of reduced sulfur species from a mafic melt can lead to isotopic depletion of  $^{34}\text{S}$  relative to  $^{32}\text{S}$  (de Hoog et al., 2001). Degassing calculations can rule out this process in the NFD. At typical basaltic oxygen fugacities, over 99.9% degassing would be required to cause the 8‰ sulfur isotopic decrease in the melt observed in the NFD (Ripley et al., 2003). This is highly implausible and inconsistent with the moderate sulfur concentrations in the dike.

The bulk assimilation of carbonates, as might accompany fault-generated brecciation, is unlikely to be the dominant assimilation mechanism for two main reasons. First, xenoliths would not be immediately digested by the magma and would lead to more heterogeneity than what is present in the smoothly varying east and west dike profiles. Brecciation should also lead to asymmetric contamination in the dike interior because of the dike's  $\approx 45^\circ$  dip. Xenoliths would settle (if denser than the magma) or rise (if more buoyant than magma), giving rise to asymmetrical chemical profiles through the NFD. The homogeneous chemical profiles through the NFD are inconsistent with extensive bulk carbonate assimilation.

Sulfur and trace metal transport in contact metamorphic fluids can be modeled to reproduce the depleted  $\delta^{34}\text{S}$  values in the dike interior, the

contaminated  $\delta^{34}\text{S}$  values in the dike margins, and the sulfur and trace metal depletion in the host carbonates. Contact metamorphic reactions liberate volatiles that may form the fluids used to transport sulfur and trace metals from sulfides destabilized by heating. Negative  $\delta^{34}\text{S}$  values in the western dike interior are found adjacent to sedimentary rocks with  $\delta^{34}\text{S}$  values as low as -25.0‰. We interpret these values as evidence that sulfur was transported from host rocks into the dike. The  $\delta^{34}\text{S}$  value of +4.1‰ in the center of the dike is similar to the range of uncontaminated sill values from +3.6 to +4.0‰. This suggests that host rock contamination did not extend throughout the entire dike, or that new uncontaminated magma was injected into the dike axis during the contamination event. Isotope-specific models of diffusive exchange between a dike and host rocks can reproduce the smoothly varying profile of  $\delta^{34}\text{S}$  values from the western carbonates to the dike center (equations 19K-1 to 19K-10 in Bird et al., 1960). Sensitivity analyses with these models lead to three major conclusions.

First, the low uniform sulfur concentrations in the dike interior require a greater effective diffusion distance of sulfur in the dike than in the sedimentary rocks. Second, the lack of a strong S-concentration gradient in the dike requires that the effective diffusion coefficient of sulfur in the magma was larger than those in the sedimentary host rocks. Third, the asymmetry in the  $\delta^{34}\text{S}$  profile between the dike and the wall rocks suggests that diffusion coefficients were subtly sensitive to isotopic mass in both the magmatic and the pore fluid environment. The implication is that flowing magma in the dike interior kept

sulfur concentrations in the dike low but maintained an isotopic gradient that drove the differential diffusion of sulfur isotopes.

It is more difficult to evaluate similar models in the eastern dike profile because of the more limited exposure restricting sample collection to areas more than 7m from the dike margin. The range of carbonate  $\delta^{34}\text{S}$  values from -0.2 to +3.5‰ in the eastern profile, which could be regarded as representing sedimentary homogeneity, is similar to those from other samples collected distally from the NFD in the study area. Application of the transport model to the eastern profile predicts lighter sulfur isotopes to preferentially diffuse into the dike along the margin and heavier isotopes to remain in the host carbonates. Although these predictions are only partly verified in the eastern profile through development of low  $\delta^{34}\text{S}$  values in the dike, spot sampling of the eastern margin of the NFD elsewhere in the study area indicates that  $^{34}\text{S}$ -enriched carbonate samples do exist adjacent to the east dike margin ( $\delta^{34}\text{S}$ =+3.4 to +6.0‰). Overall, the western and eastern Northern Feeder Dike sulfur isotope and elemental sulfur profiles are consistent with sulfur transport through metamorphic fluids in the host carbonates into flowing magma in the dike interior. As Ni and Cu exhibit similar patterns to S, we suggest that a conservative interpretation attribute their behavior to the same process. Trace metal and sulfur depletions around intrusions could be used as an exploration tool to indicate potential mass transfers of these elements into dikes.

## **2.9 CONCLUSIONS**

This study documents contamination in a magmatic plumbing system during magma transport and offers an explanation for how such contamination can occur. Typical sills are essentially sterile; with homogeneous  $\delta^{34}\text{S}$  values of +3.6 to +4.0‰ in their interiors and no evidence of significant exchange with wallrocks. Elemental sulfur and trace metal profiles in sill wallrocks are controlled by primary sedimentary heterogeneity. In contrast, dikes can be regions of dynamic contamination, where elevated magmatic throughflow drives extensive metamorphic devolatilization reactions. These reactions liberate sulfur and trace metals from host carbonates, which can then be transported into the magma of the dike. Isotopic self-diffusion leads to a significant  $^{34}\text{S}$  depletion in the dike (up to 8‰ in the system examined here) while constant replenishment by the flowing magma maintains relatively low elemental sulfur abundances. Despite this, sulfur and metal contents in dynamic magma conduits are partially a function of the interactions with host rocks during transport; sulfur-rich rocks cause the most measurable contamination.

## **2.10 ACKNOWLEDGMENTS**

We would like to acknowledge the field assistance provided by the student mapping crew, visiting scientists, and support staff associated with NRCan's Victoria Island GEM project. MJH was sponsored by a Gold Fields SEG Foundation Graduate Student Fellowship, an Alexander Graham Bell CGS-M Scholarship from the Natural Sciences and Engineering Research Council

(NSERC) of Canada, and a Natural Resources Canada Research Affiliate Program Bursary. BAW acknowledges support from an NSERC Discovery grant.

## **2.11 REFERENCES**

- Arndt, N.T., Czamanske, G.K., Walker, R.J., Chauvel, C., and Fedorenko, V.A., 2003, Geochemistry and origin of the intrusive hosts of the Noril'sk-Talnakh Cu-Ni-PGE sulfide deposits: *Economic Geology and the Bulletin of the Society of Economic Geologists*, v. 98, p. 495-515.
- Bédard, J.H., Naslund, H.R., Nabelek, P., Wimpenny, A., Hryciuk, M., Macdonald, W., Hayes, B., Steigerwaldt, K. et al., 2012, Fault-mediated melt ascent in a Neoproterozoic continental flood basalt province, the Franklin sills, Victoria Island, Canada: *Geological Society of America Bulletin*, v. 124, p. 723-736.
- Bird, R.B., Stewart, W.E., and Lightfoot, E.N., 1960, *Transport phenomena*: New York, John Wiley and Sons, 780 p.
- Breeding, C.M., and Ague, J.J., 2002, Slab-derived fluids and quartz-vein formation in an accretionary prism, Otago Schist, New Zealand: *Geology*, v. 30, p. 499-502.
- Canfield, D.E., Raiswell, R., Westrich, J.T., Reaves, C.M., and Berner, R.A., 1986, The use of chromium reduction in the analysis of reduced inorganic sulfur in sediments and shales: *Chemical Geology*, v. 54, p. 149-155.

- de Hoog, J.C.M., Taylor, B.E., and van Bergen, M.J., 2001, Sulfur isotope systematics of basaltic lavas from Indonesia: implications for the sulfur cycle in subduction zones: *Earth and Planetary Science Letters*, v. 189, p. 237-252.
- Denyszyn, S.W., Halls, H.C., Davis, D.W., and Evans, D.A.D., 2009, Paleomagnetism and U-Pb geochronology of Franklin dykes in High Arctic Canada and Greenland: a revised age and paleomagnetic pole constraining block rotations in the Nares Strait region: *Canadian Journal of Earth Sciences*, v. 46, p. 689-705.
- Dostal, J., Baragar, W.R.A., and Dupuy, C., 1986, Petrogenesis of the Natkusiak continental basalts, Victoria Island, Northwest Territories, Canada: *Canadian Journal of Earth Sciences*, v. 23, p.622-632.
- Dupuy, C., Michard, A., Dostal, J., Dautel, D., and Baragar, W.R.A., 1995, Isotope and trace-element geochemistry of Proterozoic Natkusiak flood basalts from the northwestern Canadian Shield: *Chemical Geology*, v. 120, p. 15-25.
- Ernst, R., and Bleeker, W., 2010, Large igneous provinces (LIPs), giant dyke swarms, and mantle plumes: significance for breakup events within Canada and adjacent regions from 2.5Ga to the Present: *Canadian Journal of Earth Sciences*, v. 47, p. 695-739.
- Fahrig, W.F., 1987, The tectonic settings of continental mafic dyke swarms: Failed arm and early passive margin, *in* Halls, H.C., and Fahrig, W.F., eds., *Mafic dyke swarms: Geological Association of Canada Special Paper* 34, p. 331-348.

- Grant, J.A., 1986, The isocon diagram- A simple solution to Gresens' equation for metasomatic alteration: *Economic Geology and the Bulletin of the Society of Economic Geologists*, v. 81, p. 1976-1982.
- Grinenko, L.N., 1985, Sources of sulfur of the nickeliferous and barren gabbro-dolerite intrusions of the northwest Siberian platform: *International Geology Review*, v. 28, p. 695-708.
- Heaman, L.M., LeCheminant, A.N., and Rainbird, R.H., 1992, Nature and timing of Franklin igneous events, Canada: Implications for a Late Proterozoic mantle plume and the break-up of Laurentia: *Earth and Planetary Science Letters*, v. 109, p. 117-131.
- Huppert, H.E., and Sparks, R.S.J., 1985, Cooling and contamination of mafic and ultramafic magmas during ascent through continental crust: *Earth and Planetary Science Letters*, v. 74, p. 371-386.
- Jefferson, C.W., Hulbert, L.J., Rainbird, R.H., Hall, G.E.M., Gregoire, D.C., and Grinenko, L.I., 1994, Mineral resource assessment of the Neoproterozoic Franklin igneous events of Arctic Canada: comparison with the Permo-Triassic Noril'sk-Talnakh Ni-Cu-PGE deposits of Russia: *Geological Survey of Canada Open File 2789*, 48 p.
- Kiss, F., and Oneschuk, D., 2010, First vertical derivative of the magnetic field, Minto Inlier aeromagnetic survey, Victoria Island, NTS 87 G/NE and parts of 87G/NW, 88 B/SE and 88B/SW: *Geological Survey of Canada Open-File Map 6705*, scale 1:100 000, sheet 2 of 2.

- Li, C., Ripley, E.M., and Naldrett, A.J., 2003, Compositional variations of olivine and sulfur isotopes in the Noril'sk and Talnakh Intrusions, Siberia: implications for ore-forming processes in dynamic magma conduits: *Economic Geology and the Bulletin of the Society of Economic Geologists*, v. 98, p. 69-86.
- Li, C., Ripley, E.M., Naldrett, A.J., Schmitt, A.K., and Moore, C.H., 2009a, Magmatic anhydrite-sulfide assemblages in the plumbing system of the Siberian Traps: *Geology*, v. 37, p. 259-262.
- Li, C., Ripley, E.M., and Naldrett, A.J., 2009b, A new genetic model for the Giant Ni-Cu-PGE sulfide deposits associated with the Siberian flood basalts: *Economic Geology and the Bulletin of the Society of Economic Geologists*, v. 104, p. 291-301.
- Lightfoot, P.C., and Keays, R.R., 2005, Siderophile and chalcophile metal variations in flood basalts from the Siberian trap, Noril'sk region: implications for the origin of the Ni-Cu-PGE sulfide ores: *Economic Geology and the Bulletin of the Society of Economic Geologists*, v. 100, p. 439-462.
- Long, D.G.F., Rainbird, R.H., Turner, E.C., and MacNaughton, R.B., 2008, Early Neoproterozoic strata (Sequence B) of mainland northern Canada and Victoria and Banks islands: a contribution to the Geological Atlas of the Northern Canadian Mainland Sedimentary Basin: Geological Survey of Canada Open File 5700, 24 p. +17 figures



- Mungall, J.E., 2007, Crustal contamination of picritic magmas during transport through dikes: the Expo Intrusive Suite, Cape Smith Fold Belt, New Quebec: *Journal of Petrology*, v. 48, p. 1021-1039.
- Mungall, J.E., and Naldrett, A.J., 2008, Ore deposits of the platinum-group elements: *Elements*, v. 4, 253-258.
- Nabelek, P.I., Bédard, J.H., Hryciuk, M. and Hayes, B., 2013, Short-duration contact metamorphism of calcareous sedimentary rocks by Neoproterozoic Franklin gabbro sills and dikes on Victoria Island, Canada: *Journal of Metamorphic Geology*, v. 31, p. 205-220.
- Naldrett, A.J., 1992, A model for the Ni-Cu-PGE deposits of the Noril'sk region and its application to other areas of flood basalts: *Economic Geology and the Bulletin of the Society of Economic Geologists*, v. 87, p. 1945-1961.
- Rainbird, R.H., Jefferson, C.W., Hildebrand, R.S., and Worth, J.K., 1994, The Shaler Supergroup and revision of Neoproterozoic stratigraphy in Amundsen Basin, Northwest Territories: *Geological Survey of Canada Current Research*, v. 1994-C, p. 61-70.
- Ripley, E.M., and Li, C., 2003, Sulfur isotopic exchange and metal enrichment in the formation of magmatic Cu-Ni-(PGE) deposits: *Economic Geology and the Bulletin of the Society of Economic Geologists*, v. 98, p. 635-641.
- Ripley, E.M., Lightfoot, P.C., Li, C., and Elswick, E.R. 2003, Sulfur isotopic studies of continental flood basalts in the Noril'sk region: implications for the association between lavas and ore-bearing intrusions: *Geochimica et Cosmochimica Acta*, v. 67, p. 2807-2817.

- Seal, R.R., II, 2006, Sulfur isotope geochemistry of sulfide minerals: Reviews in Mineralogy and Geochemistry, v. 61, p. 633-677.
- Shellnutt, J.G., Dostal, J., and Keppie, J.D., 2004, Petrogenesis of the 723 Ma Coronation sills, Amundsen basin, Arctic Canada: implications for the break-up of Rodinia: Precambrian Research, v. 129, p. 309-324.
- Thorsteinsson, R., and Tozer, E.T., 1962, Banks, Victoria, and Stefansson Islands, Arctic Archipelago: Geological Survey of Canada Memoir 330, 85 p.
- Young, G.M., 1981, The Amundsen Embayment, Northwest Territories; Relevance to the upper Proterozoic evolution of North America, *in* F.H.A. Campbell, ed., Proterozoic Basins of Canada; Geological Survey of Canada Paper 81-10, p. 203-218.

## FIGURE CAPTIONS

**Figure 2.1-** Geological map of the Minto Inlier, near Ulukhaktok, Northwest Territories, with sample locations for the sill and dike profiles shown. VI= Victoria Island; NFD= North Feeder Dike; S1=shale-hosted sill profile; C1= carbonate-hosted sill profile; modified from Bédard et al. (2012).

**Figure 2.2a-**  $\delta^{34}\text{S}$  values for the NFD west profile. The dike is represented by the light gray area between the solid lines and has a 26m corrected thickness. All samples outside of the dike are silty carbonates. All values are referenced to V-CDT-Vienna Canyon Diablo Troilite. The level of uncertainty ( $2\sigma$ ), is equal to  $\pm 0.20\text{‰}$ , and is less than the symbol size. The dark gray bar labeled sill values is

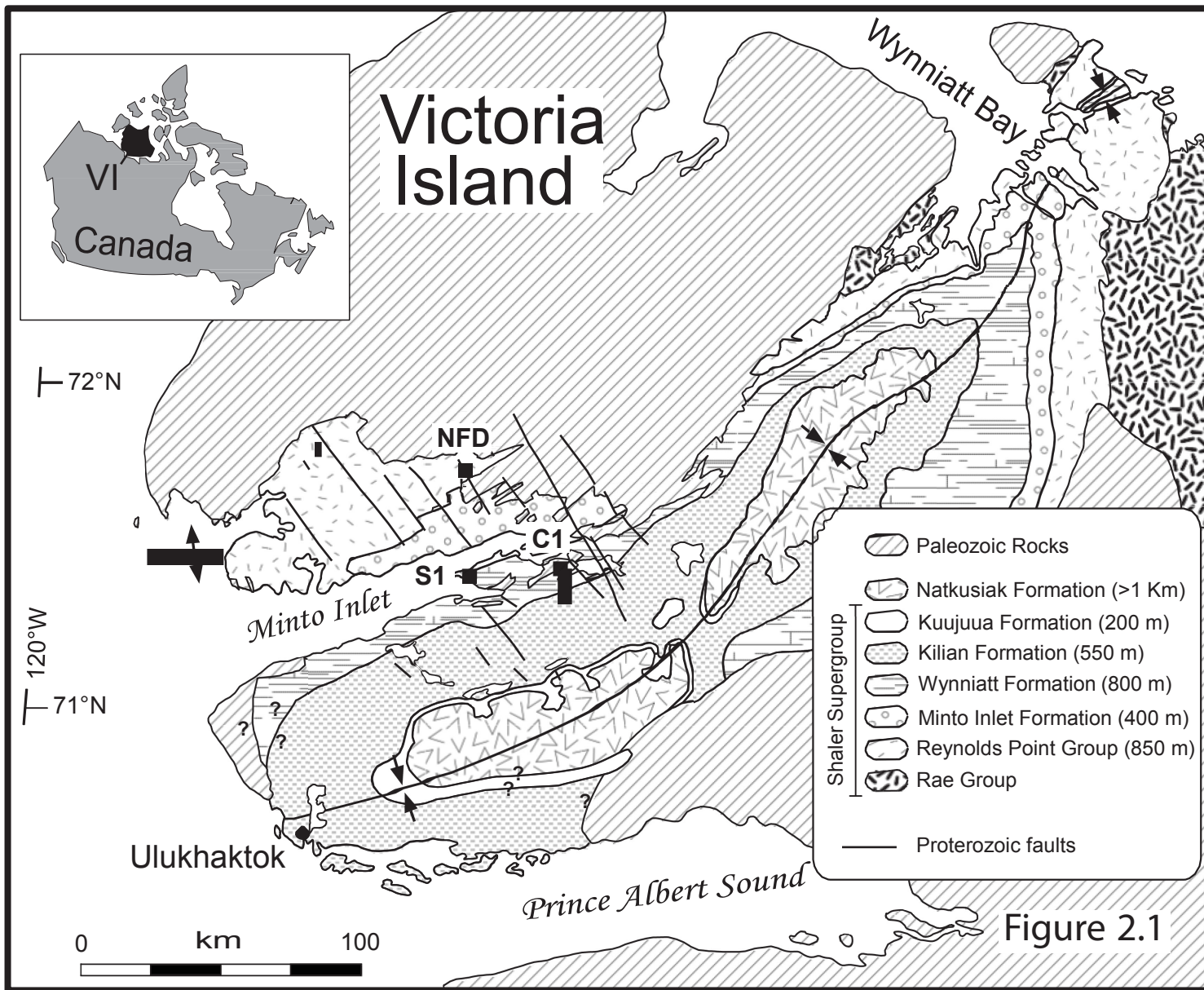
for illustrative purposes and stretches from +3 to +4‰, although sill interiors have an even more restricted range than this from +3.6 to +4.0‰.

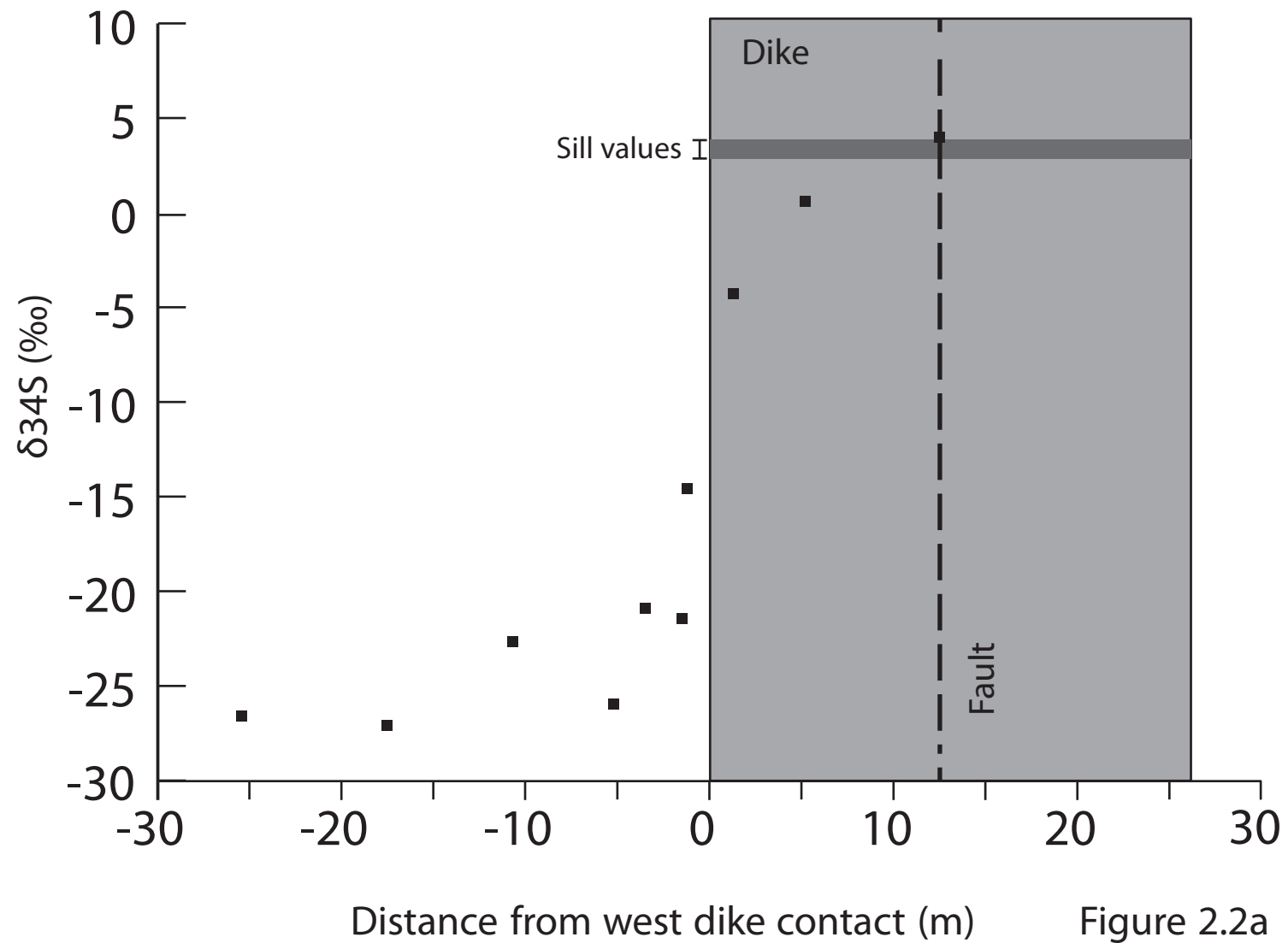
**Figure 2.2b-**  $\delta^{34}\text{S}$  values for the NFD east profile, same format as Figure 2a.

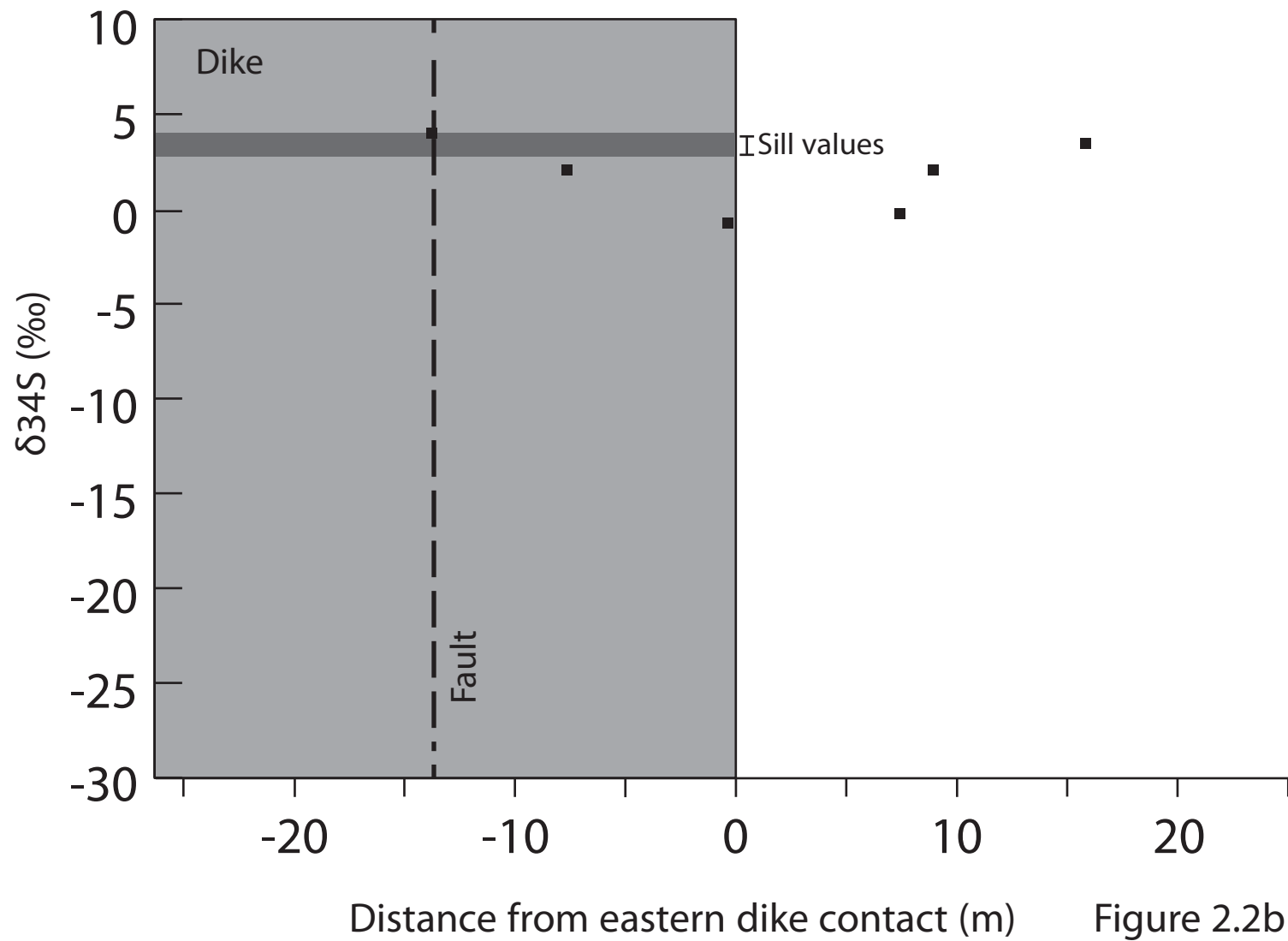
**Figure 2.2c-** Sulfur concentrations for North Feeder Dike samples (west and east profiles) in weight percent. Note that sulfur concentrations decrease towards the dike margins on the west side, and that sulfur concentrations are fairly homogeneous within the dike.

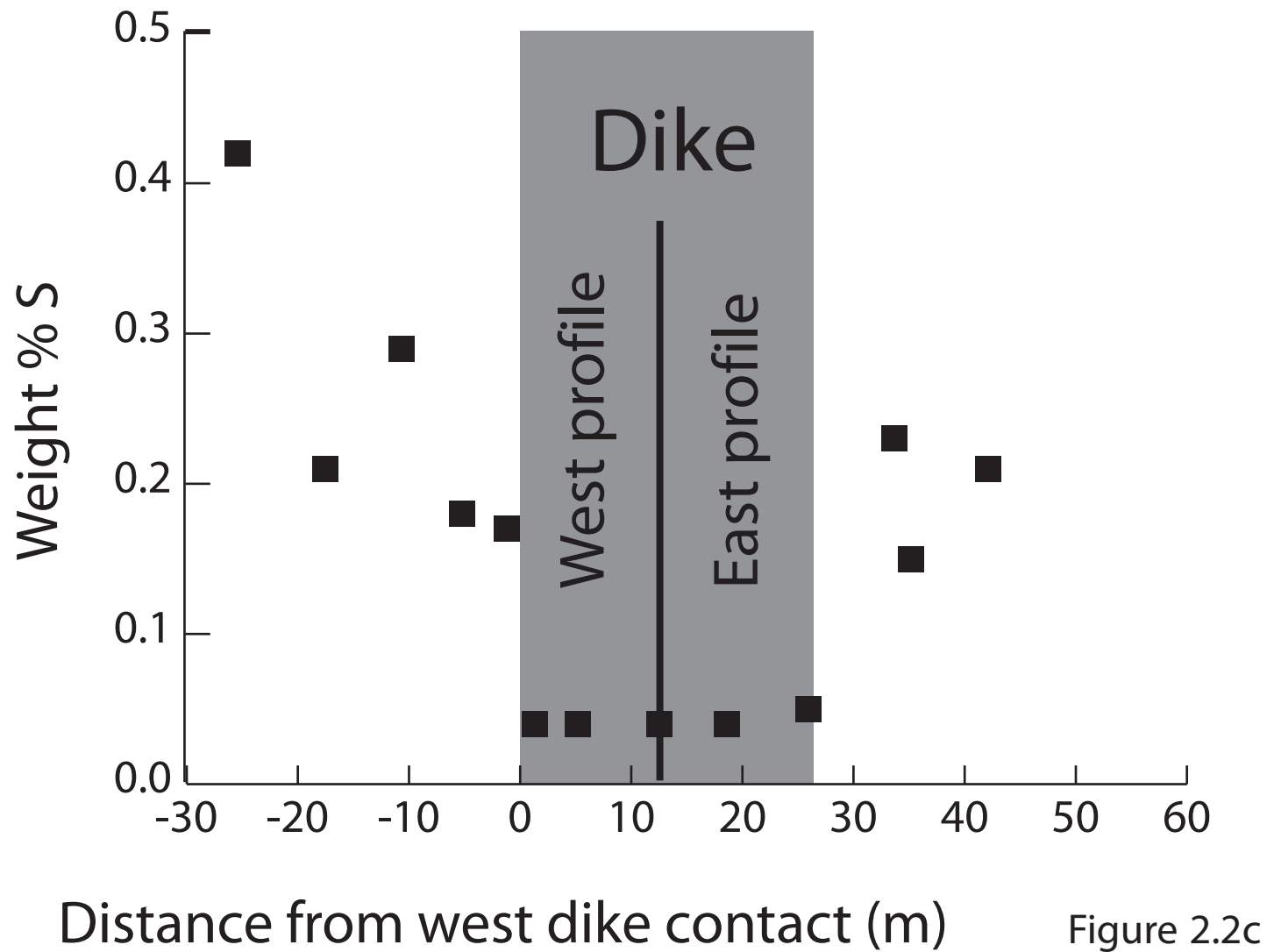
**Figure 2.3a-** Sulfur, nickel, copper and  $\text{FeO}_{\text{total}}$  mass changes relative to immobile element isocons as outlined by Grant (1986) for the North Feeder Dike west carbonate profile. HY064A1 (the leftmost data point) was selected as the most unaltered country rock in the western profile. Note the consistent mass loss and the rough correlation between Ni, Cu, S, and  $\text{FeO}_{\text{total}}$  at all samples.

**Figure 2.3b-** Sulfur, nickel, copper and  $\text{FeO}_{\text{total}}$  mass changes relative to immobile element isocons as outlined by Grant (1986) for the North Feeder Dike east carbonate profile. HY064C3 (the rightmost data point) was selected as the most unaltered country rock in the eastern profile.









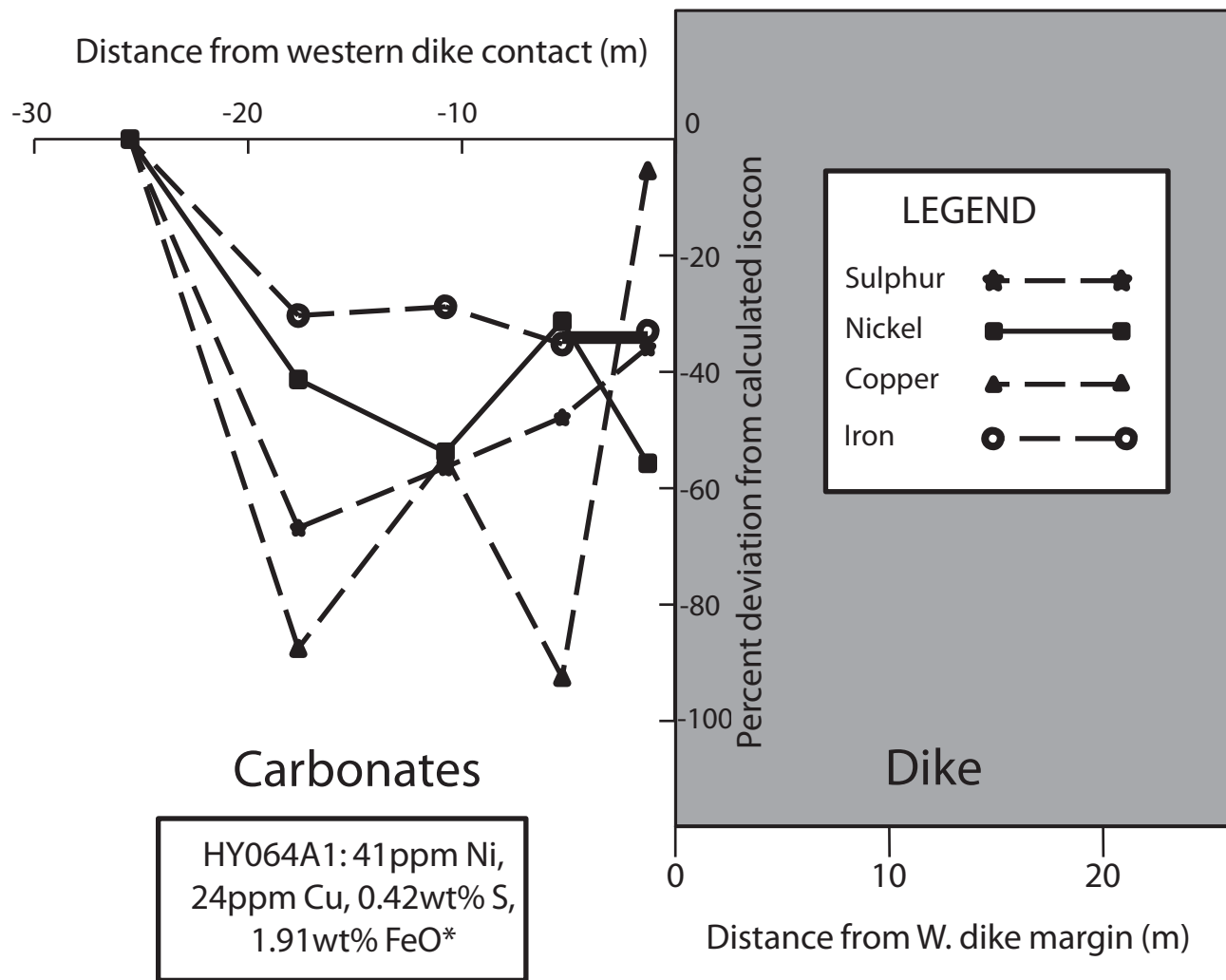


Figure 2.3a



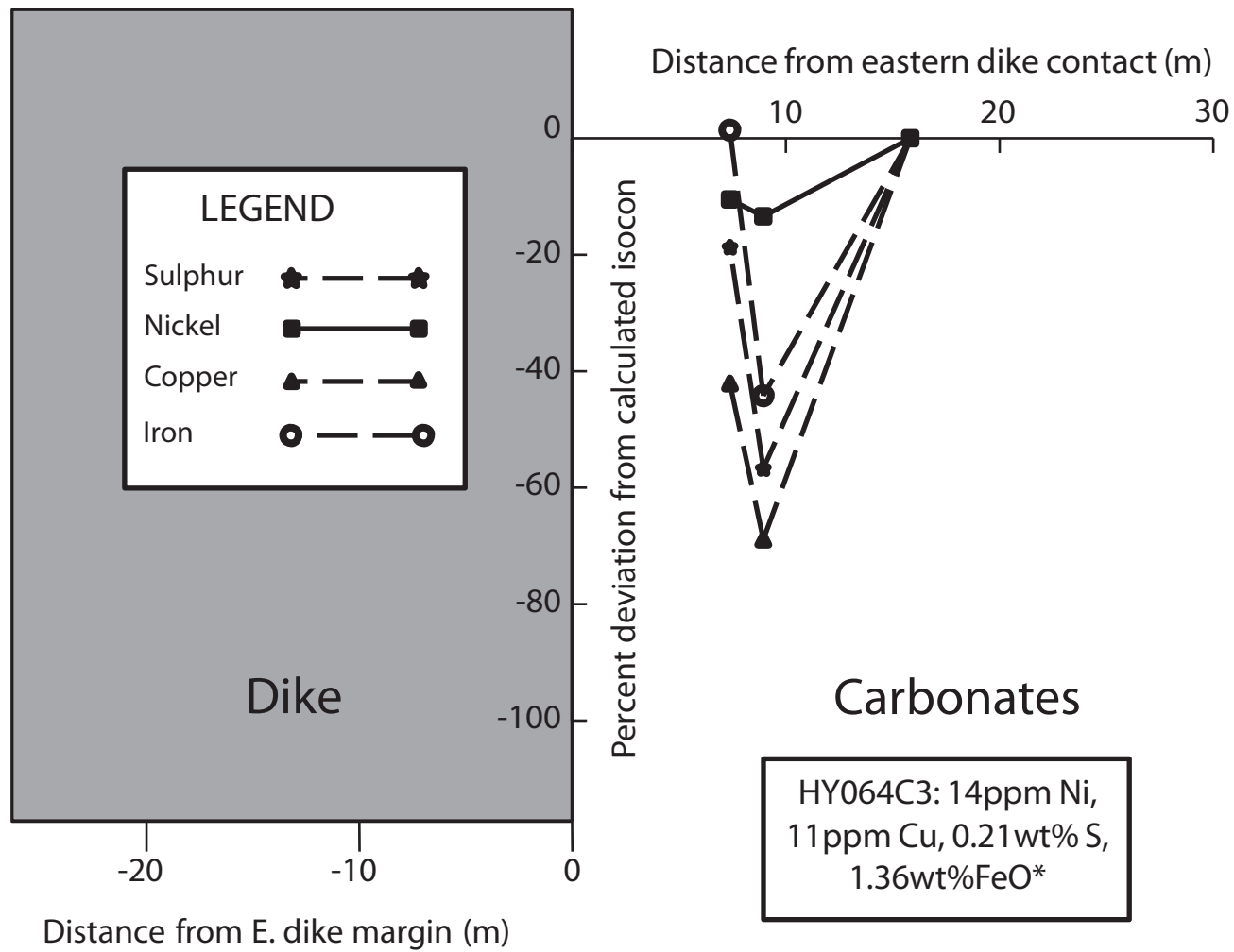


Figure 2.3b

Table 2.1: Mass changes for NFD isocon profiles

<b>Sample</b>	<b>LOI- loss on ignition (wt%)</b>	<b>Net mass change<sup>a</sup> (%)</b>	<b>SiO2 (wt %)</b>	<b>Distance from dike contact (m)</b>
<i>Western carbonates</i>				
10 RAT HY064A1 <sup>b</sup>	27.8	0.0	18.6	-25.4
10 RAT HY064A2	19.0	-34.8	31.9	-17.5
10 RAT HY064A3	18.0	-37.6	30.6	-10.7
10 RAT HY064A4	29.6	+19.0	17.5	-5.2
10 RAT HY064A5	32.7	+55.2	13.1	-1.2
<i>Eastern carbonates</i>				
10 RAT HY064C1	14.8	-27.6	43.2	7.5
10 RAT HY064C2	22.0	-40.8	30.7	9.0
10 RAT HY064C3 <sup>b</sup>	28.5	0.0	21.0	15.9

<sup>a</sup>Based on immobile element isocons (Grant, 1986)

<sup>b</sup>-least-altered host rock sample

### **Chapter 3: Connections between manuscripts**

The manuscript in Chapter 2 discusses how contamination can occur in a mafic large igneous province, the Neoproterozoic Franklin event on Victoria Island, arctic Canada. Sulfur isotopes indicate that most sills show no discernible signature of local host rock contamination. Contamination-related signatures are more commonly observed in dikes, which show more sulfur isotopic variability than sills. For example, the Northern Feeder Dike examined in Chapter 2 is emplaced in carbonates and shows a  $\delta^{34}\text{S}$  decrease of 8 per mil from its margins to its interior. Sulfur,  $\text{FeO}_{\text{total}}$  and trace metal contents in the host carbonates are depleted by 30 to 60% adjacent to the dike (relative to immobile element isocons). Sustained transport of host-rock sulfur and trace metals was proposed as a mechanism that can lead to contamination in a dynamic magma conduit.

It is inferred that dikes record higher rates and extents of magmatic throughflow relative to sills, leading to more extensive contact metamorphic reactions and inducing robust hydrothermal cells in host rocks. The greater thermal impact of fast-flowing magma can also lead to resorption of chilled margins, allowing sulfur and trace metals to assimilate into dikes. On the other hand, the elevated magmatic throughflow in dikes would dilute the local effects of contamination relative to a static intrusion, because there is a larger magma volume to contaminate, and would also spatially decouple the contamination signatures, because contaminated magma would be flushed downstream. Thus, although sulfur isotopes record evidence of contamination in the Northern Feeder Dike, sulfur concentrations were apparently kept low (around 500ppm) in the dike

interior due to replenishment by fresh magma. These concentrations are well below sulfur saturation. We suggest that sulfur-rich host rocks such as sulfate evaporites are required to trigger sulfide immiscibility in a large igneous province intrusive plumbing system.

In the manuscript in Chapter 4, we test this hypothesis by examining the effect of host-rock lithology on sulfur solubility in intrusions. Sulfur isotope profiles and sulfur concentrations were analyzed from a carbonate-hosted intrusion, a shale-hosted intrusion, and three evaporite-hosted intrusions. This was in order to clarify the effects of in-situ host rock contamination in sills, and to determine whether host rock contamination was able to generate sulfide immiscibility. Fe-Ti oxide oxybarometry was also used to evaluate the effects of host-rock contamination on sulfur solubility and the sulfur species present in a mafic magma, which are dependent on oxygen fugacity (Carroll and Rutherford, 1988).

## **Chapter 4: Evaporite assimilation and immiscible sulfides in a mafic magma conduit system: insights from the Franklin LIP, Victoria Island, Canada**

Matthew J. Hryciuk<sup>1a</sup>, Jean H. Bédard<sup>2</sup>, William G. Minarik<sup>1</sup>, and Boswell A. Wing<sup>1</sup>

<sup>1</sup>Department of Earth and Planetary Sciences, McGill University, 3450 University Street, Montreal, Quebec H3A 2A7, Canada

<sup>2</sup>Geological Survey of Canada (GSC-Quebec), 490 de la Couronne, Quebec, Quebec G1K 9A9, Canada

### **4.1 Abstract:**

Sulfate evaporite assimilation by a mafic melt can trigger sulfide immiscibility, which is a critical first step in the formation of magmatic Ni-Cu-PGE ore deposits. Constraints on evaporite assimilation in natural systems are often inferential, making the effects on oxygen fugacity ( $fO_2$ ) and sulfide immiscibility difficult to disentangle.

In the Franklin Large Igneous Province on Victoria Island, arctic Canada, exceptional preservation enables the geological and geochemical relationships between mafic sills, dikes and sulfate evaporites to be studied in detail. We used sulfur isotopes and Fe-Ti oxide oxybarometry to evaluate the extent and effects of external sulfur addition in sills and dikes.

On Victoria Island, sills hosted by carbonates and shales have homogeneous sulfur isotope compositions with  $\delta^{34}S$  values in sill interiors restricted to between +3.6 and +4.0‰. Oxygen fugacity conditions recorded by these sills are not correlated to sulfur isotope values and are in the reducing range below  $\Delta FMQ+1$  (log units relative to the fayalite-magnetite-quartz buffer) where sulfides are the dominant sulfur species in the melt.

---

<sup>a</sup> Email- [matthew.hryciuk@mail.mcgill.ca](mailto:matthew.hryciuk@mail.mcgill.ca)

In contrast, sills hosted by Minto Inlet Formation evaporites exhibit a much wider range of  $\delta^{34}\text{S}$  values and  $f\text{O}_2$ . One evaporite-hosted sill has  $\delta^{34}\text{S}$  values of less than +5‰ and recorded uniformly reducing  $f\text{O}_2$  conditions below  $\Delta\text{FMQ}-1$ , whereas another sill with intermediate  $\delta^{34}\text{S}$  values between +8.7 and +10.6‰ recorded oxygen fugacities spanning the entire range found in the other two evaporite-hosted sills. The sill with the most positive  $\delta^{34}\text{S}$  values of +11.5 to +12.9‰ in its interior also recorded the most uniformly oxidizing  $f\text{O}_2$  conditions between  $\Delta\text{FMQ}+1.1$  and  $\Delta\text{FMQ}+1.8$ , in the transitional range between sulfide and sulfate stability. Mixing calculations indicate that this sill assimilated up to 0.7 wt% anhydrite, and that over 50% of the added sulfur is presently missing from this sill. We infer that sulfide immiscibility was triggered upstream, likely in a feeder dike by evaporite assimilation. Elevated  $\delta^{34}\text{S}$  values have yet to be documented in the overlying Wynniatt Formation, so immiscible sulfides likely settled out of the melt close to where they formed. This study documents field evidence of evaporite assimilation leading to magma oxidation and sulfide saturation.

## 4.2 INTRODUCTION

Country rock sulfur addition may trigger the formation of magmatic ore deposits of nickel, copper and platinum group elements (Ni-Cu-PGE) in a large igneous province setting (Naldrett, 2005). The giant Noril'sk-Talnakh Ni-Cu-PGE deposits of Russia are considered to be a type example of ore formation that is intimately associated with evaporite assimilation (Li et al. 2009b). At Noril'sk, mineralized mafic intrusions hosted by evaporites have higher  $\delta^{34}\text{S}$  values than

uneconomic intrusions hosted by other lithologies (Grinenko, 1985). Added sulfur can potentially cause sulfide immiscibility. Interactions between segregated sulfides and large volumes of silicate melt can lead to the chalcophile enrichment required for an ore deposit (Naldrett, 1992).

Although adding anhydrite to a mafic melt increases the total sulfur content and could induce sulfide saturation, assimilation of  $\text{SO}_4^{2-}$  will also increase the oxygen fugacity (Li et al., 2009b). This suggests the possibility that oxidation of the melt during sulfate assimilation could inhibit the formation of immiscible sulfides.

Previous studies evaluating the effects of evaporite assimilation on oxygen fugacity and sulfide immiscibility in natural systems have focussed on ore-bearing intrusions and lavas, with less documentation of intrusive-host rock interactions and magmatic parameters in typical intrusions (Ripley et al., 2003; Li et al., 2009b). The Franklin Large Igneous Province on Victoria Island, Canada is an ideal field location for evaluating the effects of evaporite contamination on mafic magmas. Sills can be continuous for tens of kilometers, simplifying correlations throughout the conduit system, and dike emplacement has a clear structural control, being guided by NNW-trending faults (Bédard et al., 2012). Sections sampled across contacts, including both host rocks and intrusive facies, and ranging from proximal to distal with respect to intrusive contacts, can be used to evaluate whether contamination occurred in place or upstream. Evaporites in the Minto Inlet Formation have a restricted range of  $\delta^{34}\text{S}$  values (Prince et al., 2012) with a large isotopic contrast relative to the typical magmatic range, allowing the effects of evaporite assimilation to be detected and modeled. We use sulfur

isotopes, sulfur contents, and Fe-Ti oxide geothermometry and oxybarometry to study sills hosted by evaporites, carbonates and shales. We use this data to constrain the extent, location, timing and mechanisms of evaporite assimilation and the consequent effects on  $fO_2$  and sulfide immiscibility.

#### **4.3 BACKGROUND GEOLOGY**

The Franklin Large Igneous Province (LIP) is widely distributed in arctic and northern Canada, with an estimated volume of  $165\,000\text{km}^3$  (Robertson and Baragar, 1972). Franklin dikes extend over 2500km from Great Bear Lake (Fahrig, 1987) to western Greenland (Denyszyn et al., 2009) and Baffin Island (Pehrsson and Buchan, 1999). Uranium-Pb ages from baddeleyite and zircon constrain the emplacement of the Franklin LIP to 723Ma (Heaman et al., 1992; Pehrsson and Buchan, 1999).

In the sill-dominated Minto Inlier of Victoria Island (Figure 4.1), Franklin intrusions are emplaced into sedimentary rocks of the Neoproterozoic Shaler Supergroup, which is overlain by the consanguineous Franklin Natkusiak flood basalts (Baragar et al., 1976; Dostal et al., 1986; Dupuy et al., 1995). The Shaler Supergroup belongs to the second of three major unconformity-bounded sedimentary successions of Mesoproterozoic to Neoproterozoic age along the northwest margins of Laurentia, termed Sequence B (Rainbird et al., 1996; Long et al., 2008). These rocks were deposited in the Amundsen Basin, interpreted by Young (1981) to be the embayment of a shallow intracratonic sea.

Sedimentary rocks of the Shaler Supergroup on Victoria Island consist dominantly of carbonates (Boot Inlet, Jago Bay, and Wynniatt Fms.), but there are



also mudstones and shales (Wynniatt Fm.), sandstones (Fort Collinson and Kuujjua Fms.), and sulfate evaporites (Minto Inlet and Kilian Fms.) (Rainbird et al., 1994; Long et al., 2008). The Minto Inlet Formation contains gypsum and anhydrite layers up to 13m thick interbedded with limestone (Young, 1981). Evaporites have a variety of textures including laminations, chickenwire, nodular anhydrite, and satinspar veins. This paper reports data from sills emplaced into the Minto Inlet and Wynniatt Formations.

Franklin sills are distributed throughout the Shaler Supergroup, tend to be between a few m and 100m in thickness, and can be continuous for tens of kilometers (Heaman et al., 1992; Hulbert, 1998; Bédard et al., 2012). Sills are mainly composed of diabase or gabbro, but some are more differentiated with olivine cumulates in their lower parts and granophyric and taxitic patches in their upper parts. Dikes are associated with NNW-trending magnetic lineaments (Kiss and Oneschuk, 2010), interpreted by Bédard et al. (2012) to be syn-magmatic normal faults that guided Franklin magmas.

#### **4.4 SAMPLING**

A total of 5 sills at 4 locations were sampled for this study along with their host rocks to test the effect of lithology on magma contamination: 1 carbonate-hosted, 1 shale-hosted and 3 evaporite-hosted (Figure 4.1). All 5 sills sampled were diabasic with the exception of the shale-hosted sill S1, which has a picritic layer near its base.

Two detailed transects separated by 2.4km (Section 1 and Section 2) were collected from sills emplaced in the Minto Inlet Formation (Figure 4.2). At both

sections nodular and bedded gypsum and anhydrite are interbedded with light green to gray limestone. Section 1 includes a 17m thick lower sill (E1) and a 4m thick upper sill (E2) separated by 23m of evaporite and carbonate interbeds with 4m of host rocks below sill E1 and 4m of host rocks above sill E2. Sills E1 and E2 merge farther along-strike. Section 1 includes host rock samples from above and below both sills. No fault is apparent near section 1.

The sill exposed at Section 2 (E3) is truncated by a fault on the western side of the sampling outcrop, which is probably a splay of a larger valley-forming fault located 200m to the west. Section 2 includes 5m of sill and 4m of underlying evaporites and carbonates with no upper sedimentary rocks preserved at this location.

A complete profile was collected from a 16m thick sill (S1) emplaced in black shales of the Wynniatt Formation. Black shale and subordinate quartzarenite samples were collected up to 7m below and 15m above the sill. A partial profile was collected across the base of an approximately 20m thick sill (C1) emplaced in upper carbonates of the Wynniatt Formation. Diabase and dark nodular calcareous shale samples were collected from within 5m of the lower sill contact.

## **4.5 METHODS**

Sulfur isotopes and sulfur concentrations were analysed from whole-rock powders. Sulfur concentrations were analysed at the Institute National de la Recherche Scientifique-Eau Terre Environnement (INRS-ETE) in Québec, Québec by inductively coupled plasma atomic emission spectrometry (ICP-AES).

All samples were analysed for sulfur isotopes at McGill University. Sulfur from sulfate evaporites was extracted using a boiling “Thode” reduction solution consisting of concentrated HCl, HI and H<sub>3</sub>PO<sub>2</sub> (Forrest and Newman, 1977). Sulfur from other samples was extracted using a reduced Cr solution (Canfield, 1986). Sample powders and the extraction solutions were heated to approximately 85°C, producing H<sub>2</sub>S that was carried by nitrogen gas through an ultrapure water trap and into a 10% (w/w) zinc acetate trap. The ZnS produced was converted to an Ag<sub>2</sub>S precipitate by adding a few drops of a 0.2M AgNO<sub>3</sub> solution. The Ag<sub>2</sub>S was rinsed with ultrapure water and a solution of ammonium hydroxide and dried overnight at ≈75°C.

Approximately 3mg of Ag<sub>2</sub>S was weighed into ethanol-cleansed aluminum foil packets and fluorinated overnight in nickel bombs at 250°C with excess F<sub>2</sub> to produce SF<sub>6</sub>. Resulting SF<sub>6</sub> was purified cryogenically and chromatographically. Sulfur isotope compositions were measured on a Thermo Finnigan MAT253 mass spectrometer by monitoring SF<sub>5</sub><sup>+</sup> ion beams at a mass/charge ratio of 127 and 129. Analytical reproducibility ( $\sigma$ ) for the full measurement procedure is estimated to be better than 0.20‰ for  $\delta^{34}\text{S}$  values. All data is reported on the Vienna Canyon Diablo Troilite (V-CDT) scale, defined by a  $\delta^{34}\text{S}$  value of -0.3‰ for the international standard IAEA-S-1.

Compositions of ilmenite and magnetite were analysed using a JEOL JXA-8900L electron microprobe at McGill University. An accelerating voltage of 15kv, a beam current of 20nA and a beam diameter of 5 $\mu\text{m}$  was used. Corrections were done with the ZAF data reduction method. Oxides were analysed for SiO<sub>2</sub>, TiO<sub>2</sub>, Al<sub>2</sub>O<sub>3</sub>, FeO<sup>total</sup>, Cr<sub>2</sub>O<sub>3</sub>, MnO, MgO, ZnO and NiO.

## **4.6 RESULTS**

### **4.6.1 Carbonate-hosted and shale-hosted sills**

In the carbonate-hosted (C1) and shale-hosted (S1) sill profiles, the majority of the diabase samples have  $\delta^{34}\text{S}$  values between +3.3 and +4.0‰ (Table 4.1). The only exceptions are lower chilled margin samples, where  $\delta^{34}\text{S}$  values from samples taken within 0.20m of sill-host rock contacts are offset towards the  $\delta^{34}\text{S}$  value of the underlying host rocks. Sulfur contents in sill S1 range from 0.08 to 0.10 wt%, roughly twice the S contents of sill C1 (0.04 to 0.05 wt%, Table 4.1).

### **4.6.2 Evaporite-hosted sills**

Sulfate evaporite and carbonate interbed samples from Sections 1 and 2 are similar isotopically. All sulfate evaporite host rock sampled analysed have a very restricted range of strongly positive  $\delta^{34}\text{S}$  values between +15.6 and +16.2‰ (Table 4.2). Carbonate interbeds have a much larger range of lower  $\delta^{34}\text{S}$  values between -16.3 and +3.6‰, with samples closer to sills generally having higher values than distal samples. The evaporites have very high S contents of 17.0 to 18.0 wt% and the carbonate interbeds have much lower S contents of 0.38 to 0.42 wt%.

The  $\delta^{34}\text{S}$  values from sill E1 are similar to those in sills C1 and S1 between +3.6 and +4.9‰ (Figure 4.3), whereas sill E2 has markedly higher  $\delta^{34}\text{S}$  values between +8.7 and +10.6‰ (Table 4.2). Chilled margin samples in sills E1 and E2 have  $\delta^{34}\text{S}$  values that are lower than those from sill interiors.

Compared to sills E1 and E2, sill E3 has a larger range of  $\delta^{34}\text{S}$  values (Table 4.2). Sill interior samples have highly enriched  $\delta^{34}\text{S}$  values between +11.5

and +12.9‰ and the chilled margin has a  $\delta^{34}\text{S}$  value of +1.9‰ (Figure 4.4). The sill lower chilled margin is sulfur-poor (0.047 wt%) whereas the middle to upper part of this sill is sulfur-rich (0.089 to 0.121 wt%).

#### **4.7 FE-TI OXIDE TEMPERATURE AND OXYGEN FUGACITY CONSTRAINTS**

We estimated temperature and  $f\text{O}_2$  from the mineral compositions of ilmenite and titanomagnetite using the techniques of Ghiorso and Evans (2008; Table 4.3). Where possible, we used the compositions of coexisting ilmenite-titanomagnetite mineral pairs lacking exsolution lamellae. In the lower chilled margins of sills S1 and E3, coexisting ilmenite and titanomagnetite grains were not present so we estimated a viable range of T and  $f\text{O}_2$  values by inputting the compositions of magnetite and ilmenite crystals with the maximum and minimum  $\text{TiO}_2$  contents in the thin section of interest. When both these methods were applied, there was good agreement within  $\pm 0.2$  log units relative to  $\Delta\text{FMQ}$  (the fayalite-magnetite-quartz buffer) (Table 4.3).

Most magnetite-ilmenite temperatures are in the subsolidus range for diabase, from a minimum of 560°C to a maximum of 940°C. However, low and high temperature mineral-pairs of the same samples generally yielded very similar  $f\text{O}_2$ , suggesting that our estimated  $f\text{O}_2$  conditions were not modified significantly post-crystallization relative to the FMQ buffer (Appendix E). Minor exceptions include the oxygen fugacities presented for sills C1 and S1. Higher temperatures and more oxidizing  $f\text{O}_2$  conditions in sill C1 were recorded by euhedral ilmenite overgrowths on magnetite relative to blobby overgrowths. Higher temperatures

and more reducing  $fO_2$  conditions in sill S1 were recorded by discrete magnetite and ilmenite grain pairs than grains with both coexisting magnetite and ilmenite (Appendix F).

Most magnetite-ilmenite mineral pairs do not pass the Bacon and Hirschmann (1988) Mg/Mn partitioning equilibrium test. With the exception of magnetite-ilmenite pairs from sill C1, other magnetite-ilmenite pairs have positive deviations from the equilibrium line that can possibly be explained by increased partitioning of Mn into ilmenite in slowly cooled rocks. According to Bacon and Hirschmann (1988) this does not invalidate these oxide pairs for geothermometry. Although there may be a higher degree of uncertainty associated with magnetite-ilmenite  $fO_2$  determinations in sills than for volcanic rocks because of their slow-cooling nature, yielded oxygen fugacities are interpreted to reflect magmatic conditions.

Calculated  $fO_2$  conditions for sill C1 are  $\Delta FMQ-2.5$  to  $\Delta FMQ-1.2$ , whereas sill S1 records more oxidizing  $fO_2$  conditions of  $\Delta FMQ+0.0$  to  $\Delta FMQ+1.0$ . There are no pronounced  $fO_2$  shifts from the sill margins to the sill interiors in these sills.

In sill E3, the lower chilled margin records oxygen fugacities of  $\Delta FMQ-1.4$  to  $\Delta FMQ-0.9$ , whereas a sample from the interior of this sill shows uniformly oxidizing  $fO_2$  conditions from  $\Delta FMQ+1.1$  to  $\Delta FMQ+1.8$ . The core of sill E1 has uniformly reducing  $fO_2$  conditions from  $\Delta FMQ-1.9$  to  $\Delta FMQ-0.9$ ; whereas the core of the sill E2 has a large range of  $fO_2$  conditions from  $\Delta FMQ-1.9$  to  $\Delta FMQ+1.9$ . Overall, the range of oxygen fugacities recorded in the evaporite-hosted sills represent more oxidizing conditions (greater than  $\Delta FMQ+1$ ) as well as a greater

range of variability than the  $fO_2$  values estimated from the carbonate- and shale-hosted sills.

## 4.8 DISCUSSION

### 4.8.1 S-isotopic evolution in the Franklin magmatic plumbing system

#### *4.8.1.1 Source of sulfur isotope values and sulfur concentrations in sills C1 and S1*

Shale-hosted sill S1 and carbonate-hosted sill C1 are isotopically similar, with  $\delta^{34}S$  values in their interiors between +3.6 and +4.0‰, yet sill C1 has sulfur contents roughly half those in sill S1. Three possibilities can account for this observation: the sulfur contents represent primary magmatic concentrations, sill C1 lost immiscible sulfides, or low sulfur contents are the result of degassing. In order for sill C1 to have been contaminated enough to segregate immiscible sulfides while maintaining  $\delta^{34}S$  values similar to sill S1, a contaminant with  $\delta^{34}S$  values between +3 and +4‰ would be needed. Given the heterogeneous range of  $\delta^{34}S$  values in carbonates and shales, a contamination scenario with  $^{34}S$  isotopic homogenization and immiscible sulfide segregation is implausible.

That the low sulfur contents in sill C1 were caused by degassing is an equally implausible possibility. If sill C1 degassed at least 50% of its sulfur at reducing oxygen fugacities typical for basaltic systems ( $\Delta FMQ+1$  or less), this could have led to  $\delta^{34}S$  decreases of 0.6 per mil (de Hoog et al., 2001; Ripley et al., 2003). However, there is no discernible sulfur isotope difference between sills S1 and C1, making extensive degassing unlikely. Thus, as the most parsimonious

explanation, we interpret that the majority of magmatic sulfur concentrations are primary.

Although we infer that sulfur concentrations are commonly primary magmatic features in many Franklin intrusions, the origin of the  $\delta^{34}\text{S}$  values between +3 and +4‰ that characterize most of the Franklin intrusions we have analyzed is problematic, because mantle-derived igneous rocks generally have  $\delta^{34}\text{S}$  values near or slightly greater than 0‰ (Seal, 2006). Sills in the northeast Minto Inlier emplaced into the lower formations of the Shaler Supergroup (Escape Rapids Fm. to Grassy Bay Fm.) have near-zero  $\delta^{34}\text{S}$  values (Jefferson et al., 1994), suggesting that the elevated  $\delta^{34}\text{S}$  values in sills C1 and S1 are probably not primary mantle values. Conversely, sills in the Brock Inlier, located approximately 300km to the southwest, have mean  $\delta^{34}\text{S}$  values similar to those found in sills C1 and S1 despite being generally lower in the stratigraphy (Escape Rapids Fm. to Minto Inlet Fm., Jefferson et al, 1994). This suggests that an upper crustal source of the enriched (+3.6 to +4.0‰)  $\delta^{34}\text{S}$  values is not required. A more plausible hypothesis is that the enriched (+3.6 to +4.0‰)  $\delta^{34}\text{S}$  values were acquired in the lower to middle crust during transport from the magma source. Thus, the restricted range of  $\delta^{34}\text{S}$  values in sills C1 and S1 can be considered a magmatic feature, albeit one affected by prior crustal contamination.

#### *4.8.1.2 Sulfur isotope shifts in sill chilled margins*

In the sill profiles S1 and C1, only lower chilled margin samples (within 20cm of contacts) have  $\delta^{34}\text{S}$  values outside of the +3.6 to +4.0‰ values found in sill interiors. Sulfur contents in chilled margins are uncorrelated with  $\delta^{34}\text{S}$  values (Table 4.1). Isotopic exchange of sulfur between sills and host rocks can account



for this feature (Ripley and Li, 2003), and we believe that the  $\delta^{34}\text{S}$  values of many chilled margins were perturbed by diffusional exchanges during cooling (Bickle and McKenzie, 1987). We do not consider chilled margin data henceforth; except to point out that subsolidus diffusion through chilled margins is unlikely to have had any significant effects on the sulfur mass balance or  $\delta^{34}\text{S}$  signatures of the sill interiors.

#### *4.8.1.3 Contamination in the Evaporite-Hosted sills*

Samples from the interiors of the evaporite-hosted sills generally have more positive  $\delta^{34}\text{S}$  values (+4.6 to +12.9‰, Table 4.2) than samples from the carbonate- or shale-hosted sills (+3.6 to +4.0‰, Table 4.1). This suggests that  $^{34}\text{S}$ -enriched S was added to mafic magmas from evaporites. The large sulfur isotope contrast ( $\approx 12\text{‰}$ ) between the Minto Inlet evaporites and the original mafic magma allows contamination by sulfate evaporites to be detected at extremely low levels.

This point can be illustrated with a simple mixing model (Ripley and Li, 2003). Unlike the C1 and S1 chilled margins, the  $\delta^{34}\text{S}$  value of the E1 chilled margin of +3.6‰ falls in the inferred magmatic range of +3.6 to +4.0‰. We assume that subsolidus diffusional exchanges between evaporites and sills are less effective than those between carbonates or shales and sills described in the previous section. Therefore, the sulfur concentrations and  $\delta^{34}\text{S}$  values in evaporite-hosted sill chilled margins could represent uncontaminated magmatic values. In Section 1 no sulfur contents were available, so it was assumed that the lower chill of sill E1 had a sulfur content of 500ppm, roughly equal with what is observed in other sulfur-poor sills in the field area. Lower chilled margins were

used to infer parental magma compositions of sills E1 and E2 ( $\delta^{34}\text{S}=+3.6\text{‰}$ , 500ppm S) and sill E3 ( $\delta^{34}\text{S}=+1.9\text{‰}$ , 470ppm S).

The increase in  $\delta^{34}\text{S}$  values from sill E1 to E2 to E3 can be modeled by increasing degrees of evaporite assimilation. The  $\delta^{34}\text{S}$  values (+4.6 to +4.9‰, Table 4.2) from sill E1 can be accounted for by the assimilation of only 0.02 to 0.03 wt% of the average host sulfate evaporite (17% S,  $\delta^{34}\text{S}=+16\text{‰}$ , Figure 4.3). About 0.15 wt% anhydrite assimilation is required to contaminate the chilled margin of sill E2 ( $\delta^{34}\text{S}=+8.7\text{‰}$ , Table 4.2), with high  $\delta^{34}\text{S}$  values between +10.5 to +10.6‰ of gabbros inside the sill requiring an additional 0.12 to 0.13 wt% of anhydrite assimilation. Data from sill E3 implies it assimilated significantly more evaporites, with 0.42 to 0.71 wt% anhydrite assimilation required to explain the elevated  $\delta^{34}\text{S}$  values from +11.5 to +12.9‰ in this sill's interior (Figure 4.4, Table 4.4).

#### **4.8.2 Location and mechanisms of S incorporation**

Possible mechanisms for evaporite assimilation include partial melting and mixing, diffusive transfer, and the hydrothermal leaching of sulfate from host rocks and subsequent redeposition within the intrusion (Ripley et al., 2003). Heat from sills should have initiated evaporite dissolution and hydrothermal fluid circulation. However, uncontaminated lower chilled margins of evaporite-hosted sills suggest that chilled margin formation created an impermeable barrier between host rocks and sill interiors. This leaves stoping along upper sill contacts during sill inflation, leading to bulk rock assimilation, as the most viable contamination mechanism in sills. Magmatic overpressure and elevated heat flow along the upper contact could facilitate brecciation. An important control on the

amount of contamination is the surface area of the upper sill contact. As a result, sill E1, which is 4 times thicker than sill E2, only assimilated a maximum of  $\frac{1}{4}$  the amount of evaporites as sill E2 *in situ* based on isotopic constraints. The additional 0.15 wt% anhydrite assimilation in the base of sill E2 must be explained by contamination upstream, potentially at the site of bifurcation from sill E1.

Sill E3 is thicker than sill E2, so the extent of inferred anhydrite assimilation between 0.42 and 0.71 wt % is significantly more than the 0.13 wt% maximum anhydrite assimilation that can be explained by roof stoping *in situ* (assuming all of the in-place contamination at sill E2 was by this process). The higher calculated amounts of anhydrite assimilation for sill E3 may be linked to its location proximal to a NNW-trending fault, because it is inferred that many of these faults acted as magmatic conduits where contamination occurred more easily (Hryciuk et al., Chapter 2).

Mungall (2007) proposed that vertical dike chilled margins are mechanically less stable than horizontal sill chilled margins. This is particularly relevant to assimilation in the Franklin magmas, because field evidence (Bédard et al., 2012) indicates that the mafic dikes on Victoria Island were typically emplaced along faults, which brecciate host rocks, and were active during emplacement. Furthermore, chilled margins and wallrocks are more likely to resorb if magma flow is rapid and turbulent rather than slow and laminar (Huppert and Sparks, 1985), conditions that may be more common in dike-like feeder conduits, as opposed to more quiescent, slower flowing magmas in the Franklin sills. On Victoria Island, there are wider contact metamorphic aureoles around

dikes relative to sills, possibly recording a history of greater magmatic throughflow. More intense metamorphism around dikes could have led to devolatilization reactions liberating fluids and the destabilization of sulfur-bearing phases, with sulfur transported from host rocks contaminating the dike  $\delta^{34}\text{S}$  signatures (Hryciuk et al., Chapter 2). Chilled margin breaches induced by thermal metamorphic devolatilization reactions could have facilitated wallrock assimilation and S-rich fluid transfer into the dike. These factors suggest that dikes are where the most extensive potential for contamination exists.

#### **4.8.3 Evaporite assimilation, oxygen fugacity and sulfide immiscibility**

At  $f\text{O}_2$  conditions of  $\Delta\text{FMQ}+2.0$  or greater, sulfates are the dominant sulfur species in the melt and have a solubility of  $1.5\pm0.2$  wt% (Jugo et al., 2005). This is 10 times greater than the solubility of sulfides, which are dominant in the melt at  $f\text{O}_2$  conditions of  $\Delta\text{FMQ}+1.5$  or less, with a solubility of  $0.14\pm0.02$  wt% (Jugo et al., 2005). Sills C1, S1 and E1 recorded  $f\text{O}_2$  conditions less than  $\sim\Delta\text{FMQ}+1$  (Table 4.3). At such conditions, greater than 90% of the sulfur in the magma is dissolved as sulfide (Carroll and Rutherford, 1988; Wallace and Carmichael, 1994). Sulfur contents in these sills are below 0.10 wt%, and commonly less than 0.06 wt%, well below the sulfide solubility threshold (Jugo et al., 2005).

In contrast, oxygen fugacities of sill E2 span the range from reducing conditions of  $\Delta\text{FMQ}-1.9$  to transitional conditions of  $\Delta\text{FMQ}+1.9$ , consistent with the effects of evaporite assimilation and corresponding to elevated  $\delta^{34}\text{S}$  values relative to typical magmatic values (Figure 4.5). Sulfur contents in sill E2 (0.085 to 0.115wt%) based on the evaporite assimilation model previously described in

this manuscript start to approach but do not reach those needed for sulfur saturation and sulfide segregation ( $0.14 \pm 0.02$  wt%, Jugo et al., 2005).

Despite the extensive amounts of inferred evaporite assimilation recorded by elevated  $\delta^{34}\text{S}$  values in the core of sill E3,  $f\text{O}_2$  conditions have not reached those necessary ( $\Delta\text{FMQ}+2$  or higher) to resorb magmatic sulfides to sulfate (Figure 4.5). In Sill E3, all magnetite-ilmenite pairs recorded oxygen fugacities between  $\Delta\text{FMQ}+1$  and  $\Delta\text{FMQ}+2$ , in the transitional range where both sulfides and sulfates are stable in the melt (Figure 4.6). At such conditions S-immiscibility could occur at S-concentrations as low as 1400ppm (Jugo et al., 2005; Figure 4.6). The sulfur contents predicted by the evaporite assimilation models outlined above (0.145 to 0.214 wt%) exceed sulfur solubility by up to  $\sim 750$ ppm. However, measured sulfur contents do not match those predicted, varying between 0.089 and 0.121 wt%. Thus, the upper part of sill E3 only contains between 42 and 45% of the expected external sulfur, such that about half of the assimilated sulfur predicted to be in the magma based on modeling is missing from the system (Figure 4.7). We infer that evaporite assimilation led to the high  $\delta^{34}\text{S}$  values up to +12.9‰ in sill E3 and elevated sulfur contents past the point of saturation in the melt, and that the cause of the inferred missing sulfur was the segregation of immiscible sulfides from the melt upstream.

The inference that the majority of contamination occurred in dikes upstream from sill E3 makes it difficult to accurately predict what happened to sulfur in the immiscible sulfides after segregation. Immiscible sulfide transport, resorption or degassing at oxidizing conditions (above  $\Delta\text{FMQ}+1$ , Mandeville et al., 2009) would lead to intrusions with elevated  $\delta^{34}\text{S}$  values downstream from the

site of contamination. However, the restricted sulfur isotope values found in sills S1 and C1 ( $\delta^{34}\text{S}=+3.6$  to  $+4.0\%$ ) in the overlying Wynniatt Formation show no evidence of this signature, implying that the magmas emplaced higher in the stratigraphy did not interact with Minto Inlet sulfates during transport. Therefore the calculated missing sulfur likely remained settled out as the magma as sulfide droplets upstream from sill E3 near the site of contamination.

#### **4.8.4 Implications for Ni-Cu mineralization and LIPs**

The cause of sulfide immiscibility of the Noril'sk-Talnakh Ni-Cu-PGE sulfide ore deposits is still debated, despite the elevated  $\delta^{34}\text{S}$  values of these magmas, their high S contents, and the association with sulfate evaporite bearing strata. Sulfur isotope homogeneity and the emplacement of some economic intrusions in sulfate-free lithologies led Grinenko (1985) to conclude that evaporite assimilation *in situ* was not the cause of sulfide immiscibility and ore deposition. More recent studies used the presence of magmatic anhydrite and coexisting sulfides to argue that the assimilation of evaporites was an important ore forming process, but was not the cause of initial sulfide immiscibility (Li et al., 2009a; Li et al., 2009b; Ripley et al., 2010). We suggest that elevated homogeneous sulfur isotope values in the Noril'sk sulfide ores could have been derived from the assimilation of sulfur-rich fluids and xenoliths from sulfate evaporites in feeder dikes to the ore-bearing intrusions.

In the Franklin intrusions, the constraints provided by the S-contents, S-isotopes and  $f\text{O}_2$  determinations suggest that sulfide immiscibility would have been triggered by the assimilation of between 0.4 and 0.7 wt% anhydrite. This estimate is in excellent agreement with those of Li et al. (2009b), who argued that

sulfide immiscibility in the Kharaelakh intrusion and  $fO_2$  increases from  $\Delta FMQ-2.0$  to  $\Delta FMQ+1.5$  were caused by the assimilation of 0.9 wt% anhydrite or less. Low levels of anhydrite assimilation triggered sulfide immiscibility in the Franklin LIP.

## 4.9 CONCLUSIONS

Franklin sills hosted by carbonates and shales in the Wynniatt Formation of the Shaler Supergroup have homogeneous  $\delta^{34}S$  values between +3.6 and +4.0‰ in their interiors. These sills (S1 and C1) preserve no evidence of sulfide immiscibility. Chilled margins likely seal off sills from interactions with their host rocks. Magnetite-ilmenite pairs indicate  $fO_2$  conditions below  $\Delta FMQ+1$  in these intrusions; conditions which favor sulfides.

In sills hosted by evaporites of the Minto Inlet Formation, evaporite assimilation led to a greater range of  $\delta^{34}S$  values, sulfur contents and  $fO_2$  conditions. In evaporite-hosted sill E1, distal from any inferred dike, evaporite assimilation based on the  $\delta^{34}S$  values of +4.6 to +4.9‰ in the sill interior would have resulted in negligible increases in sulfur contents. In sill E2, which is a thin sill above sill E1, evaporite assimilation leading to  $\delta^{34}S$  values of +8.7 to +10.6‰ would have increased sulfur contents but not enough to reach sulfur saturation. In sill E3, close to a NNW-trending fault with an inferred feeder dike, evaporite assimilation leading to elevated  $\delta^{34}S$  values up to +12.9‰ in the interior could have increased sulfur contents above the point of sulfur saturation, triggering sulfide immiscibility. Calculated  $fO_2$  conditions in the interior of sill E3 were in the transitional range of sulfur stability between sulfides and sulfates of  $\Delta FMQ+1$  to  $\Delta FMQ+2$ . This indicates that evaporite assimilation can cause sulfur saturation

without oxidizing magma to the point where sulfides are converted to sulfates and resorbed.

The interior of sill E3 is missing 50% of its inferred external sulfur based on isotopic mixing constraints, we interpret that this sulfur segregated from the melt as immiscible sulfides upstream. Contamination in the Franklin magmatic plumbing system occurred preferentially in dikes, because of elevated brecciation and bulk rock assimilation associated with syn-magmatic fault movements. As well, elevated magmatic throughflow leads to increased chilled margin resorption, more extensive hydrothermal cells and more effective contact metamorphic devolatilization reactions, all of which lead to contamination of dikes by sulfur-rich fluids. Sulfate evaporite assimilation in dikes was likely required to trigger magma conduit sulfide immiscibility in the southwest Minto Inlier.

#### **4.10 ACKNOWLEDGEMENTS**

This paper is a contribution to the Geological Survey of Canada's Geomapping for Energy and Minerals project. Many people made this project possible, from those who coordinated logistics, to those who provided field support services, to the visiting scientists and mapping crew. MJH was sponsored by a Gold Fields SEG Foundation Graduate Student Fellowship, an Alexander Graham Bell CGS-M Natural Sciences and Engineering Research Council (NSERC) of Canada Scholarship, and through a Natural Resources Canada Research Affiliate Program Bursary. BAW acknowledges support from an NSERC Discovery grant



#### 4.11 REFERENCES

- Bacon, C.R., and Hirschmann, M.M., 1988, Mg/Mn partitioning as a test for equilibrium between coexisting Fe-Ti oxides: *American Mineralogist*, v. 73, p. 57-61.
- Baragar, W.R.A., 1976, The Natkusiak Basalts, Victoria Island, District of Franklin, *in* Report of Activities: Geological Survey of Canada Paper 76-1A, p. 347-352.
- Bédard, J.H., Naslund, H.R., Nabelek, P., Winpenny, A., Hryciuk, M., Macdonald, W., Hayes, B., Steigerwaldt, K. et al., 2012, Fault-mediated melt ascent in a Neoproterozoic continental flood basalt province, the Franklin sills, Victoria Island, Canada: *Geological Society of America Bulletin*, v. 124, p. 723-736.
- Bickle, M.J., and McKenzie, D., 1987, The transport of heat and matter by fluids during metamorphism: *Contributions to Mineralogy and Petrology*, v. 95, p. 384-392.
- Canfield, D.E., Raiswell, R., Westrich, J.T., Reaves, C.M., and Berner, R.A., 1986, The use of chromium reduction in the analysis of reduced inorganic sulfur in sediments and shales: *Chemical Geology*, v. 54, p. 149-155.
- Carroll, M.C., and Rutherford, M.J., 1988, Sulfur speciation in hydrous experimental glasses of varying oxidation state: results from measured wavelength shifts of sulfur X-rays: *American Mineralogist*, v. 73, p. 845-849.

- de Hoog, J.C.M., Taylor, B.E., and van Bergen, M.J., 2001, Sulfur isotope systematics of basaltic lavas from Indonesia: implications for the sulfur cycle in subduction zones: *Earth and Planetary Science Letters*, v. 189, p. 237-252.
- Denyszyn, S.W., Halls, H.C., Davis, D.W., and Evans, D.A.D., 2009, Paleomagnetism and U-Pb geochronology of Franklin dykes in High Arctic Canada and Greenland: a revised age and paleomagnetic pole constraining block rotations in the Nares Strait region: *Canadian Journal of Earth Sciences*, v. 46, p. 689-705.
- Dostal, J., Baragar, W.R.A., and Dupuy, C., 1986, Petrogenesis of the Natkusiak continental basalts, Victoria Island, Northwest Territories, Canada: *Canadian Journal of Earth Sciences*, v. 23, p. 622-632.
- Dupuy, C., Michard, A., Dostal, J., Dautel, D., and Baragar, W.R.A., 1995, Isotope and trace-element geochemistry of Proterozoic Natkusiak flood basalts from the northwestern Canadian Shield: *Chemical Geology*, v. 120, p. 15-25.
- Fahrig, W.F., 1987, The tectonic settings of continental mafic dyke swarms: Failed arm and early passive margin, *in* Halls, H.C., and Fahrig, W.F., eds., *Mafic dyke swarms: Geological Association of Canada Special Paper* 34, p. 331-348.
- Forrest, J., and Newman, L., 1977, Silver-110 microgram sulfate analysis for the short time resolution of ambient levels of sulfur aerosol: *Analytical Chemistry*, v. 49, p. 1579-1584.

- Ghiorso, M.S., and Evans, B.W., 2008, Thermodynamics of rhombohedral oxide solid solutions and a revision of the Fe-Ti two-oxide geothermometer and oxygen-barometer: *American Journal of Science*, v. 308, p. 957-1039.
- Grinenko, L.N., 1985, Sources of sulfur of the nickeliferous and barren gabbro-dolerite intrusions of the northwest Siberian platform: *International Geology Review*, v. 28, p. 695-708.
- Heaman, L.M., LeCheminant, A.N., and Rainbird, R.H., 1992, Nature and timing of Franklin igneous events, Canada: Implications for a Late Proterozoic mantle plume and the break-up of Laurentia: *Earth and Planetary Science Letters*, v. 109, p. 117-131.
- Hulbert, L.J., 1998, Mineralogical and chemostratigraphic investigation of ultramafic-bearing sills on ground held by Aber Resources in the Wynniatt Bay-Glenelg Bay-Killian Lake Area, Victoria Island: Northwest Territories Geoscience Office, 41 p.
- Huppert, H.E., and Sparks, R.S.J., 1985, Cooling and contamination of mafic and ultramafic magmas during ascent through continental crust: *Earth and Planetary Science Letters*, v. 74, p. 371-386.
- Jefferson, C.W., Hulbert, L.J., Rainbird, R.H., Hall, G.E.M., Gregoire, D.C., and Grinenko, L.I., 1994, Mineral resource assessment of the Neoproterozoic Franklin igneous events of Arctic Canada: comparison with the Permo-Triassic Noril'sk-Talnakh Ni-Cu-PGE deposits of Russia: *Geological Survey of Canada Open File 2789*, 48 p.

- Jugo, P.J., Luth, R.W., and Richards, J.P., 2005, An experimental study of the sulfur content in basaltic melts saturated with immiscible sulfide or sulfate liquids at 1300°C and 1.0GPa: *Journal of Petrology*, v. 46, p. 783-798.
- Kiss, F., and Oneschuk, D., 2010, First vertical derivative of the magnetic field, Minto Inlier aeromagnetic survey, Victoria Island, NTS 87 G/NE and parts of 87G/NW, 88 B/SE and 88B/SW: Geological Survey of Canada Open-File Map 6705, scale 1:100 000, sheet 2 of 2.
- Li, C., Ripley, E.M., Naldrett, A.J., Schmitt, A.K., and Moore, C.H., 2009a, Magmatic anhydrite-sulfide assemblages in the plumbing system of the Siberian Traps: *Geology*, v. 37, p. 259-262.
- Li, C., Ripley, E.M., and Naldrett, A.J., 2009b, A new genetic model for the giant Ni-Cu-PGE sulfide deposits associated with the Siberian Flood Basalts: *Economic Geology and the Bulletin of the Society of Economic Geologists*, v. 104, p. 291-301.
- Long, D.G.F., Rainbird, R.H., Turner, E.C., and MacNaughton, R.B., 2008, Early Neoproterozoic strata (Sequence B) of mainland northern Canada and Victoria and Banks islands: a contribution to the Geological Atlas of the Northern Canadian Mainland Sedimentary Basin: Geological Survey of Canada Open File 5700, 24 p. +17 Figures
- Mandeville, C.W., Webster, J.D., Tappen, C., Taylor, B.E., Timbal, A., Sasaki, A., Hauri, E., and Bacon, C.R., 2009, Stable isotope and petrologic evidence for open-system degassing during the climactic and pre-climactic eruptions of Mt. Mazama, Crater Lake, Oregon: *Geochimica et Cosmochimica Acta*, v. 73, p 2798-3012.

- Mungall, J.E., 2007, Crustal contamination of picritic magmas during transport through dikes: the Expo Intrusive Suite, Cape Smith Fold Belt, New Quebec: *Journal of Petrology*, v. 48, p. 1021-1039.
- Naldrett, A.J., 1992, A model for the Ni-Cu-PGE deposits of the Noril'sk region and its application to other areas of flood basalts: *Economic Geology and the Bulletin of the Society of Economic Geologists*, v. 87, p. 1945-1961.
- Naldrett, A.J., 2005, A history of our understanding of magmatic Ni-Cu sulfide deposits: *The Canadian Mineralogist*, v. 43, p. 2069-2098.
- Pehrsson, S.J., and Buchan, K.L., 1999, Borden dykes of Baffin Island, Northwest Territories: a Franklin U-Pb baddeleyite age and a paleomagnetic reinterpretation: *Canadian Journal of Earth Sciences*, v. 36, p. 65-73.
- Prince, J.K.G., Rainbird, R.H., Wing, B.A., Dix, G.R., and Thomson, D., 2012, A dynamic sulphate reservoir at the start of the Cryogenian, *in* GAC-MAC Joint Meeting St. John's 2012, Abstracts Volume 35: Geological Association of Canada and Mineralogical Association of Canada, p. 118-119.
- Rainbird, R.H., Jefferson, C.W., Hildebrand, R.S., and Worth, J.K., 1994, The Shaler Supergroup and revision of Neoproterozoic stratigraphy in Amundsen Basin, Northwest Territories: *Geological Survey of Canada Current Research*, v. 1994-C, p. 61-70.
- Rainbird, R.H., Jefferson, C.W., and Young, G.M., 1996, The early Neoproterozoic sedimentary Succession B of northwestern Laurentia: correlations and paleogeographic significance: *Geological Society of America Bulletin*, v.108, p. 454-470.

- Ripley, E.M., and Li, C., 2003, Sulfur isotope exchange and metal enrichment in the formation of magmatic Cu-Ni-(PGE) deposits: *Economic Geology and the Bulletin of the Society of Economic Geologists*, v. 98, p. 635-641.
- Ripley, E.M., Lightfoot, P.C., Li, C., and Elswick, E.R., 2003, Sulfur isotopic studies of continental flood basalts in the Noril'sk region: Implications for the association between lavas and ore-bearing intrusions: *Geochimica et Cosmochimica Acta*, v. 67, p. 2805-2817.
- Ripley, E.M., Li, C., Moore, C.H., and Schmitt, A.K., 2010, Micro-scale S isotope studies of the Kharaelakh intrusion, Noril'sk region, Siberia: Constraints on the genesis of coexisting anhydrite and sulfide minerals: *Geochimica et Cosmochimica Acta*, v. 74, p. 634-644.
- Robertson, W.A., and Baragar, W.R.A., 1972, The petrology and paleomagnetism of the Coronation Sills: *Canadian Journal of Earth Sciences*, v. 9, p. 123-140.
- Seal, R.R., II, 2006, Sulfur isotope geochemistry of sulfide minerals: *Reviews in Mineralogy and Geochemistry*, v. 61, p. 633-677.
- Toplis, M.J., and Carroll, M.R., 1995, An experimental study of the influence of oxygen fugacity on Fe-Ti oxide stability, phase relations, and mineral-melt equilibria in ferro-basaltic systems: *Journal of Petrology*, v. 36, p. 1137-1170.
- Wallace, P.J., and Carmichael, I.S.E., 1994, S speciation in submarine basaltic glasses as determined by measurements of SK $\alpha$  X-ray wavelength shifts: *American Mineralogist*, v. 79, p. 161-167.

Young, G.M., 1981, The Amundsen Embayment, Northwest Territories;  
Relevance to the upper Proterozoic evolution of North America, *in* F.H.A.  
Campbell, ed., Proterozoic Basins of Canada; Geological Survey of  
Canada Paper 81-10, p. 203-218.

## FIGURE CAPTIONS

**Figure 4.1-** Victoria Island regional geology map, modified from Bédard et al. (2012). Sample locations of shale-hosted sill S1, carbonate-hosted sill C1, and evaporite-hosted sills E1, E2 and E3 are shown.

**Figure 4.2-** Pictures of evaporite hosted sill profiles. **A:** Section 1 photo, in this sampling profile there is a 17m thick lower sill (E1) and a 4m thick upper sill (E2) separated by 23m of evaporites and interbedded carbonates. Sill E1 is laterally continuous for a few kilometers and a few hundred meters away sill E2 bifurcates from sill E1. **B:** Close up photo of sill E3 and the interbedded sulfate evaporites (white) and carbonate layers (gray) below. **C:** Sill E3 is laterally discontinuous as it is truncated by a NNW-trending fault on its west side (far side of photograph).

**Figure 4.3-** Sulfur isotope profile for the sill E1. All  $\delta^{34}\text{S}$  values are reported relative to V-CDT. The level of uncertainty ( $2\sigma$ ), is equal to  $\pm 0.20\%$ , and is less than the symbol size. Sedimentary  $\delta^{34}\text{S}$  values are only shown for MH139A1A and MH139A1B, an evaporite and a carbonate sample above the sill.

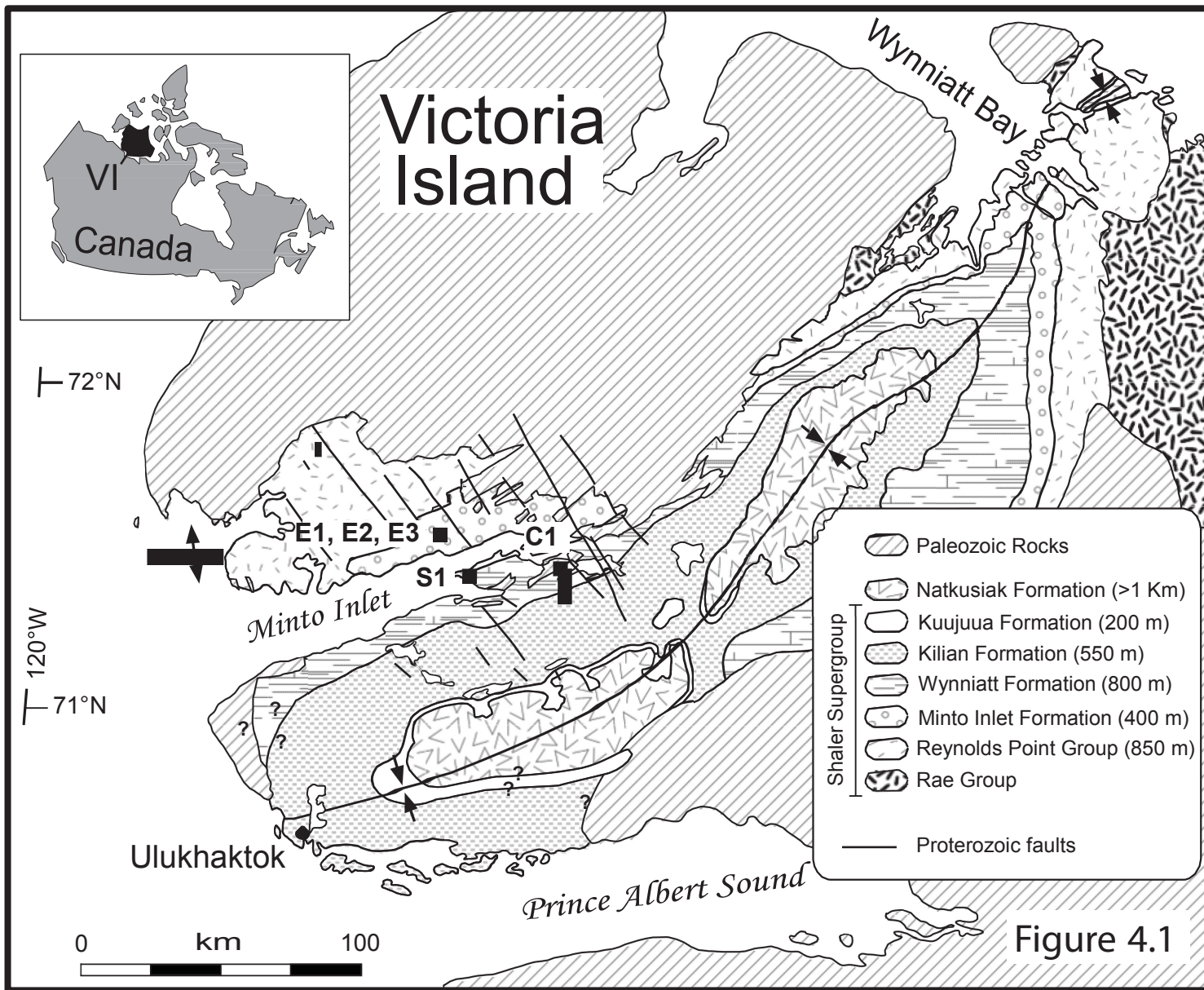
**Figure 4.4-** Sulfur isotope profile for the sill E3 and underlying sedimentary rocks. All  $\delta^{34}\text{S}$  values are reported relative to V-CDT. The level of uncertainty ( $2\sigma$ ), is equal to  $\pm 0.20\%$ , and is less than the symbol size. Sedimentary  $\delta^{34}\text{S}$  values are shown for all samples analysed, and carbonates and evaporites are interbedded.

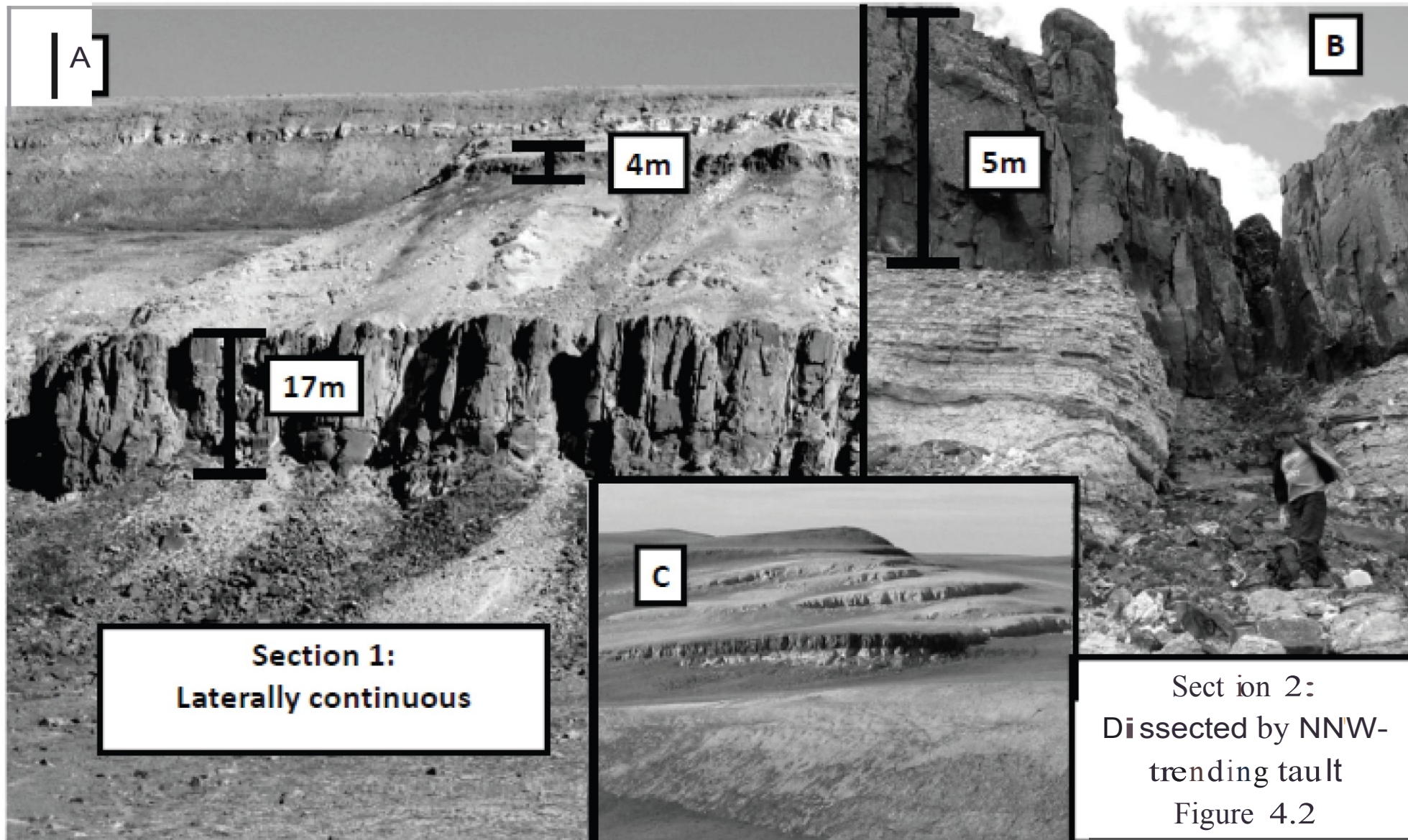
**Figure 4.5-** The effect of evaporite assimilation on oxygen fugacity and sulfur isotopes. All  $\delta^{34}\text{S}$  values are reported relative to V-CDT. The level of uncertainty ( $2\sigma$ ), is equal to  $\pm 0.20\%$ , and is less than the symbol size for each ilmenite-magnetite pair  $f\text{O}_2$  value. Oxygen fugacity is reported in log units relative to the fayalite-magnetite-quartz (FMQ) buffer. Samples shown from all 3 sections are from sill interiors and not from chilled margins.

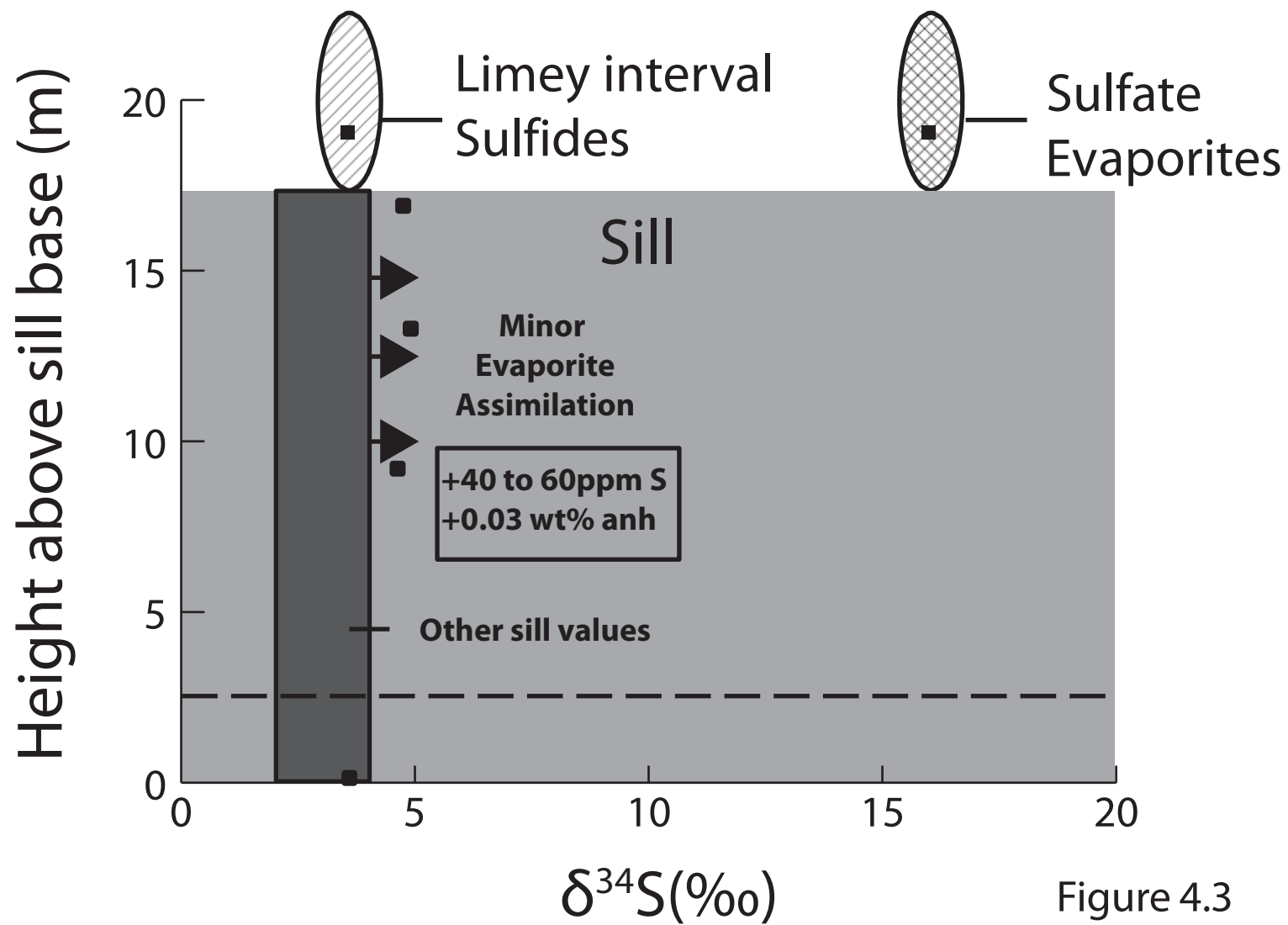
**Figure 4.6-** The effect of evaporite assimilation on oxygen fugacity and sulfur solubility, modified from Li et al. (2009b). The dashed line is the modeled sulfur solubility of mafic magmas: in reducing conditions sulfide is stable while in oxidizing conditions sulfate is stable and is 10 times more soluble (Jugo et al., 2005). Samples in sills E2 and E3 were in the transitional range of sulfur solubility, but no oxygen fugacities corresponded to the range of sulfate stability.



**Figure 4.7**-Missing sulfur in sill E3 samples. The short-dashed line is how much sulfur should be present in samples with elevated  $\delta^{34}\text{S}$  values based on a simple mixing model with sulfate evaporites (Ripley and Li, 2003); conditions are given in the inset box. The solid black line is the sulfur content baseline if no evaporites have been assimilated. The long-dashed black lines and data points indicate how much of the isotopically predicted external sulfur was actually present in the samples analysed.







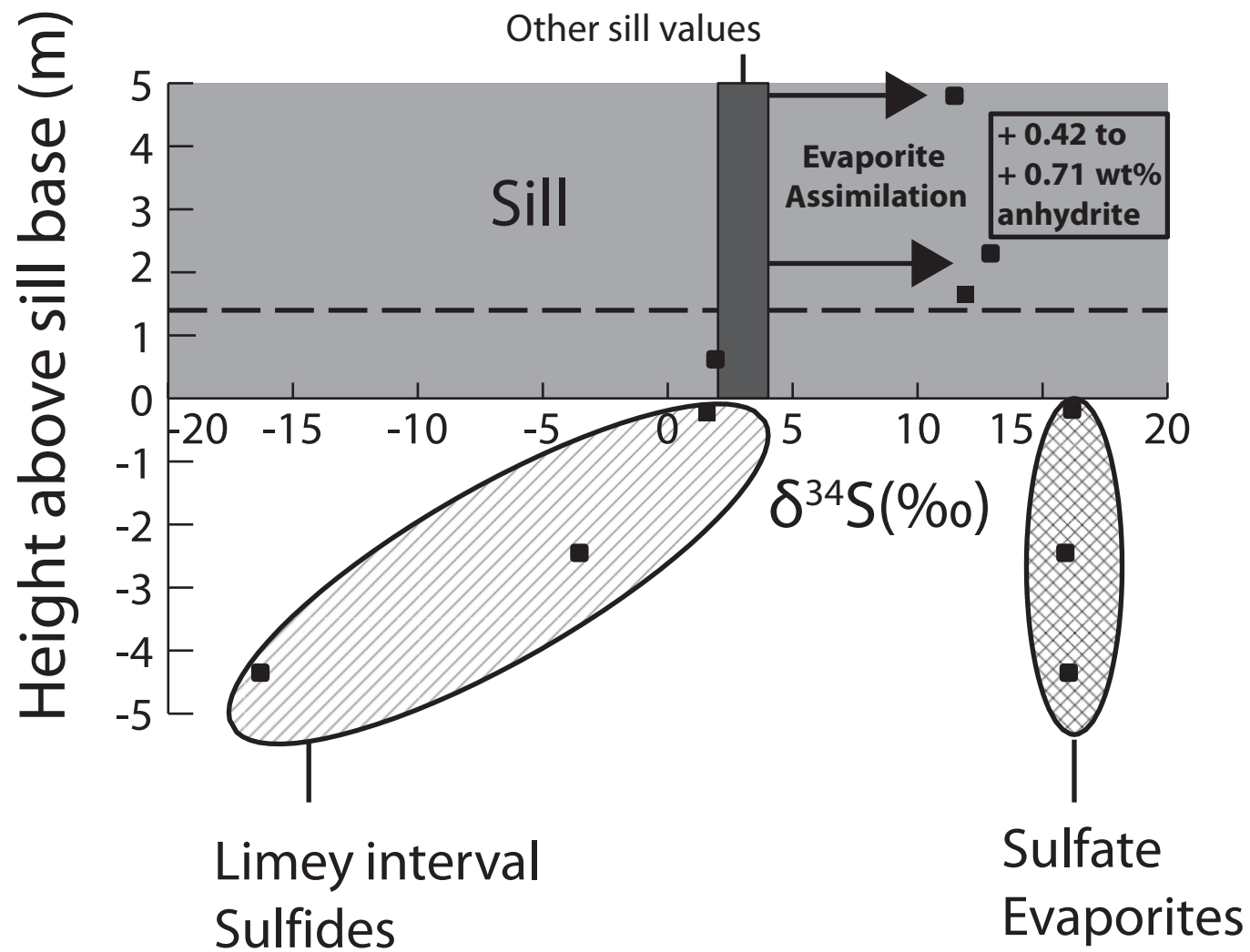


Figure 4.4

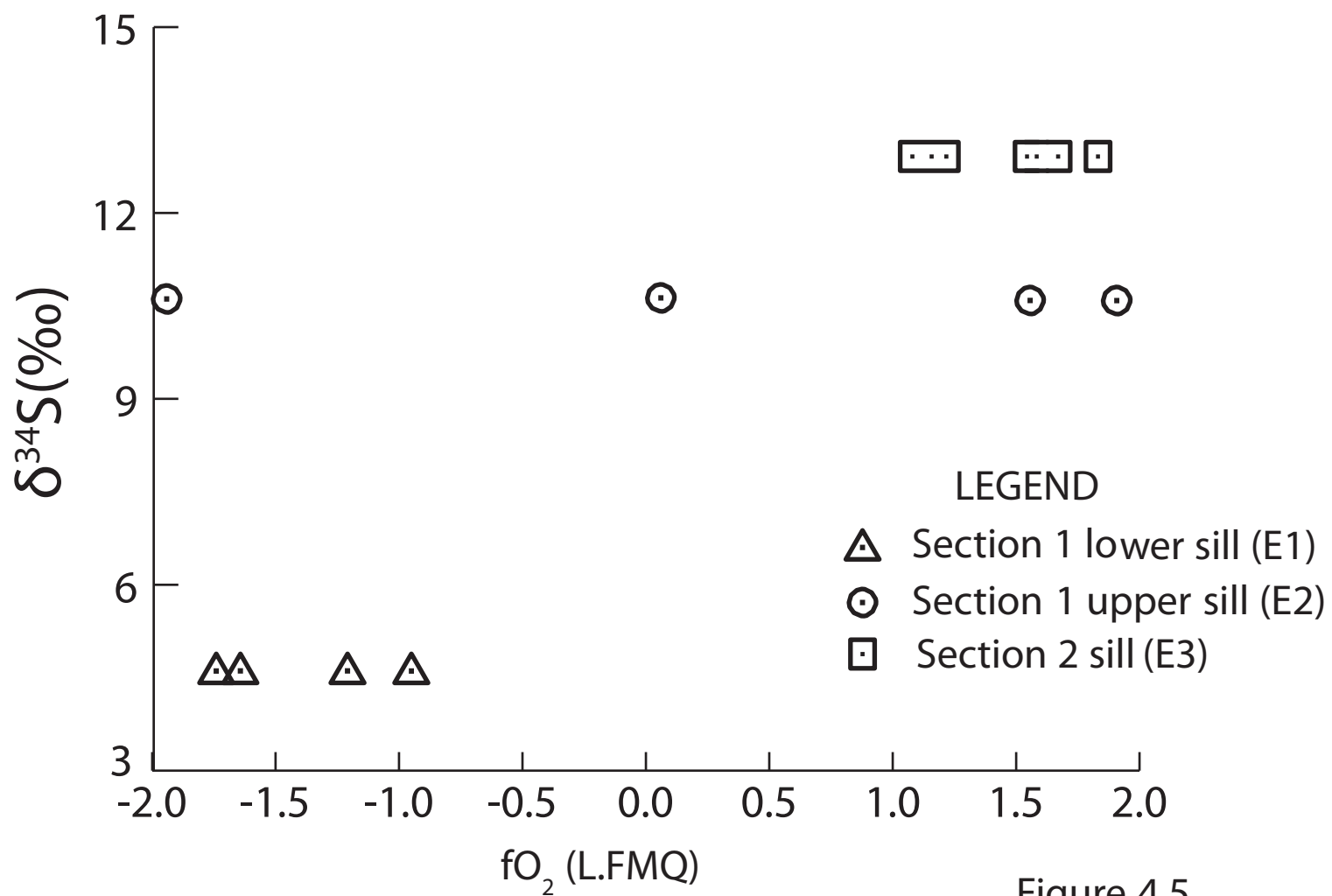
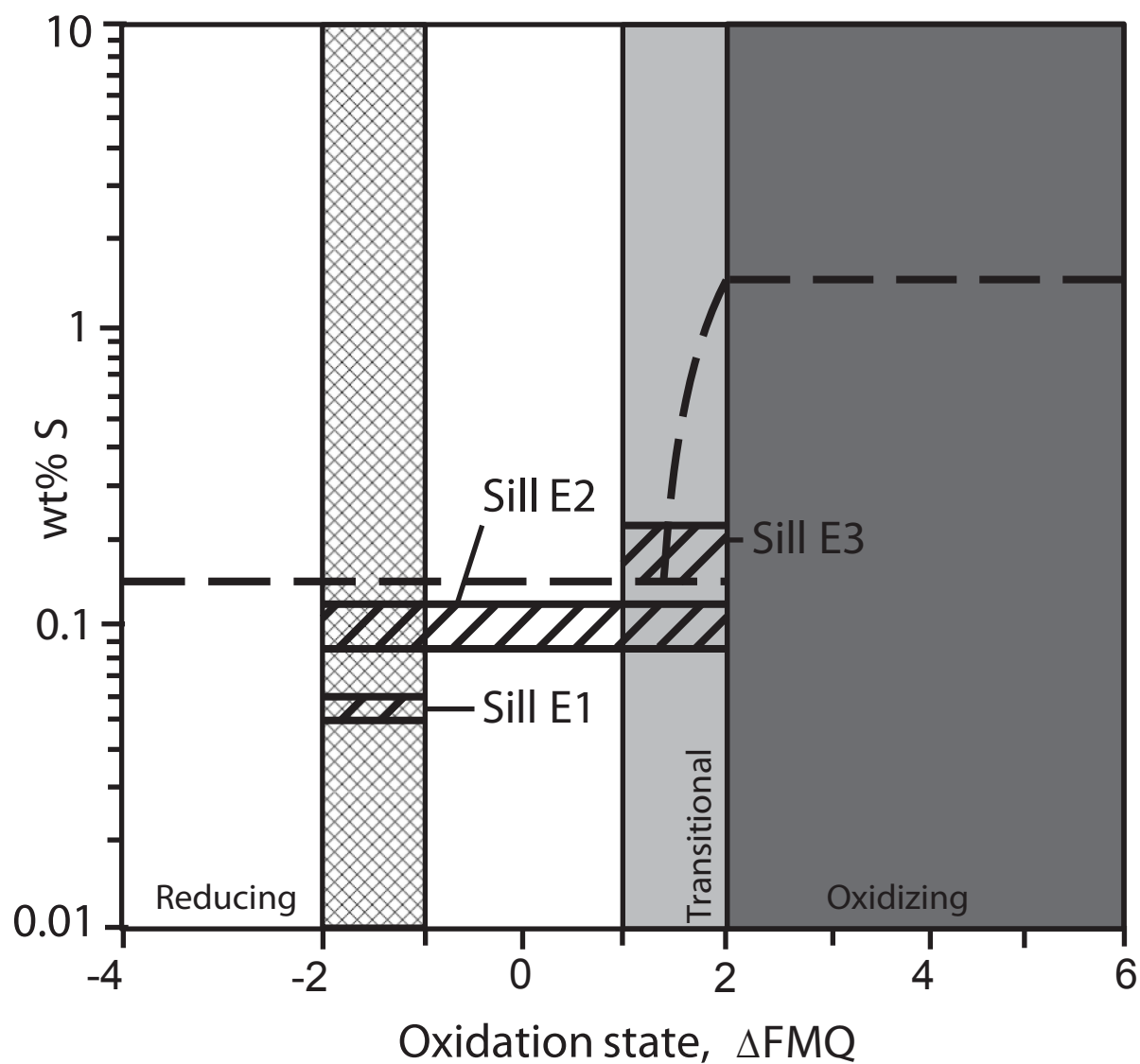


Figure 4.5





## LEGEND




-  Sill E1:  
Sulfides stable,  
magmatic  $\delta^{34}\text{S}$   
**no immiscible sulfides**
-  Sill E3:  
Sulfides stable,  
elevated  $\delta^{34}\text{S}$   
**immiscible sulfides**
-  Excess assimilation  
Sulfates stable,  
**no immiscible sulfides**

Figure 4.6

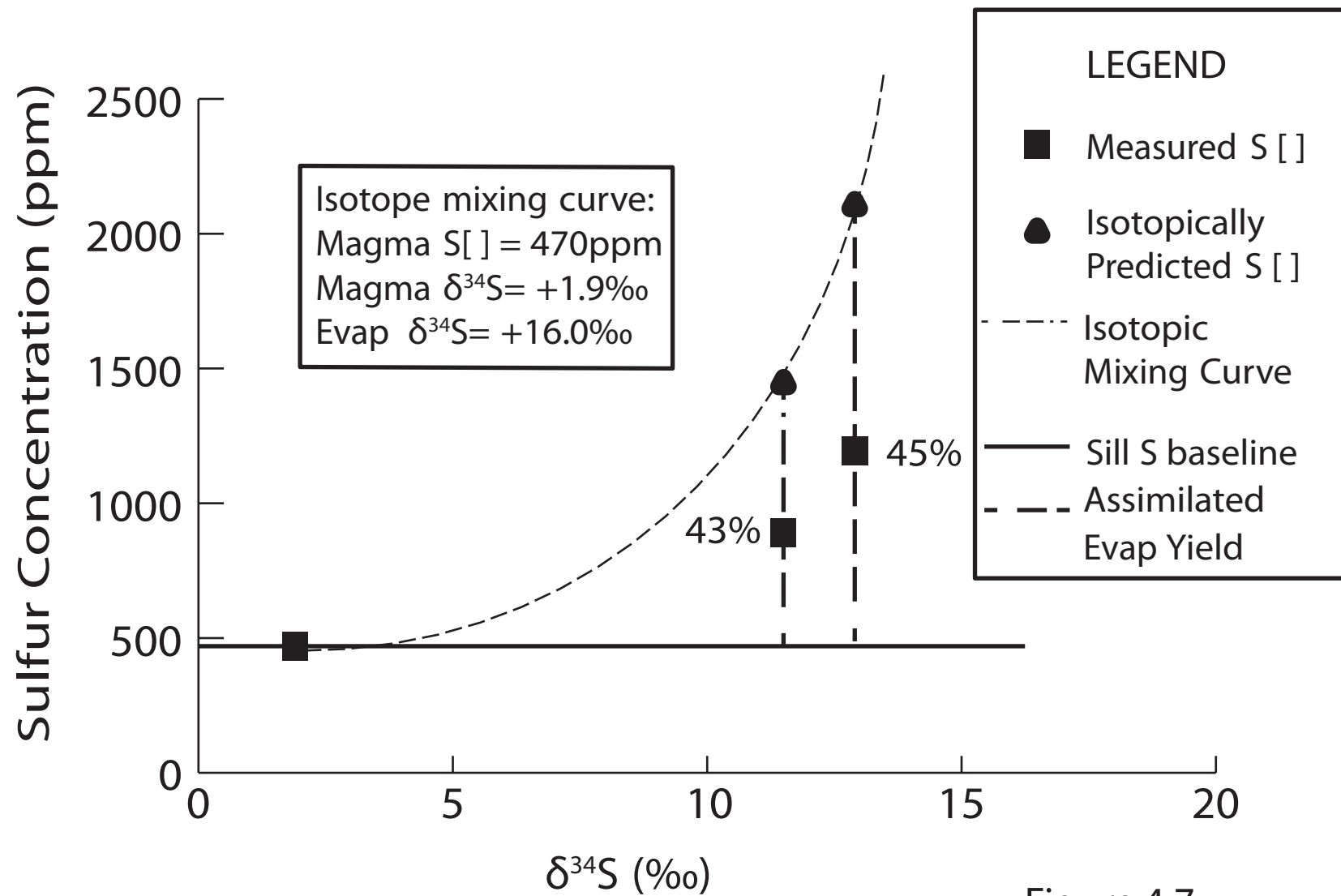


Figure 4.7



Table 4.1:  $\delta^{34}\text{S}$  values of sills hosted by the Wynniatt Formation

Sample	Lithology	$\delta^{34}\text{S}$ (‰)	Sulfur content (wt %)	Height above lower sill base (m)
<i>CI</i>				
10 RAT HY068A1B	Carbonate shale	-8.1	0.19	-3.93
10 RAT HY068A2	Carbonate shale	-10.4	0.08	-1.68
10 RAT HY068A3	Carbonate shale	-8.5	0.19	-0.13
10 RAT HY068B1A	Diabase	+3.3	0.048	0.17
10 RAT HY068B1B	Diabase	+1.0	0.044	0.17
10 RAT HY068B2	Diabase	+3.6	0.037	2.16
10 RAT HY068B3	Diabase	+3.9	0.045	4.85
<i>S1<sup>a</sup></i>				
10 RAT HY069A1	Black shale	+8.9	0.41	-6.6
10 RAT HY069A2	Black shale	+4.8	0.44	-3.8
10 RAT HY069A3	Black shale	+7.5	0.05	-2.4
10 RAT HY069A4	Black shale	+6.1	0.07	-1.3
10 RAT HY069A5	Black shale	+6.6	0.30	-0.1
10 RAT HY069B1	Diabase	+5.6	0.077	0.1
10 RAT HY069B2	Picrite	+4.0	0.081	2.4
10 RAT HY069B3	Diabase	+3.9	0.076	7.7
10 RAT HY069B4	Diabase	+3.9	0.078	13.7
10 RAT HY069B5	Diabase	+3.7	0.097	16.2
10 RAT HY069C1	Black shale	+6.9	0.26	17.0
10 RAT HY069C2	Black shale	+6.3	0.16	19.5
10 RAT HY069C3	Black shale	+3.6	0.20	21.8
10 RAT HY069C4	Sandstone	+2.0	0.18	24.2
10 RAT HY069C5	Sandstone	+7.4	0.26	31.1

<sup>a</sup>Upper sill contact of S1 is at 16.2m

Table 4.2:  $\delta^{34}\text{S}$  values and S contents of evaporite-hosted sills

Sample	Lithology	$\delta^{34}\text{S}$ (‰)	Height above lower sill base (m)	Sulfur Content (wt %)
<i>Section 1<sup>a</sup> (E1 and E2)</i>				
11 RAT MH141A1A	Evaporite	+16.1	-4.3	N/A
11 RAT MH141A1B	Carbonate	-2.1	-3.7	N/A
11 RAT MH141A2	Carbonate	-7.9	-0.35	N/A
11 RAT MH140A1	Diabase (E1)	+3.6	+0.14	N/A
11 RAT MH140A2	Diabase (E1)	+4.6	+9.2	N/A
11 RAT MH140A3	Diabase (E1)	+4.9	+13.3	N/A
11 RAT MH140A4	Diabase (E1)	+4.8	+16.9	N/A
11 RAT MH139A1A	Evaporite	+16.0	+19.05	N/A
11 RAT MH139A1B	Carbonate	+3.6	+19.05	N/A
11 RAT MH139A2	Evaporite	+15.6	+23.6	N/A
11 RAT MH139A3A	Evaporite	+15.8	+30.7	N/A
11 RAT MH139A3B	Carbonate	-9.6	+30.7	N/A
11 RAT MH138A1	Diabase (E2)	+8.7	+41.5	N/A
11 RAT MH138A2	Diabase (E2)	+10.6	+42.55	N/A
11 RAT MH138A3	Diabase (E2)	+10.5	+44.05	N/A
11 RAT MH137A1	Evaporite	+15.8	+48.2	N/A
<i>Section 2 (E3)</i>				
10 RAT HY074A1A	Evaporite	+16.0	-4.35	18.0
10 RAT HY074A1B	Carbonate	-16.3	-4.35	0.38
10 RAT HY074A2A	Evaporite	+15.9	-2.45	17.8
10 RAT HY074A2B	Carbonate	-3.5	-2.45	0.42
11 RAT MH068A1	Carbonate	+1.6	-0.23	N/A
10 RAT HY074A3	Evaporite	+16.2	-0.18	17.0
10 RAT HY074B1	Diabase (E3)	+1.9	+0.62	0.047
11 RAT MH068B1	Diabase (E3)	+11.9	+1.65	N/A
10 RAT HY074B2	Diabase (E3)	+12.9	+2.30	0.121
10 RAT HY074B3	Diabase (E3)	+11.5	+4.80	0.089

a- Upper sill contact (E1) is at +17.20m, lower sill contact (E2) is at +40.2m,  
upper sill contact (E2) is at +44.2m, upper sill (E2) is 4.0m thick

Table 4.3: Magnetite-Ilmenite  $fO_2$  and T constraints (Ghiorso and Evans 2008) for Wynniatt-hosted and evaporite-hosted sill samples

Sample	$fO_2$ (min) <sup>c</sup>	$fO_2$ (max) <sup>c</sup>	T (min) <sup>c</sup>	T (max) <sup>c</sup>	Method <sup>a</sup>	# of analyses
<i>Wynniatt-hosted</i>						
10 RAT HY068B1A (C1)	N/A	~0	N/A	~1100	Phase relationships <sup>b</sup>	0 Mt, 20 Ilm
10 RAT HY068B3 (C1)	-2.3	-1.2	560	736	General	9 Mt, 11 Ilm
10 RAT HY068B3 (C1)	-2.5	-1.2	608	734	Mineral pairs	19 pairs
10 RAT HY069B1 (S1)	+0.5	+1.0	658	805	General	2 Mt, 5 Ilm
10 RAT HY069B2 (S1)	-1.1	+0.9	587	764	General	8 Mt, 10 Ilm
10 RAT HY069B2 (S1)	0.0	+1.0	688	835	Mineral pairs	17 pairs
<i>Evaporite-hosted</i>						
11 RAT MH140A2 (E1)	-1.8	-1.4	660	764	General	4 Mt, 7 Ilm
11 RAT MH140A2 (E1)	-1.9	-1.0	676	834	Mineral pairs	10 pairs
11 RAT MH138A2 (E2)	-1.9	+2.0	688	801	General	6 Mt, 4 Ilm
11 RAT MH138A2 (E2)	-1.9	+1.9	681	809	Mineral pairs	4 pairs
10 RAT HY074B1 (E3)	-1.4	-0.9	803	941	General	11 Mt, 4 Ilm
10 RAT HY074B2 (E3)	+1.1	+1.9	640	765	General	9 Mt, 9 Ilm
10 RAT HY074B2 (E3)	+1.1	+1.8	665	748	Mineral pairs	14 pairs

a- Mineral pairs = based on specific magnetite-ilmenite mineral pairs, General = based on total range of magnetite and ilmenite compositions (some samples did not have usable magnetite-ilmenite pairs)

b- Ilmenite but no magnetite, T and  $fO_2$  constraints based on Toplis and Carroll (1995) figure 2

c- T is in °C and  $fO_2$  is relative to the  $\Delta FMQ$  buffer

Table 4.4: Sulfur isotopes and added anhydrite for evaporite-hosted sills

Sample	$\delta^{34}\text{S}_{\text{sample}}$ (‰)	$\delta^{34}\text{S}_{\text{magma}}$ (‰) <sup>a</sup>	$\delta^{34}\text{S}_{\text{segs}}$ (‰) <sup>b</sup>	S% segs	S <sub>magma</sub> (wt%) <sup>a</sup>	S <sub>sample</sub> (wt%) <sup>c</sup>	S <sub>segs</sub> (wt%)	Anhydrite wt% <sup>d</sup>
11 RAT MH140A1 (E1)	4.6	3.6	16.0	8	0.050	0.055	0.005	0.02
11 RAT MH140A2 (E1)	4.9	3.6	16.0	11	0.050	0.056	0.006	0.03
11 RAT MH140A3 (E1)	4.8	3.6	16.0	9	0.050	0.055	0.005	0.02
11 RAT MH138A1 (E2)	8.7	3.6	16.0	41	0.050	0.085	0.035	0.15
11 RAT MH138A2 (E2)	10.6	3.6	16.0	57	0.050	0.115	0.065	0.28
11 RAT MH138A3 (E2)	10.5	3.6	16.0	55	0.050	0.112	0.062	0.26
10 RAT HY074B2 (E3)	12.9	1.9	16.0	78	0.047	0.214	0.167	0.71
10 RAT HY074B3 (E3)	11.5	1.9	16.0	68	0.047	0.146	0.099	0.42
10 RAT HY074B2 (E3)	12.9	3.6	16.0	75	0.050	0.201	0.151	0.64
10 RAT HY074B3 (E3)	11.5	3.6	16.0	64	0.050	0.137	0.087	0.37

a- Two possible parental magma compositions: lower chilled margin of sill E3 ( $\delta^{34}\text{S}=+1.9\text{‰}$ , 0.047wt%S) or typical sulfur-poor diabasic sill ( $\delta^{34}\text{S}=+3.6\text{‰}$ , 0.050wt%S)

b- Local average  $\delta^{34}\text{S}$  value for Minto Inlet Formation evaporites (see Table 4.2)

c- Theoretical sulfur content of sample based on initial magmatic sulfur contents and simple isotopic mixing

d- Anhydrite wt% =  $\text{S}_{\text{segs}} (\text{wt}\%) \times (\text{molar mass CaSO}_4/\text{S} = 136.14/32.07)$ . This is the amount of anhydrite required to cause the increase between  $\delta^{34}\text{S}_{\text{magma}}$  and  $\delta^{34}\text{S}_{\text{sample}}$  using a  $\delta^{34}\text{S}_{\text{segs}}$  contaminant with  $\text{S}_{\text{magma}}$  being the sulfur content of the magma prior to evaporite assimilation

## Chapter 5: Conclusions and applications

### 5.1 Scientific contributions

The two manuscripts in this thesis provide examples of how interactions between mafic intrusions and host rocks can be studied directly. Detailed transects through intrusions and their host rocks can provide more information about the processes that occurred *in situ* in a LIP plumbing system than reverse models and inferences from ore-bearing intrusions, flood basalts, and representative country rock samples.

The first manuscript in Chapter 2 provides evidence that contamination in the part of the conduit system we have examined is concentrated in dikes relative to sills. This manuscript also proposes a mechanism by which contamination in an intrusion can occur *in situ* during magma transport. The manuscript proposes that contact metamorphism can lead to the destabilization of sulfide phases, leading to the advection of sulfur and metals in metamorphic fluids from host rocks into dikes. This process can lead to smoothly varying  $\delta^{34}\text{S}$  sulfur isotope profiles extending from distal host rocks into dike interiors; as well as depleted sulfur, iron, and trace metal contents in host rocks adjacent to dikes. In dynamic intrusions, contamination by host rocks with low to moderate sulfur contents will be insufficient to significantly raise sulfur contents.

The second manuscript in Chapter 4 provides evidence that dynamic magma conduits can be contaminated to the point of sulfur saturation by sulfur-rich host rocks like sulfate evaporites. However, sills emplaced in evaporites can show negligible  $^{34}\text{S}$ -enrichments and sulfur concentration increases, suggesting that contamination by evaporites was upstream, possibly in dikes. This study

provided field-constrained isotopic data of a sill with  $\delta^{34}\text{S}$  values as high as +13‰. We used a simple mixing model to infer that  $^{34}\text{S}$ -elevated isotopic values were caused by upstream assimilation of less than 0.7 wt% anhydrite. Measured sulfur concentrations indicated that over 50% of the isotopically-predicted external sulfur was missing from the sill. We interpreted that this missing sulfur was segregated as immiscible sulfides upstream in a feeder dike, and inferred that evaporite assimilation in dikes is the best way to create sulfide immiscibility in a dynamic magma conduit.

Previous studies of evaporite assimilation by mafic magmas in natural systems (Ripley et al., 2003; Li et al., 2009b) have inferred that evaporite assimilation leads to increases in oxygen fugacity. This can affect the sulfur species stable in a melt, therefore increasing the sulfur solubility by an order of magnitude (Carroll and Rutherford, 1988; Jugo et al., 2005). This study provides evidence of evaporite-hosted intrusions with increasing  $\delta^{34}\text{S}$  values (+4.6 to +12.9‰) relative to the assumed magmatic range (+3.6 to +4.0‰), which we used to infer increasing degrees of evaporite assimilation. Increasing  $\delta^{34}\text{S}$  values also correlate with elevated sulfur concentrations and more oxidizing  $f\text{O}_2$  conditions. This study confirmed the inference of Li et al. (2009b) that evaporite assimilation leading to sulfide immiscibility also increases oxygen fugacity to  $\Delta\text{FMQ}+1$  to  $\Delta\text{FMQ}+2$ , in the transitional range between sulfide and sulfate stability in a mafic melt. Evaporite assimilation can lead to sulfur saturation without sulfides being converted to sulfates. The more oxidizing  $f\text{O}_2$  conditions caused by the assimilation of evaporites could potentially lead to large magmatic degassing fluxes of  $\text{SO}_2$  (Li et al., 2009a).

## **5.2 From ore-forming processes to exploration models**

In order for sulfide immiscibility to lead to formation of a magmatic Ni-Cu-PGE deposit, the sulfides need to interact with a large volume of magma to upgrade their metal tenor. This is the R factor concept of Campbell and Naldrett (1979). The presence of immiscible sulfides should lead to complementary chalcophile depletion of coexisting silicate magmas (Naldrett, 1992). The efficiency of metal tenor upgrading in immiscible sulfides also depends on the olivine crystallization history and the magmatic flux. If olivine crystallization occurred before sulfide immiscibility, nickel will be extracted by olivine and the resulting magma would have lower Ni-contents and lower Ni in S tenors (Simon and Ripley, 2011). High magmatic flux might lead to metal upgrading in two ways. Sulfides interact with a large volume of silicate melt attaining a high R factor. Also, sulfide droplets are kept in suspension in the transporting magma facilitating continuous upgrading interactions (Bremond d'Ars et al., 2001).

Two case studies on Victoria Island will be used to apply the inferences from the manuscripts in Chapters 2 and 4 about host-rock contamination on sulfide immiscibility to evaluate metal tenor upgrading potential in the Franklin LIP. The first case study will be a new field area, the Uhuk Massif of Bedard et al. (2012) and the petrologically and geochemically similar and possibly correlated “Kat’s sill” which is distal to the Uhuk Massif upflow zone and has a thick olivine cumulate at its base. Kat’s sill will be used to evaluate the effects of carbonate assimilation and olivine crystallization on magmatic metal and sulfur concentrations. The second case study will revisit the evaporite-hosted sill E3

from Chapter 4, using sulfur, trace metal and PGE concentrations to determine whether or not sulfide immiscibility led to metal tenor upgrading.

### **5.3 Application: carbonate contamination**

#### *5.3.1 Sampling*

In order to evaluate the effect of carbonate assimilation on the metal budget of the Franklin plumbing system, the feeder system at the Uhuk Massif in the Jago Bay Formation (Bedard et al., 2012) and a related distal sill profile (“Kat’s sill”) were sampled. Kat’s sill preserves the effects of contamination upstream from a feeder zone, which may correspond to the Uhuk Massif, 33km to the east. Definitive correlation of Kat’s sill with the upper sill at Uhuk is difficult because of the presence of many fault blocks. However, this sill is distinct because of the presence of a thick olivine cumulate layer in its lower half, and because this sill occupies the same stratigraphic position (immediately above the contact between the Fort Collinson and Jago Bay Formations). Upper and lower host siltstone and carbonate samples were collected for the Kat’s sill profile. Representative diabase, calc-silicate and Fe-rich skarn samples were collected from the Uhuk Massif.

#### *5.3.2 S-Isotope Results*

At the Uhuk Massif, 3 out of 5 diabase samples have  $\delta^{34}\text{S}$  values between +2.3 and +3.8‰ (Appendix B). These samples come from the Main block lower sill and the Horst block of Bedard et al. (2012) and represent the sulfur isotope values of magma entering the Uhuk system prior to contamination. Higher  $\delta^{34}\text{S}$  values of +4.9 and +7.7‰ come from the Main block feeder gabbro, domain 2 in



Bedard et al. (2012). These are sulfur-enriched coarse-grained diabases sampled very close to the contact of the discordant gabbro with the capping limestones. Thus, the Uhuk Massif contains both normal Franklin igneous signatures (+2 to +4‰) and enriched (+4.9 to +7.7‰) S-isotopic signatures. Of the 10 host rock samples collected at the Uhuk Massif, 2 samples are calc-silicates (contact-metamorphosed limestones) with  $\delta^{34}\text{S}$  values of +8.5 to +10.4‰. The other 8 are magnetite-rich exoskarns and carbonated gabbro endoskarns with  $\delta^{34}\text{S}$  values of +5.0 to +7.9‰, intermediate between normal igneous signatures and those of the host limestones.

In Kat's sill, all 5 lower picrite samples have typical igneous  $\delta^{34}\text{S}$  values less than +3.8‰ (Appendix B). The upper diabase samples have homogeneous enriched  $\delta^{34}\text{S}$  values of +6.2 and +6.8‰, whereas the upper chilled margin has a  $\delta^{34}\text{S}$  value of +8.5‰. The sample directly below the sill has a  $\delta^{34}\text{S}$  value of +0.9‰, whereas the other 8 carbonate shale samples above and below the sill have  $\delta^{34}\text{S}$  values between +5.0 and +11.1‰.

### *5.3.3 Element abundances*

The Wynniatt Formation hosted sill profiles S1 and C1, which were interpreted to be uncontaminated (Chapter 2), are used as a baseline to evaluate how S and Ni abundances have been modified during crystallization of Kat's sill (Appendix C). The carbonate-hosted sill C1 and the shale-hosted sill S1 have dramatically different abundances of S and Ni. The Wynniatt Upper Carbonate Sill has low sulfur contents between 0.037 and 0.048 wt%, as well as low uniform Ni contents between 86 and 124ppm and low uniform MgO contents between 7.3 and 8.0wt%. This sill sets the baseline for low Ni contents; and anything below

100ppm Ni will henceforth be described as depleted. The Wynniatt Black Shale Sill has higher sulfur contents between 0.076 and 0.097 wt%. Nickel contents are variable, with 485ppm in 10 RAT HY069B2, an olivine gabbro with 16.5wt% MgO, and between 101 and 143ppm in the rest of the sill (with 7.9 to 10.5wt% MgO).

In Kat's sill, there is a dramatic difference between the picritic lower sill and the diabasic upper sill. The lower chilled margin resembles sill S1 with 0.078 wt% S and 397ppm Ni. The samples in the picritic lower sill have low S contents between 0.040 and 0.045 wt% and high Ni contents between 795 and 988ppm, reflecting abundant cumulus olivine (22.8 to 23.2 wt% MgO). The diabasic upper part of the sill has high S contents between 0.106 and 0.162 wt%, depleted Ni contents between 86 and 97ppm, and low MgO contents between 7.1 and 9.2 wt%. Nickel concentrations are highest where olivine is most abundant and where sulfur concentrations are low.

#### *5.3.4 Discussion*

At the Uhuk Massif, there is evidence of typical Franklin LIP magmas with uncontaminated  $\delta^{34}\text{S}$  signatures between +2 and +4‰. However, in the Main block feeder gabbro leading up to the eastern upper sill,  $\delta^{34}\text{S}$  values of +4.9 and +7.7‰ indicate that localized contamination is taking place. The likely sources of the positive contamination signature are the sedimentary rocks metamorphosed to calc-silicates with  $\delta^{34}\text{S}$  values between +8.5 and +10.3‰. The overlap in  $\delta^{34}\text{S}$  values between +4.9 and +7.9‰ in the contaminated magma, endoskarns and exoskarns indicates that fluids and sulfur are moving both into and out of the feeder system.

In Kat's sill the range of contaminated diabase  $\delta^{34}\text{S}$  values in the upper part of the sill between +6.2 and +6.8‰ is similar to the +4.9 to +7.7‰ range of contaminated magmas in the Uhuk Massif and the narrower isotopic range likely indicates that some homogenization took place. In the picritic lower part of Kat's sill there is minimal evidence of sulfur contamination even after over 30km of inferred magma transport. That all 5 picrite samples in Kat's sill have  $\delta^{34}\text{S}$  values between +3 and +4‰ despite the transport distance is consistent with the interpretation from Chapter 2 that the contamination of sills does not take place *in situ*. Sample 10 RAT KS075A14, the upper chilled margin, can provide some insight into why this is the case. The high S contents of this sample of 0.16wt% and elevated  $\delta^{34}\text{S}$  value of +8.5‰ are indicative of extensive contamination and inconsistent with diffusion, as diffusion in chilled margins in other sills does not significantly increase sulfur contents. However, the elevated sulfur isotope values and sulfur contents do not extend to the underlying diabase samples. This could indicate that even if stoping of the upper sill contact is taking place, xenoliths are frozen by the crystallization of the upper chilled margin and do not interact with the underlying magma.

In Kat's sill there is a distinctive decoupling of sulfur and nickel contents. Although the upper diabasic part of the sill has high sulfur contents and shows nickel depletion, the simplest interpretation is that magma in the diabasic part of the sill was depleted in Ni by olivine crystallization. The olivine cumulate at the base of the sill has the highest nickel contents out of all Franklin samples analysed to date, yet has low sulfur contents, indicating that in-situ immiscible sulfide segregation did not occur.

The following is a genetic model for the formation of the Uhuk Massif feeder system and Kat's sill. Contamination of the diabasic magma in the feeder system takes place, mainly by bulk rock assimilation, leading to heterogeneously enriched  $\delta^{34}\text{S}$  values in a boundary layer. However, addition of S through contamination was not enough to cause sulfide immiscibility. During transport, xenoliths are melted and assimilated by the magma causing the homogenization of  $\delta^{34}\text{S}$  values. The loss of heat from magma in the feeder system to the host rocks causes olivine to crystallize and settle, concentrating nickel from the passing magma. As the magma flux starts to wane, chilled margins solidify, minimizing host rock contamination.

At some stage the system is rejuvenated by the influx of primitive olivine-rich magmas that show lesser amounts of prior contamination. These low sulfur magmas use the same conduits and inject laterally into the pre-existing sills, underplating the diabasic parts of these sills. The result is a sulfur-poor, nickel-rich olivine cumulate with homogeneous  $\delta^{34}\text{S}$  values in Kat's sill distal from the feeder system. Overall, although carbonate contamination of a feeder system can lead to elevated  $\delta^{34}\text{S}$  values and sulfur concentrations, carbonates lack sufficient sulfur to cause sulfide immiscibility, so magmas concentrate nickel in olivine.

#### **5.4 Application: evaporite contamination**

Mixing calculations in evaporite-hosted sill E3 samples indicate a loss of over 50% of the external sulfur calculated from the isotopic data; suggesting sulfide immiscibility may have been linked with the assimilation process that occurred upstream of the sampled sill. Whether or not the formation of immiscible

sulfides led to metal enrichment or depletion is the focus of this section. Sill E3 has low MgO contents (5.6 to 6.8 wt%), low to depleted Ni contents (67 to 129ppm) and high Cu contents (222 to 260ppm) (Appendix C). The lower sill chilled margin is sulfur poor (0.047 wt%) whereas the middle to upper sill is sulfur rich (0.089 to 0.121 wt%). Platinum concentrations in sill E3 drop from 9.88ppb in the lowermost sample to 6.83ppb in the uppermost sample; palladium shows the opposite trend increasing from 23.4 to 27.4ppb (Appendix D).

In the Uhuk feeder system, host-rock contamination appears to have been insufficient to trigger widespread sulfide immiscibility, allowing nickel to be sequestered in olivine. In the upper part of the evaporite-hosted sill E3, elevated  $\delta^{34}\text{S}$  values and sulfur contents are coupled with nickel and platinum depletion. These features are all consistent with widespread rather than localized sulfide immiscibility in this sill. However, in samples with depleted Ni and Pt contents, there are elevated Pd, Cu, and Au contents.

In a traditional metal tenor upgrading model (Naldrett, 1992), if immiscible sulfides are exchanging trace metals and PGEs with passing magma, either all of the PGEs, Ni, Cu, and S should be enriched (sulfide accumulation) or depleted (sulfide segregation). The inconsistent behaviour of Ni, Cu, Pt, and Pd suggests that something has disrupted the magmatic systematics. There could have been some unknown fluid effect (Boudreau and Meurer, 1999) or kinetic factors (Mungall, 2002). Because the contamination in Sill E3 was interpreted to have occurred upstream it is impossible to know for certain whether sulfur forming immiscible sulfides was eventually resorbed or degassed. Speculating further on the inconsistent behaviour of chalcophile elements is beyond the scope

of this thesis. However, the important point is that immiscible sulfide formation does not automatically mean that there will be chalcophile enrichment in sulfides and chalcophile depletion in associated silicate magmas.

## **5.5 Concluding Statements and Future Research Directions**

Large magmatic fluxes and evaporite assimilation in dikes may be required for significant metal tenor upgrading. Significant upward flux of magma is required to provide a large R factor for immiscible sulfides, to keep them in suspension in the magma, and to prevent intrusions from cooling significantly allowing olivine to crystallize. With high throughflow rates, host rocks are heated up faster allowing sulfur-rich fluids from devolatilized carbonates, shales and evaporites to be added to the magma in the earlier magma stages. Early-forming immiscible sulfides can potentially interact with large volumes of magma to upgrade Ni, Cu and PGE concentrations in the absence of olivine crystallization.

The most pressing need for future study is to collect sections through dikes hosted by evaporites, and to analyse host rocks and intrusive samples for sulfur isotopes and abundances and trace metal and PGE abundances. If dike S, Ni, Cu, Pt, and Pd concentrations are all consistently enriched or depleted and  $\delta^{34}\text{S}$  values are enriched relative to primary magmatic values it could be a sign of a significant magmatic upflow zone with sulfide immiscibility and metal tenor upgrading. If evaporite-hosted dikes consistently record discordant S, Ni, Cu, Pt, and Pd concentrations then traditional magmatic Ni-Cu-PGE ore formation models would have to be re-evaluated.

## REFERENCES

(other than from Chapters 2 and 4)

Bedard, J.H., Naslund, H.R., Nabelek, P., Winpenny, A., Hryciuk, M.,

Macdonald, W., Hayes, B., Steigerwaldt, K. et al., 2012, Fault-mediated melt ascent in a Neoproterozoic continental flood basalt province, the Franklin sills, Victoria Island, Canada: Geological Society of America Bulletin, v. 124, p. 723-736.

Boudreau, A.E., and Meurer, W.P., 1999, Chromatographic separation of the platinum-group elements, gold, base metals and sulfur during degassing of a compacting and solidifying igneous crystal pile: Contributions to Mineralogy and Petrology, v. 134, p. 174-185.

Bremond d'Ars, J. de, Arndt, N.T., and Hallot, E., 2001, Analog experimental insights into the formation of magmatic sulfide deposits: Earth and Planetary Science Letters, v. 186, p. 371-381.

Campbell, I.H., and Naldrett, A.J., 1979, The influence of silicate:sulfide ratios on the geochemistry of magmatic sulfides: Economic Geology and the Bulletin of the Society of Economic Geologists, v. 74, p. 1503-1506.

Carroll, M.C., and Rutherford, M.J., 1988, Sulfur speciation in hydrous experimental glasses of varying oxidation state: results from measured wavelength shifts of sulfur X-rays: American Mineralogist, v. 73, p. 845-849.

de Hoog, J.C.M., Taylor, B.E., and van Bergen, M.J., 2001, Sulfur isotope systematics of basaltic lavas from Indonesia: implications for the sulfur cycle in subduction zones: Earth and Planetary Science Letters, v. 189, p. 237-252.

- Frost, B.R., and Lindsley, D.H., 1992, Equilibria among Fe-Ti oxides, pyroxenes, olivine, and quartz: Part II. Application, *American Mineralogist*, v. 77, p. 1004-1020.
- Ghiorso, M.S., and Evans, B.W., 2008, Thermodynamics of rhombohedral oxide solid solutions and a revision of the Fe-Ti two-oxide geothermometer and oxygen-barometer, *American Journal of Science*, v. 308, p. 957-1039.
- Janecky, D.R., and Shanks, W.C., III, 1988, Computational modeling of chemical and sulfur isotopic reaction processes in seafloor hydrothermal systems: chimneys, massive sulfides, and subjacent alteration zones: *Canadian Mineralogist*, v. 26, p. 805-825.
- Jugo, P.J., Luth, R.W., and Richards, J.P., 2005, An experimental study of the sulfur content in basaltic melts saturated with immiscible sulfide or sulfate liquids at 1300°C and 1.0GPa: *Journal of Petrology*, v. 46, p. 783-798.
- Keays, R.R., and Lightfoot, P.C., Crustal sulfur is required to form magmatic Ni-Cu sulfide deposits: evidence from chalcophile element signatures of Siberian and Deccan Trap basalts: *Mineralium Deposita*, v. 45, p. 241-257.
- Li, C., Naldrett, A.J., and Ripley, E.M., 2001, Critical factors for the formation of a nickel-copper deposit in an evolved magma system: lessons from a comparison of the Pants Lake and Voisey's Bay sulfide occurrences in Labrador, Canada: *Mineralium Deposita*, v. 36, p. 85-92.
- Li, C., Ripley, E.M., Naldrett, A.J., Schmitt, A.K., and Moore, C.H., 2009a, Magmatic anhydrite-sulfide assemblages in the plumbing system of the Siberian Traps: *Geology*, v. 37, p. 259-262.
- Li, C., Ripley, E.M., and Naldrett, A.J., 2009b, A new genetic model for the giant



- Ni-Cu-PGE sulfide deposits associated with the Siberian Flood Basalts: Economic Geology and the Bulletin of the Society of Economic Geologists, v. 104, p. 291-301.
- Mandeville, C.W., Webster, J.D., Tappen, C., Taylor, B.E., Timbal, A., Sasaki, A., Hauri, E., and Bacon, C.R., 2009, Stable isotope and petrologic evidence for open-system degassing during the climactic and pre-climactic eruptions of Mt. Mazama, Crater Lake, Oregon: *Geochimica et Cosmochimica Acta*, v. 73, p 2798-3012.
- Mungall, J.E., 2002, Kinetic controls on the partitioning of trace elements between silicate and sulfide liquids: *Journal of Petrology*, v. 43, p. 749-768.
- Naldrett, A.J., 1992, A model for the Ni-Cu-PGE deposits of the Noril'sk region and its application to other areas of flood basalts: *Economic Geology and the Bulletin of the Society of Economic Geologists*, v. 87, p. 1945-1961.
- Ripley, E.M., 1983, Sulfide mineralogy and sulfur isotope geochemistry of layered sills in the Deer Lake Complex, Minnesota: *Mineralium Deposita*, v. 18, p. 3-15.
- Ripley, E.M., and Li, C., 2003, Sulfur isotope exchange and metal enrichment in the formation of magmatic Cu-Ni-(PGE) deposits: *Economic Geology and the Bulletin of the Society of Economic Geologists*, v. 98, p. 635-641.
- Ripley, E.M., Lightfoot, P.C., Li, C., and Elswick, E.R., 2003, Sulfur isotopic studies of continental flood basalts in the Noril'sk region: Implications for the association between lavas and ore-bearing intrusions: *Geochimica et Cosmochimica Acta*, v. 67, p. 2805-2817.

- Ripley, E.M., and Li, C., 2007, Applications of stable and radiogenic isotopes to magmatic Cu-Ni-PGE deposits: examples and cautions: *Earth Science Frontiers*, v. 14, p. 124-132.
- Seal, R.R., II, 2006, Sulfur isotope geochemistry of sulfide minerals: Reviews in *Mineralogy and Geochemistry*, v. 61, p. 633-677.
- Simon, A.C., and Ripley, E.M., 2011, The role of magmatic sulfur in the formation of ore deposits: Reviews in *Mineralogy and Geochemistry*, v. 73, p. 513-578.

## **Appendix A: Sample descriptions**

### *List of abbreviations:*

c/g- coarse grained  
cpx- clinopyroxene  
dk- dark  
EC- eastern (dike) contact  
f/g- fine grained  
Fm.- Formation  
LCM- lower (sill) chilled margin  
LS- limestone  
lt- light  
NFD- Northern Feeder Dike  
ol- olivine  
plag- plagioclase  
py- pyrite  
seds- sedimentary rocks  
UCM- upper (sill) chilled margin  
vf- very fine  
WC- western (dike) contact

### ***Northern Feeder Dike***

#### *(10 RAT) HY064*

NFD, main section near top where ~30m wide. Boot Inlet Fm. Limestone with dolomitic algal brown laminae, more siliceous layers, thin bedded LS weathers light grey-brown; fresh light grey. Diabase has chills on both sides and coarsens in the middle of the dike, grey-brown weathering.

HY064 A1: WC-35.90m, Limestone, weathered surface, mostly thicker bedded limestone with some visible pyrite.

HY064 A2: same as A1, more algal layers, WC-24.80m

HY064 A3: same as A1, blocky tan weathering, WC-15.10m

HY064 A4: same as A1, brown layers, light brown weathering, parallel bedded, WC-7.40m

HY064 A5: low to ground frost-shattered blocks, significant weathering and alteration (grey-green fresh), WC-1.76m

Western dike contact: straight, widens upsection towards upper sill, rubbly

HY064 B1: very fine grained diabase, chilled margin, WC+1.85m

HY064 B2: medium grained diabase, corner block, WC+7.36m

HY064 B3: medium grained diabase, from medium brown resistant fresh block, WC+17.70m

HY064 B4: coarse grained diabase, from vertical face parallel to the dike margin, WC+26.30m

HY064 B5: very fine grained diabase, chilled margin, from block right by contact, WC+36.64m

Eastern dike contact: straight, rubbly, poor sedimentary outcrops on bench up to sill, WC+37.00m, rubbly below B5. Lower down, fault offset block to W (calc-silicate skarn HY065) forms isolated hill; dike with gossan and calc-silicate even lower down (HY066)

HY064 C1: greenish-grey limestone, good outcrop, no outcrop between here and EC, EC+10.6m.

HY064 C2: same as C1, poor outcrop, altered, EC+12.8m

HY064 C3: light grey, tan weathering, very weathered limestone, sample has lots of greenish-yellow alteration (chlorite, etc.) poor outcrop, EC+22.5m

Note: Samples C4 and C5 offset by post-magmatic fault, unrelated to samples C1 to C3

HY064 C4: cooked up limestone, very dark grey, less alteration, altered layer from C4/C5 seems continuous and altered for at least another 50m away from the dike, EC+34.3m

HY064 C5: cooked up limestone, dark grey, very weathered (green-yellow), calcite veins, abundant oxidation/pyrite, EC+42.0m

*(10 RAT) HY065*

NFD, downhill from HY064, in area with a fault offset dike, calc-silicates, skarn, gossan, mini sill and shear zone, thinly bedded limestone altered by the dike

HY065 A1: medium grained diabase, EC-9.50m

HY065 A2: fine grained diabase, EC-0.36m

HY065 B1 to B4: thick bedded limestone, massive and algal layers, microbially laminated layers alter more green, progressively less altered towards B4, B4 bedding 060°08'

*(10 RAT) HY066*

NFD, just to the south of HY065: 2 sides of dike and gossan/skarn on east, EC=WC+14.8m

HY066 A1: limestone, less altered, normal algal layers, WC-13.2m

HY066 A2: limestone, somewhat altered, WC-7.3m

HY066 B1: west chill, very fine grained diabase, WC +0.32m

HY066 B2: medium grained diabase mid-dike, WC+7.9m

HY066 B3: east chill, very fine grained diabase, WC+14.52m

HY066 C1: gossan, EC+1.13m

HY066 C2: skarn, EC+12.5m

HY066 C3: dark limestone near shear zone, EC+46.7m

*(11 RAT) MH066*

Base of NFD, sampled upper part of lower sill and the overlying sed ~15m from where the dike propagates.

MH066A1: fine grained diabase with cubic grains (pyrite/biotite?), UCM-0.16m

MH066A2: stromatolitic dolostone, light grey fresh, less calc-silicates than at base of dike, UCM+3.17m

*(11 RAT) MH067*

resampling 10 RAT HY064 (NFD).

MH067 A1: stromatolitic limestone, WC-5.00m

MH067 A2: more green than A1, contact metamorphism, at same level as HY069 A4, WC-2.13m

*Other samples*

MH144A1: thickly parallel laminated LS, ~4m below HY064A1, medium yellow grey weathered, dolosiltite not microbially laminated, medium grey/lt grey fresh.

MH143A1: microbially laminated LS, grey brown weathered, lt grey fresh, ~1%py concentrated near muddy layers vs. limey; there is a contact between the microbial LS of MH143 and the darker non-microbial LS of MH144 above

MH145: lt grey weathered and fresh microbially laminated LS, ~ in line with HY064C5 laterally, ~4m stratigraphically below HY064C1

***Shale-hosted sill S1***

*(10 RAT) HY069*

Black shale section capped by stromatolitic dolostone on peninsula above Minto Inlet. Shale below and above sill well exposed (Wynniatt Fm. black shale member), rusty red/yellow in weathered surfaces, medium grey/silty in fresh surfaces

HY069 A1: shale is black to dark grey, crumbly and with some rusty/white parts, LCM-6.60m

HY069 A2: shale is more competent than A1, light green-grey, LCM-3.82m.

HY069 A3: very competent dark grey layer, rusty red weathering, LCM-2.42m

HY069 A4: more siliceous/blocky than A3 with sulfide-rich pockets, LCM-1.31m

HY069 A5: just below lower chill, similar to A4 with visible sulfides, some copper sulfides (minor bornite/chalcopyrite?) bedding 085°10', LCM-0.09m

HY069 B1: lower chill of diabase sill, some coarser-grained crystals right above the contact, very fine grained, LCM+0.09m

HY069 B2: medium grained diabase sill, some layering, low in plagioclase, olivine-rich and melanocratic, LCM+2.37m

HY069 B3: somewhat dubiously in place coarse-grained brown-weathering diabase, LCM+7.65m

HY069 B4: coarse grained diabase below upper contact, LCM+13.70m

HY069 B5: upper chill zone contact of sill, very fine grained diabase, LCM+16.15m

HY069 C1: outcrop approximately 100m E of outcrop where A and B sampled, stream cut (possible modern alteration?), cut grey-green shale, weathers grey, UCM+0.80m

HY069 C2: medium grey shale, sulfidized, more siliceous than C1. UCM+3.27m

HY069 C3: same as C2, red weathering, UCM+5.62m

HY069 C4: quartzite with many sulfides including pyrite and chalcopyrite, UCM+8.02m

HY069 C5: altered/sulfidized medium grey shale to quartzarenite, weathered black/red/yellow; altered all the way up to the overlying dolostone, UCM+14.9m

***Carbonate-hosted sill C1***

*(10 RAT) HY068*

Nodular black calcareous shale near base of Upper Carbonate member of Wynniatt near waterfall section. Some vertical fluid flow with oxidation/sulfidation, lots of subvertical joints, lower sill preserved, upper sedimentary rocks not preserved

HY068 A1A: black calcareous shale, lots of recrystallized calcite (toothpaste), LCM-3.93m; A1B is calcite nodules

HY068 A2: shale above calcite nodules, LCM-1.68

HY068 A3: limestone below contact, lighter coloured more blocky more lithified, LCM-0.13m

HY068 B1A: lower chill of diabase sill, B1B vertical S-rich alteration zone, ~0.3m wide at lower chill, LCM+0.17m

HY068 B2: medium grained gabbro, LCM+2.16m

HY068 B3: medium grained gabbro, LCM+4.85m

***Evaporite-hosted sills E1 and E2 (Section 1)***

MH141A1A: weathered outcrop, crumbly white bedded gypsum with lt green blocky limey layers, LCM1-4.30m

MH141A1B: limey layer from same outcrop as MH141A1A, LCM1-3.70m

MH141A2: parallel laminated limestone, beige weathered, aquamarine fresh, vf crystalline, LS only for 2m below lower sill base, LCM1-0.35m

MH140A1: lower chill of lower sill, dk grey weathered, melanocratic fresh, f/g, LCM1+0.14m

MH140A2: LCM1+9.20m, c/g diabase, dk grey weathered, elongate cpx laths diabasic

MH140A3: c/g gabbro, elongate and equant plag xtyls, dk greenish grey weathered, LCM1+13.30m

MH140A4: LCM1+16.9m, UCM1 is 17.20m above LCM1, f/g diabase chill of lower sill, dk greenish grey, weathered

MH139A1A: UCM1+2.85m, bedded gypsum interlayered with lt green LS, fairly fresh overall, this sample is the gypsum

MH139A1B: UCM1+2.85m, limey interval from MH139A1A

MH139A2: UCM1+6.40m, mainly bedded gypsum, weathered outcrop, not much LS

MH139A3A: UCM1+13.50m, nodular gypsum, some marble/anhydrite layers. Gypsum chunk, may not be 100% in place

MH139A3B: marble/anhydrite layer, competent, 100% in place, UCM1+13.30m, LCM2=UCM1+23.0m

MH138A1: black weathering diabase, very fractured and weathered, f/g, LCM2+1.30m, UCM2=LCM2+4.00m

MH138A2: fractured/veined diabase, black weathering, LCM2+2.35m

MH138A3: f/g dk green to black weathering diabase, upper chill of upper sill, 5-10% sulfides, fractured, LCM2+3.85m.

MH137A1: bedded gypsum, broken up/folded, very thin shale layers, sample is from pink more competent layer (slightly marbleized?), UCM2+4.00m

***Evaporite-hosted sill E3 (Section 2)***

*(10 RAT) HY074*

Mostly nodular gypsum (white, soft) approximately 25 percent lime mud layers (light green weathered, light grey fresh), sill is approximately 5m thick, seds above can't be included in section because of a fault running N/S

HY074 A1A: gypsum, fairly solid chunk, LCM-4.35m

HY074 A1B: lime mud layer (adjacent to A1B)

HY074 A2A: gypsum, crumbly, altered, LCM-2.45m

HY074 A2B: limestone mud layer

HY074 A3: weathered gypsum just below sill, LCM-0.18m

HY074 B1: fine grained to very fine grained diabase matrix with plagioclase phenocrysts, lower chilled zone, LCM+0.62m

HY074 B2: medium grained gabbro, LCM+2.30m

HY074 B3: fine grained to very fine grained matrix with plagioclase phenocrysts, upper chill zone, LCM +4.8m

(11 RAT) MH068A1: Shaly limestone from below sill, LCM-0.23m



(11 RAT) MH068B1: medium grained diabase above sill contact LCM+1.65m

**“Kat’s sill”**

Sampled by K. Steigerwaldt, H.R. Naslund. See Appendix 2 for summary of samples from sill

BH082A1: dolostone, silty, parallel bedded (3-5cm) and thinly laminated, some cross bedding, carbonaceous layers (dark grey, black shale?) weathers light brown/tan; fresh light grey, bedding 035°05' (RHR), visible pyrite cubes, LCM-7.8m, W outcrop

BH082 A2: same as A1, bedding 030°02' (RHR), W. outcrop, LCM-6.1m

BH082 A3: laminated dolosiltstone, medium grey fresh, lt brown weathered. Some sandy laminae with quartz, E. outcrop, LCM-4.4m

BH082 A4: 305°02' bedding (RHR), dolosiltstone, LCM-2.8m, E. outcrop

BH082 A5: shaly, limey, some very weathered, creamy, W. outcrop, LCM-1.2m

KS076A1- limestone, parallel bedded (dolosiltite?) shaly, some visible sulfides  
Fine crystalline, light grey to white, highly silicified

**KS076A2**

Fine to fine crystalline quartzite, calcite cement, mostly planar to weakly wavy laminated with some low angle cross-laminae in a more quartz-rich bed. ~85 percent light grey brown quartz-rich layers with 15 percent dark grey fine crystalline layers with scattered light grey specks inside <.5mm diameter. Trace pyrite, moderately layer controlled, highly oxidized

**KS076A3**

Medium crystalline quartzite, calcite cement, light grey fresh with mottled cinnamon brown layering, trace disseminated pyrite, very fine grained

**KS076A4**

Medium crystalline quartzite, calcite cement, light grey fresh, light brown weathered, 5 percent dark grey low angle cross laminae (pyrite rich, highly oxidized to hematite)

**KS076A5**

Quartzite with calcite cement (highly silicified marlstone? fine grained sandstone protolith?), light grey brown fresh, medium crystalline, weakly layered, ~1 to 2 percent relict pyrite (highly oxidized to hematite, disseminated but somewhat layer controlled, partially concentrated in loose bands)

Appendix B: Supplemental  $\delta^{34}\text{S}$  values of Franklin igneous samples and their host sedimentary rocks

Sample	Lithology	Host Formation	$\delta^{34}\text{S}$ (‰)	Comment
<i>Northern Feeder Dike</i>				
10 RAT HY064B1	Diabase	Boot Inlet	-4.2	upper dike western chilled margin
10 RAT HY064B2	Diabase	Boot Inlet	+0.7	upper dike interior
10 RAT HY064B3	Diabase	Boot Inlet	+4.1	upper dike interior
10 RAT HY064B4	Diabase	Boot Inlet	+2.1	upper dike interior
10 RAT HY064B5	Diabase	Boot Inlet	-0.7	upper dike eastern chilled margin
10 RAT HY065A1	Diabase	Boot Inlet	-3.9	middle dike interior
10 RAT HY065A2	Diabase	Boot Inlet	+1.9	middle dike eastern chilled margin
10 RAT HY066B2	Diabase	Boot Inlet	-3.2	middle dike
10 RAT JB097A1	Diabase	Boot Inlet	+0.3	lower dike
10 RAT JB099B	Diabase	Boot Inlet	+0.4	lower dike
10 RAT JB100C	Diabase	Boot Inlet	-2.0	lower dike
10 RAT JB102B	Diabase	Boot Inlet	-2.3	lower sill window
11 RAT MH066A1	Diabase	Boot Inlet	+2.7	lower sill upper chilled margin
10 RAT HY064A1	Carbonate	Boot Inlet	-26.5	western carbonates, upper dike
10 RAT HY064A2	Carbonate	Boot Inlet	-27.0	western carbonates, upper dike
10 RAT HY064A3	Carbonate	Boot Inlet	-22.6	western carbonates, upper dike
10 RAT HY064A4	Carbonate	Boot Inlet	-25.9	western carbonates, upper dike
10 RAT HY064A5	Carbonate	Boot Inlet	-14.5	western carbonates, upper dike, right beside dike
11 RAT MH067A1	Carbonate	Boot Inlet	-20.8	western carbonates, upper dike
11 RAT MH067A2	Carbonate	Boot Inlet	-21.4	western carbonates, upper dike
11 RAT MH143A1	Carbonate	Boot Inlet	-29.88	western carbonates, upper dike
11 RAT MH144A1	Carbonate	Boot Inlet	-18.7	western carbonates, middle dike
10 RAT HY064C1	Carbonate	Boot Inlet	-0.2	eastern carbonates, upper dike
10 RAT HY064C2	Carbonate	Boot Inlet	+2.2	eastern carbonates, upper dike
10 RAT HY064C3	Carbonate	Boot Inlet	+3.5	eastern carbonates, upper dike

Appendix B (continued): Supplemental  $\delta^{34}\text{S}$  values of Franklin igneous samples and their host sedimentary rocks

Sample	Lithology	Host Formation	$\delta^{34}\text{S}$ (‰)	Comment
<i>Northern Feeder Dike</i>				
10 RAT HY065B1	Carbonate	Boot Inlet	+3.4	eastern carbonates, middle dike
10 RAT HY065B2	Carbonate	Boot Inlet	-0.2	eastern carbonates, middle dike
10 RAT HY065B4	Carbonate	Boot Inlet	-0.6	eastern carbonates, middle dike
10 RAT HY066C1	Carbonate	Boot Inlet	+6.0	eastern carbonates, middle dike
10 RAT HY066C3	Carbonate	Boot Inlet	+14.3	eastern carbonates, middle dike
11 RAT MH145A1	Carbonate	Boot Inlet	+3.2	eastern carbonates, middle dike
11 RAT MH066B1	Carbonate	Boot Inlet	+7.2	eastern carbonates, above lower sill
<i>Uhuk Massif<sup>a</sup></i>				
10 RAT AW063	Diabase	Jago Bay	+2.4	Horst, domain 7
10 RAT HY062A2	Diabase	Jago Bay	+2.3	Main block, lower sill, domain 4
10 RAT JB155B	Diabase	Jago Bay	+3.8	Main block, lower sill, domain 2
10 RAT JB156B1	Diabase	Jago Bay	+4.9	Main block, feeder gabbro, domain 2
10 RAT JB156B2	Diabase	Jago Bay	+7.7	Main block, feeder gabbro, domain 2
10 RAT JB 155A	Skarn	Jago Bay	+7.7	Main block, domain A
10 RAT JB 155AS	Skarn	Jago Bay	+7.9	Main block, domain A
10 RAT JB 155B2	Skarn	Jago Bay	+7.3	Main block, domain A
10 RAT JB 155C	Calc-silicate	Jago Bay	+10.4	Main block, domain A
10 RAT JB 157A	Skarn	Jago Bay	+6.5	Main block, domain C
10 RAT AW064	Calc-silicate	Jago Bay	+8.5	Horst, domain F
10 RAT AW065	Skarn	Jago Bay	+6.1	Horst, domain F
10 RAT JB163B	Skarn	Jago Bay	+5.8	Northern Block, south side, domain G
10 RAT JB166BM	Skarn	Jago Bay	+5.8	Northern Block, west side, domain G
10 RAT JB166BV	Skarn	Jago Bay	+5.0	Northern Block, west side, domain G

a-domains refer to location in Bedard et al. (2012) Figure 4

Appendix B (continued): Supplemental  $\delta^{34}\text{S}$  values of Franklin igneous samples and their host sedimentary rocks

Sample	Lithology	Host Formation	$\delta^{34}\text{S}$ (‰)	Comment
<i>"Kat's sill"</i>				
10 RAT KS072B	Picrite	Jago Bay	+3.8	lower chilled margin
10 RAT KS074A10	Picrite	Jago Bay	+3.5	olivine cumulate, lower sill
10 RAT KS074A11	Picrite	Jago Bay	+3.7	olivine cumulate, lower sill
10 RAT KS074A7	Picrite	Jago Bay	+3.3	olivine cumulate, lower sill
10 RAT KS074A9	Picrite	Jago Bay	+3.1	olivine cumulate, lower sill
10 RAT KS075A3	Diabase	Jago Bay	+6.8	diabasic upper sill
10 RAT KS075A8	Diabase	Jago Bay	+6.2	diabasic upper sill
10 RAT KS075A14	Diabase	Jago Bay	+8.5	upper chilled margin
10 RAT BH082A1	Carbonate shale	Jago Bay	+7.7	lower sedimentary rocks
10 RAT BH082A2	Carbonate shale	Jago Bay	+5.2	lower sedimentary rocks
10 RAT BH082A3	Carbonate shale	Jago Bay	+9.9	lower sedimentary rocks
10 RAT BH082A4	Carbonate shale	Jago Bay	+5.0	lower sedimentary rocks
10 RAT BH082A5	Carbonate shale	Jago Bay	+0.9	lower sedimentary rocks
10 RAT KS076A1	Carbonate shale	Jago Bay	+7.0	upper sedimentary rocks
10 RAT KS076A3	Carbonate shale	Jago Bay	+10.4	upper sedimentary rocks
10 RAT KS076A4	Carbonate shale	Jago Bay	+11.1	upper sedimentary rocks
10 RAT KS076A5	Carbonate shale	Jago Bay	+8.9	upper sedimentary rocks

Appendix C: Sulfur, nickel and copper concentrations of Section 2 diabase and sedimentary samples and representative sill and dike diabase and picrite samples

<b>Sample</b>	<b>Lithology</b>	<b>MgO (wt %)</b>	<b>Sulfur content (wt %)</b>	<b>Nickel content (ppm)</b>	<b>Copper content (ppm)</b>
<i>Section 2 (Sill E3)</i>					
10 RAT HY074A1A	Evaporite	0.01	17.96	11	2
10 RAT HY074A1B	Carbonate	17.2	0.38	b.d.l <sup>a</sup>	2
10 RAT HY074A2A	Evaporite	0.05	17.83	15	b.d.l <sup>a</sup>
10 RAT HY074A2B	Carbonate	18.2	0.42	20	10
10 RAT HY074A3	Evaporite	0.03	16.98	17	2
10 RAT HY074B1	Diabase	6.77	0.047	129	222
10 RAT HY074B2	Diabase	6.60	0.121	106	238
10 RAT HY074B3	Diabase	5.58	0.089	67	260
<i>Sills</i>					
<i>Carbonate-hosted (C1)</i>					
10 RAT HY068B1A	Diabase	7.38	0.048	86	131
10 RAT HY068B1B	Diabase	7.34	0.044	103	130
10 RAT HY068B2	Diabase	8.04	0.037	124	131
10 RAT HY068B3	Diabase	7.56	0.044	102	122
<i>Shale-hosted (S1)</i>					
10 RAT HY069B1	Diabase	10.5	0.077	137	243
10 RAT HY069B2	Picrite	16.5	0.081	485	115
10 RAT HY069B3	Diabase	9.25	0.076	143	108
10 RAT HY069B4	Diabase	7.93	0.078	101	143
10 RAT HY069B5	Diabase	8.06	0.097	116	123
<i>"Kat's sill"</i>					
10 RAT KS072B	Diabase	13.1	0.078	397	131
10 RAT KS074A07	Picrite	23.2	0.045	988	89
10 RAT KS074A09	Picrite	23.2	0.040	884	66
10 RAT KS074A10	Picrite	22.8	0.044	795	82
10 RAT KS074A11	Picrite	23.2	0.041	862	542
10 RAT KS075A03	Diabase	7.58	0.110	97	139
10 RAT KS075A08	Diabase	7.08	0.106	86	177
10 RAT KS075A14	Diabase	9.20	0.162	87	154
<i>Northern Feeder Dike</i>					
10 RAT HY064B1	Diabase	7.05	0.044	100	188
10 RAT HY064B2	Diabase	6.35	0.043	76	179
10 RAT HY064B3	Diabase	6.58	0.045	88	184
10 RAT HY064B4	Diabase	6.91	0.039	84	150
10 RAT HY064B5	Diabase	7.10	0.051	115	170
10 RAT HY065A1	Diabase	7.24	0.094	101	159
10 RAT HY066B2	Diabase	6.80	0.058	142	169

a- b.d.l= below detection limit, 0.02wt% S, 1.1ppm Cu, 10ppm Ni

Appendix D: PGE and Au concentrations of Section 2, sill S1, and north feeder dike diabases and host sedimentary rocks<sup>ab</sup>

Sample	Lithology	Ru (ppb)	Rh (ppb)	Pd (ppb)	Os (ppb)	Ir (ppb)	Pt (ppb)	Au (ppb)
<i>Section 2 (sill E3)</i>								
10 RAT HY074A1A	Evaporite	b.d.l	b.d.l	0.30	b.d.l	b.d.l	b.d.l	b.d.l
10 RAT HY074A1B	Carbonate	b.d.l	0.01	0.11	b.d.l	0.00	0.11	b.d.l
10 RAT HY074A2B	Carbonate	b.d.l	0.01	0.19	b.d.l	b.d.l	0.19	b.d.l
10 RAT HY074B1	Diabase	0.34	0.67	23.42	0.02	0.05	9.88	5.23
10 RAT HY074B2	Diabase	0.32	0.59	22.69	0.04	0.04	9.15	5.16
10 RAT HY074B3	Diabase	0.18	0.56	27.44	0.01	0.02	6.83	5.88
<i>Shale-hosted sill S1</i>								
10 RAT HY069A1	Black shale	b.d.l	0.02	0.72	b.d.l	0.00	0.27	b.d.l
10 RAT HY069A3	Black shale	b.d.l	0.02	0.06	b.d.l	b.d.l	0.19	0.21
10 RAT HY069A5	Black shale	b.d.l	0.01	0.32	b.d.l	b.d.l	0.23	b.d.l
10 RAT HY069C2	Black shale	b.d.l	0.01	0.31	b.d.l	b.d.l	0.15	b.d.l
10 RAT HY069C4	Sandstone	b.d.l	b.d.l	b.d.l	b.d.l	b.d.l	b.d.l	b.d.l
10 RAT HY069C5	Sandstone	b.d.l	0.00	b.d.l	b.d.l	0.01	0.02	b.d.l
10 RAT HY069B1	Diabase	0.47	0.63	12.13	0.00	0.23	12.65	2.85
10 RAT HY069B2	Picrite	1.11	0.55	8.73	0.26	0.25	8.93	1.33
10 RAT HY069B3	Diabase	0.40	0.54	10.55	0.04	0.19	11.28	2.39
10 RAT HY069B4	Diabase	0.21	0.47	11.95	b.d.l	0.16	12.52	0.27
10 RAT HY069B5	Diabase	0.47	0.55	11.56	0.15	0.21	11.55	0.63
<i>North Feeder Dike</i>								
10 RAT HY064A1	Carbonate	b.d.l	0.02	b.d.l	b.d.l	0.00	0.19	b.d.l
10 RAT HY064A5	Carbonate	b.d.l	0.01	0.01	b.d.l	b.d.l	0.08	b.d.l
10 RAT HY064C1	Carbonate	b.d.l	0.01	0.14	b.d.l	b.d.l	0.14	b.d.l
10 RAT HY064C5	Carbonate	b.d.l	0.01	0.09	b.d.l	b.d.l	0.08	0.48
10 RAT HY064B1	Diabase	0.19	0.45	15.67	b.d.l	0.00	5.31	2.44
10 RAT HY064B2	Diabase	0.36	0.78	29.68	b.d.l	b.d.l	7.82	7.03
10 RAT HY064B3	Diabase	0.25	0.57	19.10	b.d.l	b.d.l	5.39	3.87
10 RAT HY064B5	Diabase	0.31	0.52	19.89	b.d.l	0.01	6.42	0.52

a- based on measured concentrations of <sup>99</sup>Ru, <sup>103</sup>Rh, <sup>105</sup>Pd, <sup>189</sup>Os, <sup>193</sup>Ir, <sup>195</sup>Pt and <sup>197</sup>Au

b- b.d.l = below detection limit, 0.12ppb Ru, 0.08ppb Rh, 0.47ppb Pd, 0.07ppb Os, 0.03ppb Ir, 0.84ppb Pt, 0.48ppb Au

Appendix E: Magnetite-Ilmenite  $fO_2$  and T constraints (Ghiorso and Evans 2008) for specific mineral pairs

Mineral pair	$fO_2$ ( $\Delta FMQ$ )	T ( $^{\circ}C$ )	Mineral pair	$fO_2$ ( $\Delta FMQ$ )	T ( $^{\circ}C$ )
<i>Sills</i>					
<i>10 RAT HY068B3</i>			<i>Session 1<sup>a</sup></i>		
Oxides 1	-1.84	703	Oxides 2	-2.08	668
Oxides 3	-1.21	616	Oxides 6	-2.23	631
Oxides 7	-2.51	608	Oxides 8	-2.15	617
Oxides 9	-1.78	634	Oxides 10	-1.8	632
Oxides 11	-1.68	722			
<i>10 RAT HY068B3</i>			<i>Session 3<sup>a</sup></i>		
Oxides 1 (1)	-1.69	716	Oxides 1 (2)	-1.37	707
Oxides 2 (1)	-1.48	695	Oxides 2 (2)	-1.98	696
Oxides 3 (1)	-1.56	640	Oxides 3 (2)	-1.74	660
Oxides 4 (1)	-2.49	659	Oxides 4 (2)	-1.27	647
Oxides 6 (1)	-1.67	708	Oxides 6 (2)	-1.34	734
<i>10 RAT HY069B2 (low Mg)</i>			<i>Session 1<sup>a</sup></i>		
Oxides 2	+0.60	761	Oxides 4	+0.61	730
Oxides 6	+0.69	771			
<i>10 RAT HY069B2 (low Mg)</i>			<i>Session 3<sup>a</sup></i>		
Oxides 1	+0.97	695	Oxides 2 (1)	+0.96	709
Oxides 2 (2)	+0.57	766	Oxides 3	+0.77	763
Oxides 4	+1.02	706	Oxides 5 (1)	+0.55	798
Oxides 5 (2)	+0.76	789	Oxides 7 (1)	+0.59	736
Oxides 7 (2)	+0.81	688			
<i>10 RAT HY069B2 (high Mg)</i>			<i>Session 1<sup>a</sup></i>		
Oxides 8	+0.25	741	Oxides 9	+0.73	718
Oxides 10	-0.04	739	Oxides 12	+0.31	809
<i>10 RAT HY069B2 (high Mg)</i>			<i>Session 3<sup>a</sup></i>		
Oxides 6	+0.56	835			

a- Session 1: December 15<sup>th</sup> and 16<sup>th</sup>, 2011; Session 2: May 18<sup>th</sup> and 22<sup>nd</sup>, 2012; Session 3: July 11<sup>th</sup>, 2012

Appendix E (continued): Magnetite-Ilmenite  $fO_2$  and T constraints (Ghiorso and Evans 2008) for specific mineral pairs

Mineral pair	$fO_2$ ( $\Delta FMQ$ )	T ( $^{\circ}C$ )	Mineral pair	$fO_2$ ( $\Delta FMQ$ )	T ( $^{\circ}C$ )
<i>Dike</i>					
<i>10 RAT HY064B1</i>			<i>Session 2<sup>a</sup></i>		
Oxides 1	-0.06	686	Oxides 2	-0.30	679
Oxides 3	+0.57	682	Oxides 4	-0.07	662
Oxides 5	+0.04	573	Oxides 6	+0.31	714
<i>10 RAT HY064B2</i>			<i>Session 2<sup>a</sup></i>		
Oxides 2	-2.11	639	Oxides 6	-1.49	694
Oxides 7	-1.52	690			
<i>Evaporite-hosted sills</i>					
<i>10 RAT HY074B2</i>			<i>Session 1<sup>a</sup></i>		
Oxides 1	+1.22	684	Oxides 2	+1.67	748
Oxides 4	+1.22	715	Oxides 5	+1.16	687
Oxides 6	+1.83	713	Oxides 7	+1.08	689
Oxides 10	+1.55	665	Oxides 11	+1.58	695
<i>10 RAT HY074B2</i>			<i>Session 3<sup>a</sup></i>		
Oxides 1 (1)	+1.64	718	Oxides 1 (2)	+1.76	716
Oxides 6	+1.81	707	Oxides 7	+1.61	732
Oxides 8 (1)	+1.61	691	Oxides 8 (2)	+1.61	682
<i>11 RAT MH138A2</i>			<i>Session 2<sup>a</sup></i>		
Oxides 2	+1.91	681	Oxides 3	+1.56	809
Oxides 4	+0.06	689	Oxides 6	-1.94	785

a- Session 1: December 15<sup>th</sup> and 16<sup>th</sup>, 2011; Session 2: May 18<sup>th</sup> and 22<sup>nd</sup>, 2012; Session 3: July 11<sup>th</sup>, 2012



Appendix E (continued): Magnetite-Ilmenite  $fO_2$  and T constraints (Ghiorso and Evans 2008) for specific mineral pairs

Mineral pair	$fO_2$ ( $\Delta FMQ$ )	T ( $^{\circ}C$ )	Mineral pair	$fO_2$ ( $\Delta FMQ$ )	T ( $^{\circ}C$ )
<i>11 RAT MH140A2</i>			<i>Session 2<sup>a</sup></i>		
Oxides 1	-0.95	834	Oxides 2	-1.64	715
Oxides 3	-1.21	702	Oxides 7	-1.74	719
<i>11 RAT MH140A2</i>			<i>Session 3<sup>a</sup></i>		
Oxides 3 (1)	-1.30	701	Oxides 3 (2)	-1.57	734
Oxides 4 (1)	-1.86	749	Oxides 5 (1)	-1.63	700
Oxides 5 (2)	-1.78	676	Oxides 6	-1.89	732

a- Session 1: December 15<sup>th</sup> and 16<sup>th</sup>, 2011; Session 2: May 18<sup>th</sup> and 22<sup>nd</sup>, 2012; Session 3: July 11<sup>th</sup>, 2012

Appendix E (continued): Magnetite-Ilmenite  $fO_2$  and T constraints (Ghiorso and Evans 2008) for specific mineral pairs

Mineral pair	$fO_2$ ( $\Delta FMQ$ )	T ( $^{\circ}C$ )	Mineral pair
<i>Discarded mineral pairs</i>			<i>Reason</i>
10 RAT HY074B2- ox2 (S3)	+2.28	678	Too close to immiscible sulfides, local not sample $fO_2$
10 RAT HY074B2- ox 3 (S3)	+2.22	686	Too close to immiscible sulfides, local not sample $fO_2$
10 RAT HY064B2- ox3 (S2)	-0.91	442	T way too low, disequilibrium
11 RAT MH140A1- ox1 (S3)	-0.87	534	Low T anhedral blobby ilmenite
11 RAT MH140A1- ox2(1) (S3)	-0.97	520	Low T anhedral blobby ilmenite
11 RAT MH140A1- ox2(2) (S3)	-0.84	544	Low T anhedral blobby ilmenite

a- Session 1 (S1): December 15<sup>th</sup> and 16<sup>th</sup>, 2011; Session 2 (S2): May 18<sup>th</sup> and 22<sup>nd</sup>, 2012; Session 3 (S3): July 11<sup>th</sup>, 2012